Functional Electrospun Nanofibrous Membranes

for water filtration

Dissertation

zur Erlangung des akademischen Grades

Doktor der Ingenieurwissenschaften

(Dr. –Ing.)

der Technischen Fakultät

der Christian-Albrechts-Universität zu Kiel

Seyed Shahin Homaeigohar

Kiel

2011

1. Gutachter:

Prof. Dr. Mady Elbahri

2. Gutachter:

Prof. Dr. Franz Faupel

3. Gutachter:

Prof. Dr. Rainer Adelung

4. Gutachter:

Prof. Dr. Christine Selhuber-Unkel

Datum der mündlichen Prüfung: 16.12.2011

Table of Contents *Page*

List of Tables *Page*

List of Figures *Page*

Chapter 1.

Introduction

Chapter 1. Introduction

1.1 water filtration as a global challenge for the coming century and nanofibers as an advanced solution

The term of **Water crisis** is often used by the United Nations and other world organizations for depiction of the present status of world's water resources relative to human demand. In general, scarcity of usable water and water pollution constitute the major aspects of the water crisis.[1]

The distribution mode of water on earth is seen in figure 1.1A. The oceans contain around 97 percent of all water as saline water, while the rest is fresh water produced through the water cycle as shown in figure 1.1B. The major part of this fresh water source (about 69 percent) is confined in glaciers and icecaps, mainly in Greenland and Antarctica. Figure 1.1C shows that surprisingly the remaining freshwater, almost all of it exists as ground water and not accessible. Of all the freshwater on earth, only about 0.3 percent is contained in rivers and lakes and usable for human's daily life.[2] Despite such limited capacity of usable water, the human kind is also polluting the water thereby minimizing the available fresh usable water. As seen in figure 1.2A, the pollution released from industry into the atmosphere is ruining the quality of the environment and intensifying the water scarcity problem continuously. According to the released statistics shown in figure 1.2B, it is estimated that more than 50% of nations in the world will experience freshwater shortages by 2025, while by 2075, this percentage will increase to 75% of all nations. [3]

Considering the shortage of the usable water and the progressive pollution as a recognized threat to the world's environment, the attention must be switched, as quickly as possible, towards addressing these critical challenges and directing global research to develop advanced technology and devices for creation of a clean environment. Filtration technology is one of such advanced approaches for making a healthier and cleaner environment. For instance, tapping alternative sources of water, such as seawater, rainwater, wastewater effluent etc. and removal of available contaminants through a filtration process to increase the water quality can be a potential solution for the problem of water shortage.

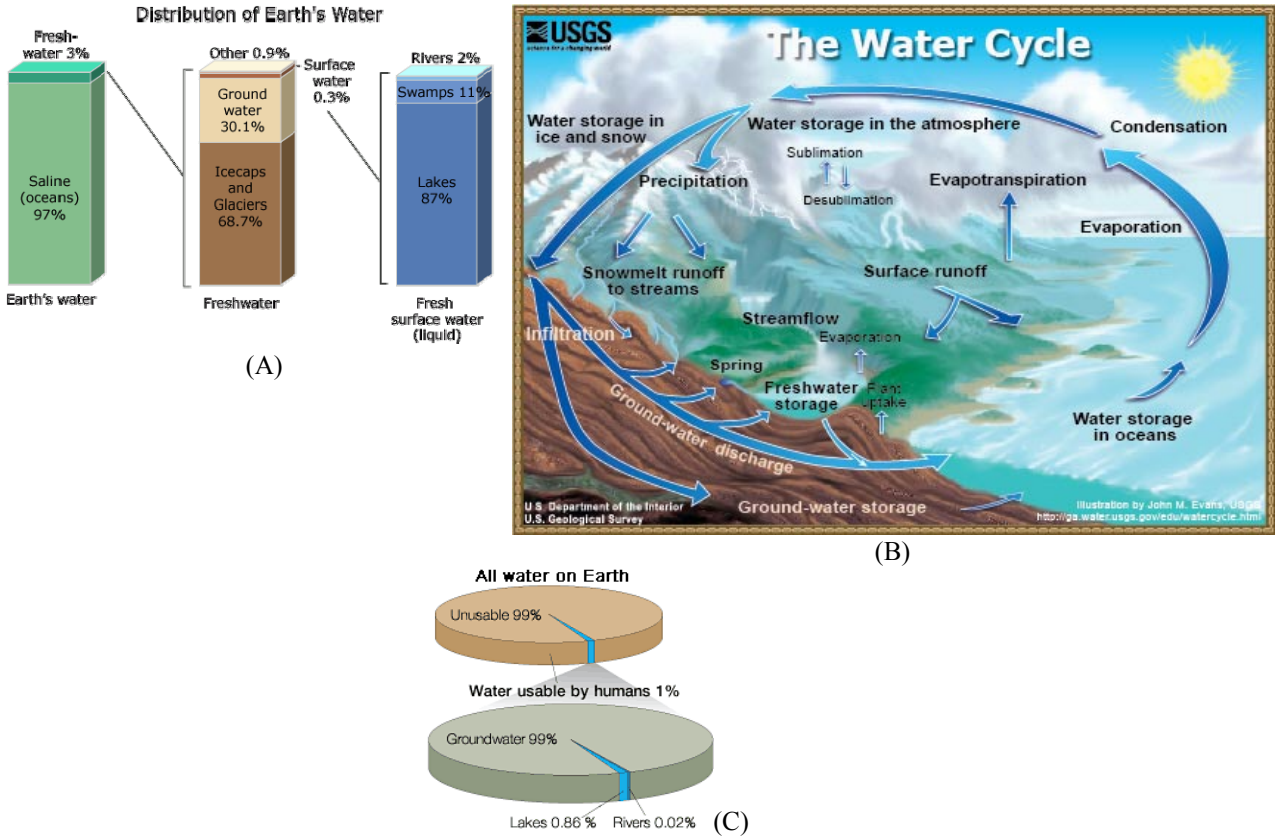

Figure 1.1: A)Distribution of earth's water [2] B) The water cycle supplying the limited capacity of the fresh water [2]C) Scarcity of the water usable for human needs [2]

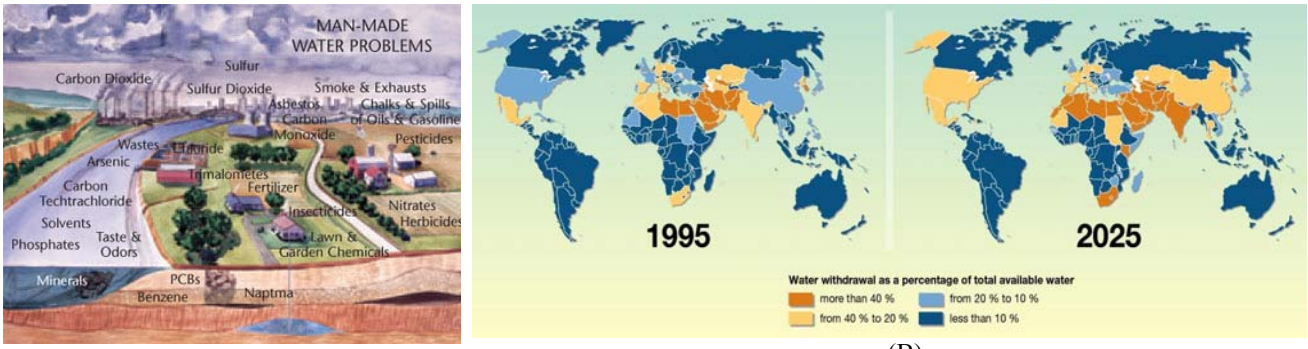

Figure 1.2: A) Common water problems due to industrialization [4] B)Water shortage as a global challenge [5]

The necessity of benefiting breakthrough filtration technology has led to increasing attention in advanced functional nanosized materials such as nanofibers for filtering devices. Water and air purification can be effectively achieved using nanofibrous membranes due to their high interconnected porosity and tunable pore size. These structural features can create very promising filtration abilities in terms of permeability, selectivity and low fouling.

Nanofibers can be produced via several different methods including: drawing, template synthesis, phase separation, self-assembly and electrospinning. Among these

methods, electrospinning because of its easiness and low cost has become more popular [3].

Briefly, this PhD research work deals with implementation of electrospun polymeric nanofibers for water filtration. As the main membrane material, polyethersulfone (PES) has been selected due to its high mechanical property, high thermal resistance, also high chemical resistance to various acids and alkalis. Additionally, it is easily fabricable in a wide variety of configurations and modules, and has a relatively low cost. A combination of desirable material and structural properties (i.e. high porosity and surface area) are assumed to make the PES electrospun nanofibrous membrane (ENM) a highly efficient filter for water filtration.

The structure of this PhD thesis consists of several chapters including:

Chapter 1- Introduction

Chapter 2- Theoretical background: including a brief description regarding nanofibers and their production techniques especially electrospinning, the controlling parameters in electrospinning, and diverse applications of electrospun nanofibers especially in the filtration area.

Chapter 3- Experimental and Characterizations: The experimental part of the PhD study including preparation of the samples and main characterization tests is described from two views of theory and practice.

Chapter 4- Preparation and filtration characterization: Chapter 4 mainly deals with the results of the first experimental part of thesis concerning preparation of the PES ENM and its subsequent filtration characterization. Filtration potentials of the PES ENM are evaluated by using a Polystyrene heterodisperse suspension in terms of permeability, rejection ability also transmembrane pressure.

Chapters 5, 6 and 7- Modification: These chapters are about modification of the PES ENM to obtain the optimum efficiency for water filtration application.

Despite promising filtration features, an electrospun membrane possesses a very high surface area to volume ratio which makes it more exposed to mechanical stresses applied while filtration. Without mechanical stability, the membrane undergoes mechanical failures such as compaction which reduces the porosity and affects the filtration efficiency. Furthermore, in case of using a hydrophobic membrane material, the wettability of the membrane is drastically decreased giving rise to its fouling tendency. Therefore, an electrospun nanofibrous membrane should possess sufficient mechanical strength and wettability. To fulfill such requirements,

the PES ENM is mechanically reinforced and hydrophilized through different approaches. As a progressive trend, the mechanical stability and wettability of the membrane are improved through a heat treatment approach also incorporation of zirconia and titania nanoparticles. The zirconia nanoparticles are in fact a novel nanofiller in membrane technology. Fabrication method for the nanocompoites containing each kind of nanofiller is different depending on the main purpose of addition.

Chapter 8- Outlook: The outlook of the current PhD study is to the advanced functionalized electrospun nanofibrous membranes. Despite the desirable filtration performance of the PES ENM in terms of permeability, the rejection ability is limited to coarse suspended solids as a microfiltration membrane. Functionalization of the nanofibers could bring about a high capacity for rejection of even nanoparticles much smaller than the pore size. Functionalization of PES is a very complicated approach, however a novel polymer like Poly(acrylonitrile-co-glycidyl methacrylate) (PANGMA) can easily be functionalized through protein immobilization. As a preliminary study, PANGMA nanofibers are biofunctionalized by Bovine Serum Albumin (BSA) protein and their separation efficiency is evaluated for gold nanoparticles.

1.2 References

[1] http://en.wikipedia.org/wiki/water_crisis

[2] http://ga.water.usgs.gov/edu/earthwherewater.html

[3] V. Thavasi, G. Singh and S. Ramakrishna, Electrospun nanofibers in energy and environmental applications Energy Environ. Sci.1(2008) 205–221.

[4] www.planetperformance.org/water/water.htm

[5] maps.grida.no/go/graphic/increased-global-water-stress

Chapter 2.

Theoretical background

Chapter 2. Theoretical background

2.1 Nanofibers and their importance

Reduction of the diameter of polymeric fibers from micrometers (e.g. 10–100 μm) to sub-microns or nanometers (e.g. 0.01–0.1 μm) leads to creation of some amazing characteristics such as an extraordinary surface area to volume ratio (as large as 10^3 times of that of a microfiber), flexibility in surface functionalities, excellent mechanical properties and versatility of design. Such desirable features make the polymer nanofibers optimal choices for many important applications such as composites, protective clothing, catalysis, electronics, biomedicine, agriculture and filtration.[1,2]

Figures 2.1A,B show electrospun nanofibers compared to conventional microfibers and a normal human hair (70 μm in diameter), respectively.

2.2 Production techniques

Drawing, template synthesis, phase separation, self-assembly and electrospinning are the main processing techniques for preparation of polymer nanofibers. Here, the drawing is performed in a similar way to dry spinning in fiber industry, thereby one-by-one very long single nanofibers are formed. However, only those viscoelastic materials which are able to tolerate strong deformations while pulling can be made into nanofibers through drawing.

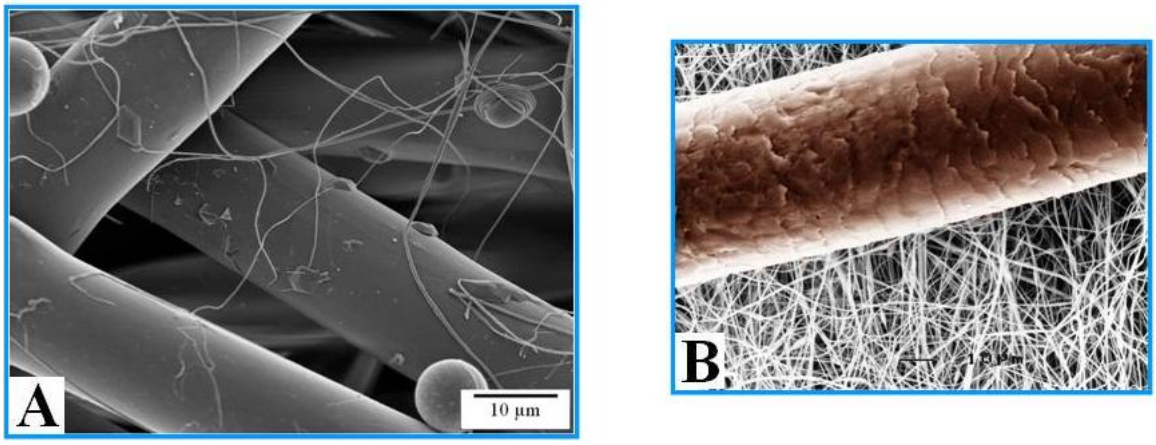

Figure 2.1: A) Size comparison of PES electrospun nanofibers and PET microfibers; B) Electrospun nanofibers compared to a normal human hair [3]

In the template synthesis, a nanoporous membrane is used as a template to make solid or hollow nanofibers of a diverse range of raw materials including electronically conducting polymers, metals, semiconductors and carbons. Nevertheless, production of one-by-one continuous nanofibers is not feasible by this method. The phase separation is another technique consisting of dissolution, gelation, extraction using a different solvent, freezing and drying which finally results in formation of a nanoporous foam. The whole process of conversion of the solid polymer into the nanoporous foam takes relatively long period of time. The self-assembly is the process of self-arrangement of randomly dispersed pre-existing components thereby formation of an organized structure or pattern. Specific, local interactions among the components themselves is the cause of such organization. This technique same as the phase separation is time-consuming in production of continuous polymer nanofibers. Thus, electrospinning process seems to be the only suitable method for mass production of continuous nanofibers from various polymers.[1,4]

Electrospinning is a novel production technique of continuous ultrafine fibers (with diameters of 10 μm down to 10 nm) based on forcing a polymer melt or solution through a spinnerette with an electrical driving force.[4,5] The main advantages of this technique are relatively easiness (easy to setup), high speed, low cost of the process, high versatility allowing control over fiber diameter, microstructure and arrangement and vast materials selection.[4,6,7]

2.3 Electrospinning

2.3.1 Processing

2.3.1.1. Fundamental Aspect

Electrospinning process of polymer nanofibers is shown schematically in figure 2.2. This technique is based on three main components: a high voltage supplier, a capillary tube equipped to a needle of small diameter and a metallic collecting plate. In this process, to make an electrically charged jet of polymer solution or melt out of the needle, a high voltage is applied between two electrodes connected to the spinning solution/melt and to the collector which is normally grounded, respectively. The electric field is subjected to the tip of the needle containing a droplet of the polymer solution. The surface of the droplet is electrified by the electric field. The repulsion of

the present charges at the surface also their contraction to the opposite electrode creates a force overcoming the surface tension. Increase of the intensity of the electric field changes the hemispherical surface of the fluid at the tip of the needle to a conical shape known as the Taylor cone. After a special intensity of the electric field, the repulsive electrostatic force dominates the surface tension and a charged jet of the polymer solution/melt is ejected from the tip of the Taylor cone. Due to the mutually repulsive forces of the electric charges of the jets, the polymer solution jet undergoes an instability (bending instability) and is elongated. The bending instability makes the jet very long and thin. Evaporation of the solvent while occurrence of bending instability results in formation of a charged polymer fiber which is collected as an interconnected web on the collector.[1,2,5,6,8]

The polymer solution jet is subject to three opposing forces including electrostatic and viscoelastic forces and surface tension. Similar to mechanical drawing in conventional fiber spinning, as stretching force, electrostatic repulsion of the charges in the jet increases its surface area by reduction of the fiber diameter. Gradually evaporation of the solvent intensifies this effect. On the other hand, the surface tension of the polymer solution tries to lower the total surface of the jet through an instability called "Rayleigh instability" by breaking up the jet into spherical droplets.

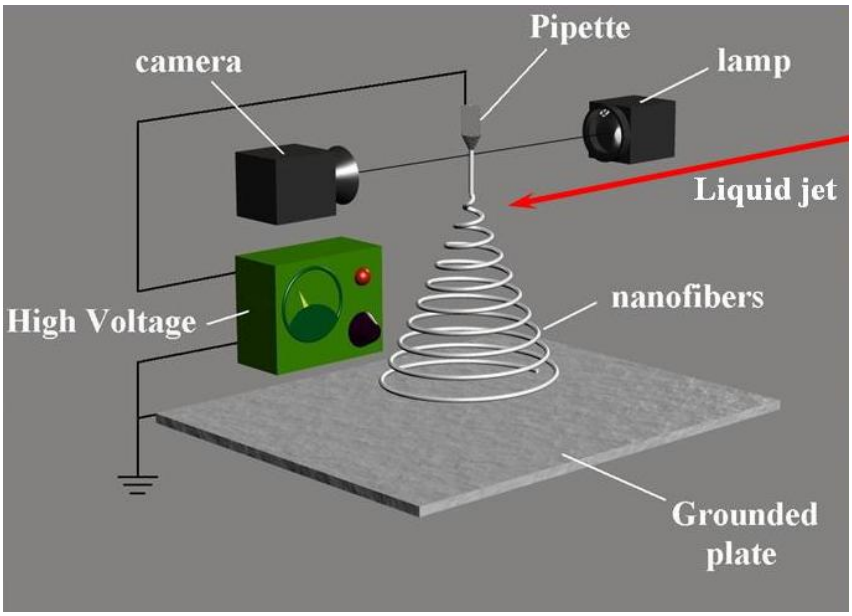

Figure 2.2: A schematic diagram to interpret electrospinning of polymer nanofibers [9]

In the polymer solution being electrospun, entanglement of polymer chains results in a viscoelastic force that resists against the stretching of the jet by electrical force. Also viscoelastic force withstand any rapid change in shape of the jet by surface tension. The nature and mechanical properties of the polymer solution including its viscosity and surface tension are determining factors for privilege of one of these forces to the other one.[8,10]

For the solutions containing long-chain molecules that cannot be easily broken up into discrete droplets, Rayleigh instability creates a "pearls-on-a-string" morphology (so-called "beading"). Formation of the beaded nanofibers strongly depends on the processing variables including viscosity (i.e. concentration of the polymer solution) also surface tension.[8]

Other than the polymer solutions, polymer melts can also be electrospun into nanofibers. Similarly, the polymer melt is introduced into the capillary tube, however the whole electrospinning process is done in a vacuum condition.[1]

2.3.1.2 Parameter Investigation

Conversion process of polymer solution into nanofiber through electrospinning is affected by several different parameters including: (a) the solution properties such as viscosity, elasticity, conductivity and surface tension, (b) governing parameters such as pump feed pressure, electrical voltage and the collecting distance between the tip and the collector, and (c) ambient parameters such as solution temperature, humidity also air velocity in the electrospinning chamber.[1,8]

The optimum morphological characteristics of electrospun nanofibers can be summarized in (1) consistency and controllability of the diameter, (2) absence of any surface defects like pores and beads, and (3) continuity of single nanofibers as much as possible.[1] The nanofibers possessing such optimum morphological features are made only by regulation of the above mentioned influential parameters. For example the fiber diameter is mainly controllable through the solution viscosity adjustment. A higher viscosity results in a larger fiber diameter.[1] Since, the solution viscosity is proportional to the polymer concentration, hence increase of the polymer concentration leads to formation of thicker nanofibers.[1] In fact, the higher polymer concentration makes more chain entanglement and restricts chain mobility, as a result

less extension of the solution jet thickens the fibres.[10,11] Increase of fiber diameter with polymer concentration follows a power law relationship. [12,13]

Other than the importance of control over the fiber diameter and its uniformity, the formation of defects such as beads and surface pores - as shown in figures 2.3 A,B, respectively- should be minimized as well. In contrary to the beads which lower the surface area of the nanofibers, the pores can enhance it and for some special applications such as catalysis and tissue engineering they are also beneficial.

The formation of the beads is also dependent on the polymer concentration such that higher polymer concentrations result in fewer beads.[14] Doshi and Reneker [15] state that when surface tension of a polymer solution decreases, beadless fibers could be obtained. This does not mean that solely increase of polymer concentration decreases surface tension. Rather than the polymer concentration, the surface tension is assumed to depend more to solvent compositions.[14,16]

Moreover, adding filler materials such as salt into a polymer solution increases the electric charge density on the surface of the solution jet thereby make beadless fibers.[17] Increase of the charges density of the jet equals with increase of electrostatic repulsion force and applying a higher stretching force to the jet and subsequently formation of thinner nanofibers with smaller beads. However, increase of the electrical voltage has no effect on the number of beads or surface morphology of nanofibers i.e. formation of smoother nanofibers.[1] Inversely, it has been shown that with increase of the electrical potential, the electrospun nanofibers become rougher. [12]

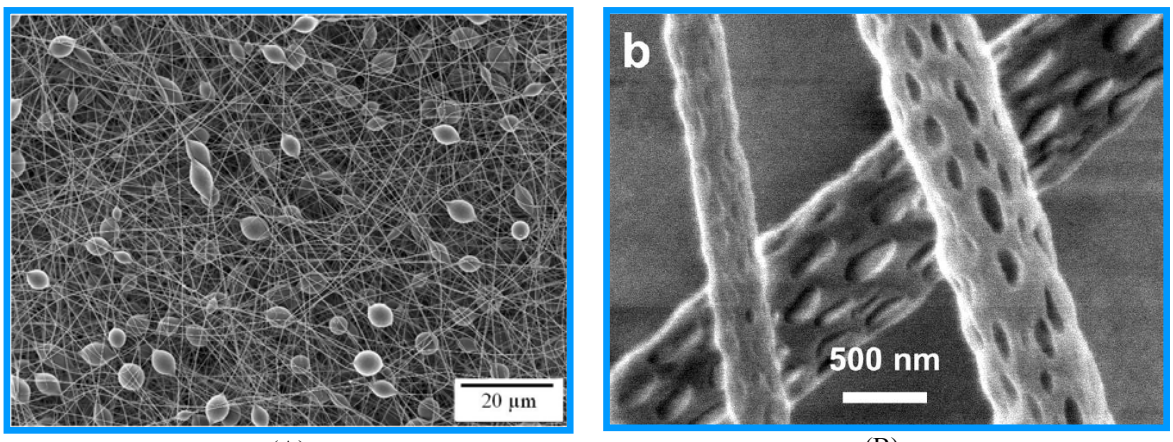

(A) (B)

Figure 2.3: A) Beaded electrospun nanofibers; B) Porous Poly-L-lactide (PLLA) nanofibers [18]

2.3.2 Applications

For electrospun nanofibers a diverse range of applications has been proposed so far. Among them, composite applications, medical prostheses (e.g. grafts and vessels) and filtration applications are the most important ones.[1,4,5,19] Reviewing the number of electrospinning related patents as seen in figure 2.4A reveals that approximately two-thirds of all applications are in the medical field. Of the rest, one-half are about filtration applications, and the remaining half belongs to all other applications.[8] In fact, the small diameter of electrospun nanofibers is advantageous for filtration and composite applications, while their high surface area makes them attractive as catalyst supports and in targeted drug delivery.[5,11] A more detailed list of proposed applications is given in figure 2.4B. Important to note that most of these applications are still at a laboratory research and development stage. However, the highly promising potential of the electrospun nanofibers makes us optimistic about their major contribution to the future industry.[1,6]

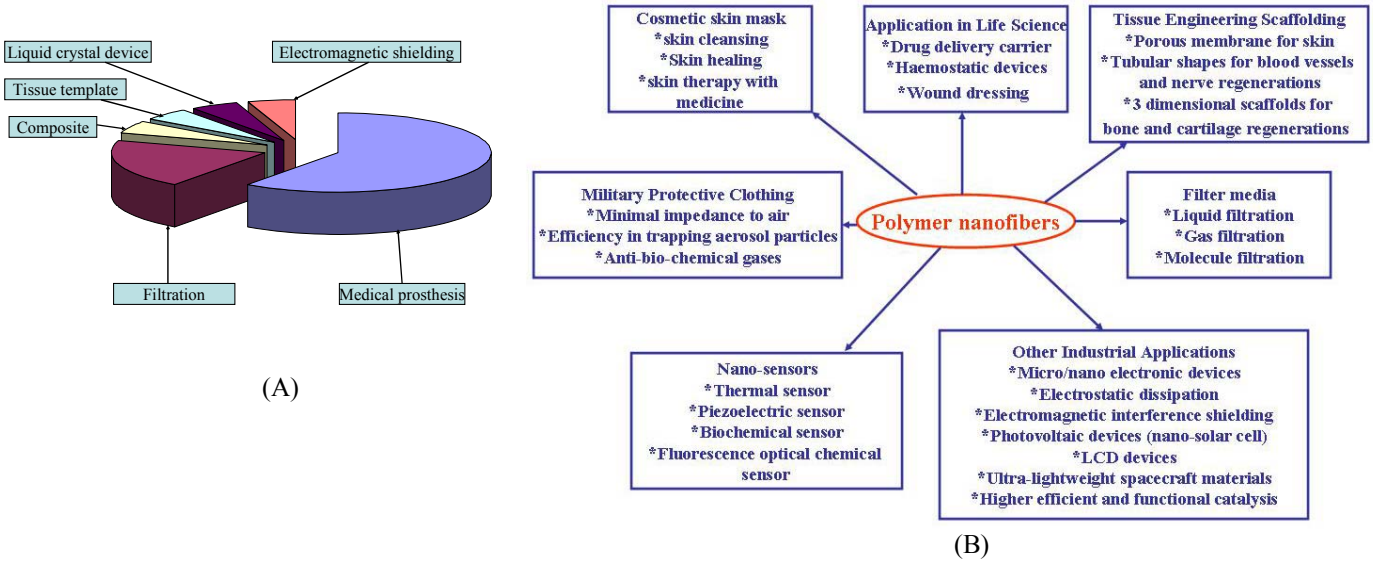

Figure 2.4: A) The application domains of electrospun nanofibers according to US patents [1] ; B) Future applications of electrospun polymer nanofibers [1]

2.3.2.1 Composite applications

Generally, composite structures consist of a matrix (polymer/ metal/ ceramic) reinforced with a filler. The reinforcement materials conventionally used are in the forms of particles also traditional (micro-size) fibers (e.g. engineering fibers such as carbon, glass and Kevlar fibers). Such reinforcements create outstanding structural properties in the composite materials compared to monolithic ones including high modulus and strength to weight ratios. Considering better mechanical properties than micro fibers, nanofibers will also eventually find a similar role to microfibers as a reinforcement material in making nanocomposites with superior structural properties. In addition to higher mechanical properties, nanofiber reinforced composites may possess some other advantages to traditional (microfiber) composites. For instance, in case of incorporation of nanofibrous reinforcements with a diameter much smaller than the wavelength of visible light into a transparent matrix, a completely transparent composite materials can be fabricated.[1,8]

2.3.2.2 Biomedical applications

Bone, dentin, collagen, cartilage, skin and so many other human tissues and organs are formed with a nanofibrous structures. Such biological tissues are characterized by well organized hierarchical fibrous structures realigning in nanometer scale. Hence it is not illogical to consider electrospun nanofibers for replacement or repairing of such biological structures. The application instances encompass various biomedical areas e.g. medical prostheses, tissue template, wound dressing, drug delivery, pharmaceutical composition and cosmetics. [1,4]

2.3.2.3 Filtration applications

The potential of nanofibrous webs as a filtering medium is highly promising. Since the main orientation of the current PhD research, this topic will be discussed more precisely.

To commence, it is interesting to know that future filtration market is estimated to be up to US $700b by the year 2020. [20] But why?

One main reason should be sought in rapid urbanization and industrialization in the past decades developing many new environmental problems such as air

pollution. As air pollution, presence of tiny particles (<2.5 μm) in air is a major cause of cardiovascular and respiratory illness. Additionally, the presence of sulfur dioxide, ozone and nitrogen dioxide is harmful especially for the people with asthma. Such pollutants can also be a cause for allergic reactions. Water similar to air has also been subjected to pollution. The pollutants such as arsenic in drinking water can cause bladder, lung, kidney, liver and skin cancer.

In addition to the need to a clean environment for a healthier life, filtration is also a necessity for industry. The control over airborn and waterborn pollutants, hazardous biological agents also allergens is of the main requirements of industrial manufacturing and processing companies in food, pharmaceuticals, biotechnology and semiconductor business. This need can be optimally circumvented through implementation of an efficient filtration technology. [21]

Functional nanoparticles (e.g. fullerene, carbon nanotubes, metals and semiconductors) in case of release into the environment are the other group of pollutants which can make special environmental concerns. This issue has newly found a higher importance due to a large scale manufacturing with economically viable processes. [22] Various studies have shown that some of these nanoparticles e.g. metal and metal oxide nanoparticles and carbon nanotubes are cytotoxic and can induce granulomas in animal lungs.[23,24,25]

Overall, the necessity of equipping the industrial factories to a highly efficient filtration technology to prevent spread of harmful substances into the environment is being felt nowadays much more than ever before. In this case, the conventional separation methods are not effective enough to prevent pollution of the environment and a more advanced qualified technology is required.[22]

Electrospun nanofibrous membrane based filtration can be an optimum solution for addressing the present environmental concerns. Electrospun nanofibers due to their extremely high length (even up to hundreds of kilometers long) are one of the safest nanomaterials that never become airborne and diffuse into the body. Moreover, considering other promising properties including a very high surface area, large porosity (up to over 90%) and the possibility of using safe (excluding functional polymers), nanofibers as the scaffolding materials can significantly improve separation efficiency, that is, a better capacity to remove pollutants from gas and liquid environments, accompanied by a higher permeability i.e. a lower energy consumption.[22,26]

2.4 Electrospinning for filtration applications

As seen in figure 2.5A, a membrane principally can be resembled to a barrier separating two distinct phases under a driving force such as pressure or concentration gradient. It remains impermeable to specific particles, molecules, or substances. In fact, some components of a feed stream are transported by the membrane into the permeate stream, whereas others are retained by it. Generally, membranes not only are able to accomplish all sorts of separations but also the advantages such as their compactness, cost and energy-efficiency and high throughput make them superior to the other conventional separation processes like adsorption, distillation and extraction.[19]

Functionality of a membrane is defined by two key factors including: flux and selectivity. Flux is about the rate of transportation of species through the membrane, while selectivity depends on the surface properties of membrane assessing the type of the species able to pass through. The structural properties of a membrane such as its porosity, pore size and distribution, hydrophilicity, transmembrane pressure and thickness influence on flux and selectivity of the membrane and subsequently its performance and application in filtration technology.[19]

Fibrous membranes are one of well-known categories of synthetic membranes possessing advantages such as high filtration efficiency and low fluid (air or water) resistance.[27] In such group of membranes, as shown in figure 2.5B, the filtration efficiency and performance is significantly dependent on the fiber diameter.[1,21,26] Accordingly, nanofibrous membranes show a highly promising filtration potential in terms of high permeability and selectivity (due to a very small pore size), making them a suitable candidate for a wide range of filtration applications.

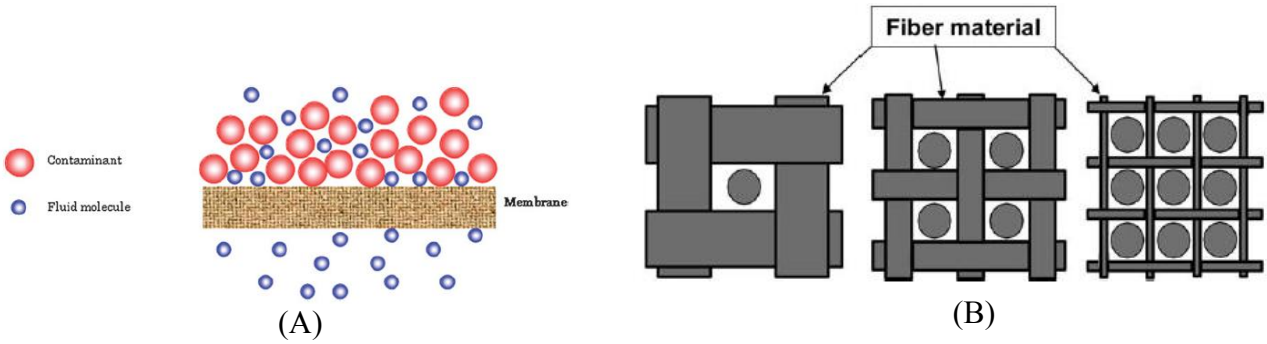

Figure 2.5: A) Schematic of the performance of a membrane [28] ;B) The efficiency of a filter increases with decrease in fiber diameter [1]

In addition, unique properties like high specific surface area (1 to 35 m^2/g depending on the fiber diameter), interconnectivity of pores and potential to be functionalized on nanoscale are of the other important advantages of such kind of membranes. All these desirable features have motivated the researchers all around the world for an extensive study on nanofibrous membranes for air and liquid filtration.[21] Especially, removal of undesirable submicron particles can be a very important objective sought through using this kind of membranes. The good match between the size of the particles or droplets to be captured in the membrane with the channels and structural elements of the membrane is the rationale of such an aim.[29]

Chemical functionalization and electrostatically charging of polymer nanofibers can be also beneficial in more attraction of particles and increase of the filtration efficiency. The nanofibers produced through electrospinnning process are inherently charged and therefore show such an optimum property.[30] For particular applications such as molecular filters which are used for the detection and filtration of chemical and biological weapon agents, the constituting nanofibers are made of some specific polymers or coated with some selective agents.[31]

Despite optimum filtration characteristics especially in pressure-driven liquid separations as micro-(MF), ultra- (UF) or nano-(NF) filtrations, electrospun nanofibrous membranes have also their own proprietary problems.[19] One of the major problems with such kind of membranes is their difficult handling due to accumulation of electrostatic charges during the electrospinning process. To address such a problem, electrospun nanofibers are deposited on a support layer forming a hybrid membrane. Commercial air filters are one of the most known example of such hybrid filters. Hybrid structure of an electrospun nanofibrous membrane can also be based on sandwiching the nanofibrous layer between various layers or blending the nanofibers with microfibers.[10,19]

2.4.1 Nanofibrous membranes for air and water filtrations

2.4.1.1 Air filtration

The first nanofibrous membranes used for air filtration were employed in the early eighties and since then further developed up to now. The air pollution as an environmental concern, the need to removal of hazardous particles from work environments and other specialized applications such as protection against toxic

gaseous agents in the air are all instances in which air should be purified by using an efficient air filter.[28]

Compared to conventional filtration microfibers, nanofibers possess a much smaller diameter thereby offering a more optimum filtration efficiency due to a higher inertial impaction and interception. Moreover, by virtue of slip flow at the nanofiber surface (for the nanofibers with diameter smaller than 500 nm), drag force on the fiber and consequently pressure drop decreases. Slip flow also results in passing more contaminants near the surface of the nanofibers, hence the inertial impaction and interception efficiencies and generally filtration efficiency of the nanofibrous membrane increases for the same pressure drop as compared with conventional fiber mats. Such a benefit besides the very high surface area of the nanofibers facilitating adsorption of contaminants from air are the main reasons for increasing attention to nanofibrous membranes for air filtration applications.[28] In figure 2.6 a commercial air filter produced by Donaldson company is seen which is based on polyamide electrospun nanofibers.

Figure 2.6: Commercial air filtration cartridge using nanofiber filter media [32]

2.4.1.2 Water filtration

Similar to air, water pollution is also another important environmental concern for the present era. To circumvent water scarcity mainly due to the pollution of the very limited available fresh water supplies, the only present solution is tapping and filtering the alternative sources of water (e.g. seawater, rainwater, wastewater effluent etc) to remove the contaminants and enhancement of water quality. Such an approach is only performed through implementing an efficient filtration technology. Recently, in order to develop advanced filtration devices, the attention has been focused on novel functional nanomaterials such as nanofibers. The reason is the possibility of obtaining a high filtration efficiency at lower energy costs. As an example, nanofibrous membranes due to their higher porosities and interconnected porous structures are much more water permeable than their conventional counterparts,[28] hence consume much lower energy and reduce the filtration cost.

Below, some examples of nanofibrous membranes studied for water filtration are explored :

2.5 Filtration of micron sized particles and suspended solids

One important task in water filtration is removal of micron sized particles and suspended solids such as flocs, bacteria etc. The pathogenic microorganisms like *Cryptosporidium parvum* and *Giardia lamblia* are so hazardous that can make serious illnesses and in many countries removal of them from water is compulsory. The rejection of such micron scale unwanted species is usually done optimally through membrane processes such as microfiltration (MF) and ultrafiltration (UF). In fact, two main objectives of water filtration including purification and disinfection are met by these processes. MF and UF membranes are often manufactured by the phase inversion and dry formed methods such as spun bonded and melt blown techniques for the film and fibrous membranes, respectively. Furthermore, electrospinning is another method which is assumed to grow considerably in near future.[28] MF and UF electrospun nanofibrous membranes proposed for water treatment seem to have a highly promising potential, hence they are under extensive research and study.

2.5.1 liquid microfiltration

According to the Baker's definition:" Microfiltration refers to filtration processes that use porous membranes to separate suspended particles with diameters

between 0.1 and 10 μm".[33] The electrospun nanofibrous membranes could be good candidates for liquid microfiltration. These membranes possess a pore size distribution from sub-micron levels to a few micrometers in the range of microfiltration membranes. Besides, compared to conventional phase inverted membranes they contain a higher porosity leading to a higher hydraulic permeability.

The filtration potential of some electrospun nanofibrous membranes (ENMs) of polyvinylidene fluoride (PVDF) and polysulfone (PSU) have been investigated using Polystyrene (PS) particulate suspensions.[19, 34] The prepared microfiltration membranes possessed a flow pore sizes larger than 1 micron (4.0–10.6 μm for PVDF, 1.2–4.6 μm for PSU). When a suspension containing PS particles bigger than 3 μm was used, a higher rejection rate (>92%) was obtained compared to that containing smaller particles (<1 μm) (14–47%). In fact, for big particles, the electrospun membranes act as a screen filter easily washable while for smaller particles as a depth filter forming a cake layer and non-washable i.e. significantly fouled.[22,34] Figure 2.7 shows a PSU nanofiber membrane before and after filtration using a PS particulate suspension (~1 μm in size). Cake layer formation is evident in this picture.

In one study by Kaur et al. [35], the filtration performance of PVDF electrospun nanofibrous membranes have been compared with their commercial counterparts. To evaluate the filtration performance of both membranes in equal conditions i.e. pore size, grafting with methacrylic acid has been carried out on the top layer of the ENM to reduce its pore size to the range of the commercial MF membrane. The results reveal an up to two times higher water flux for the electrospun nanofiber membrane (ENM) than the commercial membrane at the same applied pressure and pore size distribution. The higher water flux for this ENM confirms the better efficiency of the MF membrane with a nanofibrous structure leading to a lower energy consumption.

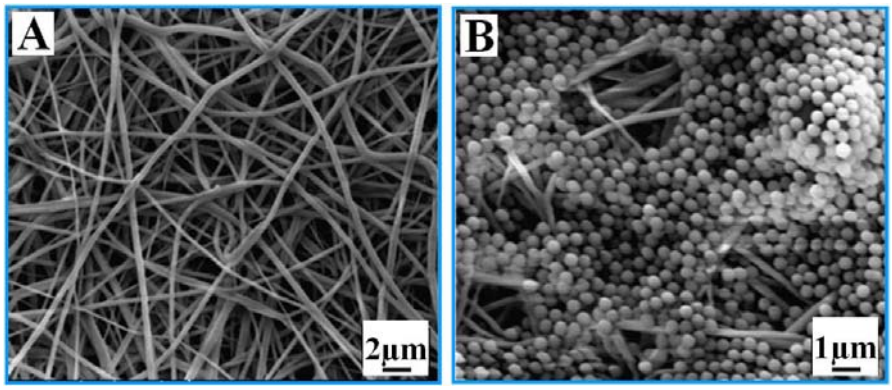

Figure 2.7: SEM micrograph of A) clean nanofiber membrane before filtration and B) nanofiber membrane after filtration with 1 μm polystyrene particles [28]

2.5.2 liquid ultrafiltration

Ultrafiltration (UF) is another filtration process discriminating a diverse range of particulates, such as viruses, emulsions, proteins, and colloids as big as about 1 to 100 nm in the liquid environment.[33] Electrospun nanofibrous membranes can be also used as an UF membrane in case of having a surface pore size less than 0.1μm. Nevertheless, these kind of membranes with such a pore size and high surface area to volume ratio are very prone to a rapid fouling with significant loss of flux while filtration. Unless, they are used with a thin film as coating i.e. as a thin film composite (TFC) membrane based on the nanofibrous support.[22] This UF TFC membrane consists a nonwoven microfibrous substrate, an electrospun nanofibrous mid-layer and a barrier layer (fabricated by coating or interfacial polymerization). The electrospun nanofibrous mid-layer with a very high porosity creates a high permeability and hence compared to the conventional TFC membranes containing an asymmetric porous phase inverted mid-layer the filtration efficiency is enhanced considerably.[22]

Some recent studies have proved this hypothesis. For example, as presented in figure 2.8, a cross-linked polyvinyl alcohol (PVA) electrospun nanofibrous scaffold with nanofiber diameter of 130 to 300 nm and porosity (bulk and surface) of 83% was used as the mid-layer in such a TFC membrane. As the hydrophilic barrier top layer, both cross-linked PVA hydrogel and PEBAX® 1074 (a polyamide–polyethylene glycol copolymer) were employed. In order to evaluate this nanofibrous TFC membrane, a model suspension of bilge water, containing soybean oil (1350 ppm) and DC 193 (polysiloxane–polyethylene glycol) emulsifier (150 ppm) was used. The results showed a flux rate considerably higher for nanofibrous TFC compared to conventional TFCs having the same barrier layer. The permeate flux and rejection rate were strongly dependent to the cross-linking density of the PVA barrier layer controllable by the amount of glutaraldehyde as the cross linker. Moreover, when oxidized multi-wall carbon nanotubes (MWNTs) (up to 10 wt% of the polymer weight) were added to the barrier layer, the permeate flux enhanced up to 3 times for PEBAX® and 5 times for cross-linked PVA (while maintaining the same high rejection ratio around 99.8%). The increase of the flux in the TFC nanofibrous membranes with MWNT incorporated barrier layer was more than 10-fold of that in a typical UF TFC membrane. This significant increase of flux is assumed to be due to the new water channels exposed on the surface of oxidized carbon nanotubes.[36]

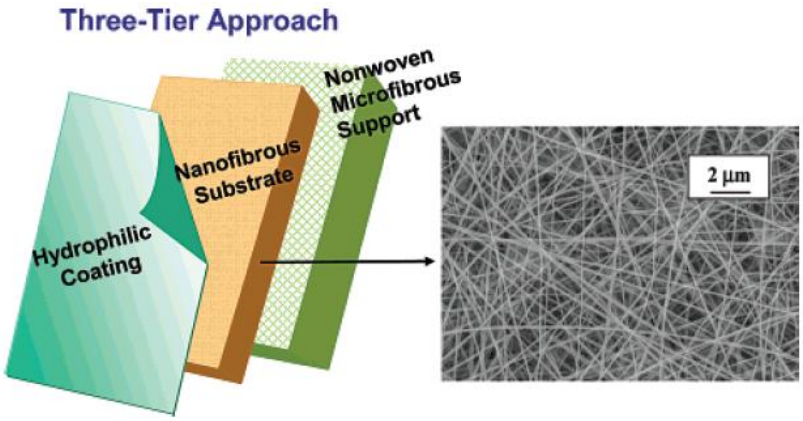

Figure 2.8: Schematic structure of the UF TFC electropun nanofibrous membrane (left) and representative SEM image of electrospun PVA substrate (right) [36]

2.6 Other liquid separations (functionalized nanofibers)

Heavy metals such as copper, cadmium, and chromium present in aquatic systems show a high toxicity and easily can accumulate in living organisms, hence they as a serious biological problem in water should be strictly regulated in the level of around a few tenths of ppb (parts per billion) or less.[22,28]

Two conventional methods for elimination of such pollutants are adsorption and filtration. Interestingly, the electrospun nanofibrous membranes (ENMs) due to possessing a tunable small pore size and high surface area are able to offer both techniques and show a promising potential for this objective.[28] For example, silk fibroin and a blend of silk fibroin with wool keratose ENMs have shown a high removal efficiency for heavy metals as compared to conventional materials like wool silver and filter paper.[37]

Organic materials like oil, protein, humic acid etc. are also of harmful water pollutants and need to be somehow removed from drinking water. Electrospun nanofibrous membrane as functionalized can remove such organic molecules in water effectively.[28] For example, a poly(methylmethacrylate) (PMMA) nanofibrous membrane functionalized with phenylcarbomylated and azidophenylcarbomylated β-cyclodextrins has shown the ability of the removal of phenolphthalein from water.[38]

Functionalized nanofibrous membranes can also be beneficial in disinfection and removal of bacteria from water.[28] Implementation of substances such as elemental silver and silver salts, silver–TiO_2 systems, and quaternary ammonium salt-containing

cationic polymers can induce good antimicrobial properties to the water membranes. By virtue of available high surface area, antimicrobial agents incorporated electrospun nanofibrous membranes can offer a very promising efficiency in removal of such pollutants.[22] One of such efficient electrospun nanofibrous membranes have been developed by Lala et al.[39] They fabricated several silver impregnated polymeric nanofibrous antimicrobial membranes and evaluated their efficiency using two gram negative bacterial groups: *E. coli* and *P. aeruginosa*. The results were quite promising in term of antimicrobial activity of the membranes when incubated with bacteria.[28] Figure 2.9 shows (A) a SEM image of nanofibers possessing antimicrobial properties and (B) the TEM image of a single fiber containing silver nanoparticles on its surface.

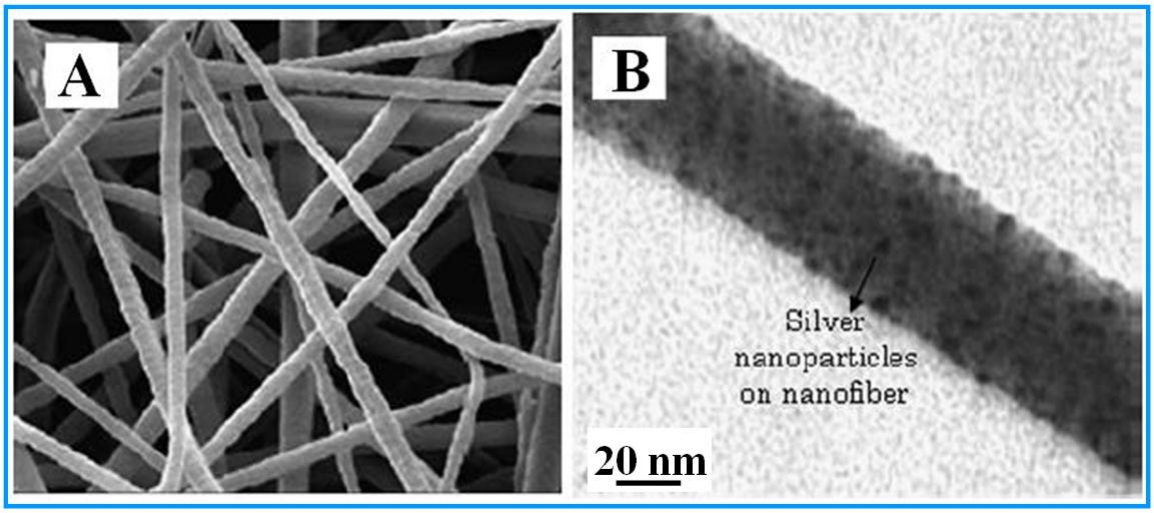

Figure 2.9: A) SEM image of electrospun nanofibers containing silver nanoparticles photoreduced by UV irradiation. B) TEM image of a single nanofiber with the surface resided silver nanoparticles [28]

2.7 References

[1] Zheng-Ming Huang, Y.-Z. Zhang, M. Kotaki, S. Ramakrishna, A review on polymer nanofibers by electrospinning and their applications in nanocomposites, Composites Science and Technology 63 (2003) 2223–2253.

[2] Katarzyna M. Sawicka and Perena Gouma, Electrospun composite nanofibers for functional applications, Journal of Nanoparticle Research 8(2006)769–781.

[3] www.epa.gov

[4] Vince Beachley, Xuejun Wen, Polymer nanofibrous structures: Fabrication, biofunctionalization, and cell interactions, Progress in Polymer Science, In press,2010.

[5] Ji-Huan He, Yu-Qin Wan, Jian-Yong Yu, Application of Vibration Technology to Polymer Electrospinning, International Journal of Nonlinear Sciences and Numerical Simulation 5(3)(2004) 253-262.

[6] Yuris Dzenis, Spinning continuous fibers for nanotechnology, Science 304(June25,2004)1917-1919.

[7] Seema Agarwal, Andreas Greiner, and Joachin H. Wendorff, Electrospinning of manmade and biopolymer nanofibers-progress in techniques, materials, and applications. Adv. Funct. Mater. 19 (2009)2863-2879.

[8] Christian Burger, Benjamin S. Hsiao, and Benjamin Chu, Nanofibrous materials and their applications, Annu. Rev. Mater. Res. 36(2006)333-68.

[9] www.fluid.ippt.gov.pl/sblonski/nanofibres.html

[10] Asis Patanaik, Valencia Jacobs, Rajesh D.Anandjiwala, Performance evaluation of electrospun nanofibrous membrane, Journal of membrane science 352(2010)136-142.

[11] Shu Zhang, Woo Sub Shim, Jooyoun Kim, Design of ultra-fine nonwovens via electrospinning of Nylon 6: Spinning parameters and filtration efficiency, Materials and Design 30 (2009) 3659–3666.

[12] Deitzel JM, Kleinmeyer J, Harris D, Tan NCB. The effect of processing variables on the morphology of electrospun nanofibers and textiles. Polymer 42(2001)261–72.

[13] Demir MM, Yilgor I, Yilgor E, Erman B. Electrospinning of polyurethane fibers. Polymer 43(2002)3303–9.

[14] Fong H, Reneker DH. Elastomeric nanofibers of styrene-butadiene-styrene triblockcopolymer. J Polym Sci: Part B Polym Phys 37(24)(1999)3488–93.

[15] Doshi J, Reneker DH. Electrospinning process and applications of electrospun fibers. J Electrostatics 35(2-3)(1995)151–60.

[16] Liu HQ, Hsieh YL. Ultrafine fibrous cellulose membranes from electrospinning of cellulose acetate. J of Polyer Sci Part B:Polymer Physics 40(2002)2119–29.

[17] Zussman E, Yarin AL, Weihs D. A micro-aerodynamic decelerator based on permeable surfaces of nanofiber mats. Experiments in Fluids 33(2002)315–20.

[18] Bognitzki M, Czado W, Frese T, Schaper A, Hellwig M, Steinhart M, et al. Nanostructured fibers via electrospinning. Adv Mater 13(2001)70–2.

[19] R. Gopal, S. Kaur, Z. Ma, C. Chan, S. Ramakrishna, T. Matsuura, Electrospun nanofibrous filtration membrane, J. Membrane Sci. 281 (2006) 581–586.

[20] Suthat A, Chase G. Chemical Engineer (2001)26–8.

[21] R.S. Barhate, Seeram Ramakrishna, Nanofibrous filtering media: Filtration problems and solutions from tiny materials Journal of Membrane Science 296 (2007) 1–8.

[22] Kyunghwan Yoon, Benjamin S. Hsiao and Benjamin Chu, Functional nanofibers for environmental applications, J. Mater. Chem., 18(2008) 5326–5334.

[23] Günter Oberdörster, Eva Oberdörster, Jan Oberdörster, Nanotoxicology: An emerging discipline evolving from studies of ultrafine particles, Environmental Health Perspective 113(2005) 823-839.

[24] Guang Jia, Haifang Wang, Lei Yan, Xiang Wang, Rongjuan Pei, Tao Yan, Yuliang Zhao, and Xinbiao Guo, Cytotoxicity of Carbon Nanomaterial : Single-Wall Nanotube, Multi-Wall Nanotube, and Fullerene, Environmental sci. and Tech 39(2005)1378-1383.

[25] Chiu-Wing Lam, John T. James, Richard McCluskey, Robert L. Hunter, Pulmonary toxicity of single wall carbon nanotubes in Mice 7 and 90 days after intratracheal instillation, Toxicol. Sci.77(1)(2004) 126-134.

[26] Andreas Holzmeister, Markus Rudisile, Andreas Greiner, Joachim H. Wendorff, Structurally and chemically heterogeneous nanofibrous nonwovens via electrospinning, European Polymer Journal 43(2007) 4859-4867.

[27] Tsaia PP, Schreuder-Gibson H, Gibson P. Different electrostatic methods for making electret filters. Journal of Electrostatics 54(2002)333–41.

[28] V. Thavasi, G. Singh and S. Ramakrishna, Electrospun nanofibers in energy and environmental applications Energy Environ. Sci.1(2008) 205–221.

[29] Graham K, Ouyang M, Raether T, Grafe T, McDonald B, Knauf P. Fifteenth Annual Technical Conference & Expo of the American Filtration & Separations Society, Galveston, TX; 9–12 April 2002.

[30] Tsaia PP, Schreuder-Gibson H, Gibson P. Different electrostatic methods for making electret filters. Journal of Electrostatics 54(2002) 333–41.

[31] Graham S. 'Smart' silicon dust could help screen for chemical weapons. Scientific American 2002:3.

[32] Timothy Grafe, Kristine Graham, Polymeric Nanofibers and Nanofiber Webs: A New Class of Nonwovens, Non woven-technology Review INJ spring (2003) 51–55.

[33] R.W. Baker, Membrane Technology and Applications, 2nd ed., Wiley, 2004.

[34] R. Gopal, S. Kaur, C.Y. Feng, C. Chan, S. Ramakrishna, S. Tabe, T.Matsuura, Electrospun nanofibrous polysulfone membranes as pre-filers:particulate removal, J. Membrane Sci. 289 (2007) 210–219.

[35] S. Kaur, Z. Ma, R. Gopal, G. Singh, S. Ramakrishna and T. Matsuura, Plasma-Induced Graft Copolymerization of Poly(methacrylic acid) on Electrospun Poly(vinylidene fluoride) Nanofiber Membrane Langmuir, 23(2007) 13085–13092.

[36] X. Wang, X. Chen, K. Yoon, D. Fang, B. S. Hsiao and B. Chu, High Flux Filtration Medium Based on Nanofibrous Substrate with Hydrophilic Nanocomposite Coating, Environ. Sci. Technol. 39(2005) 7684-7691.

[37] C. S. Ki, E. H. Gang, I. C. Um and Y. H. Park, Nanofibrous membrane of wool keratose/silk fibroin blend for heavy metal ion adsorption. J. Membr. Sci. 302(2007) 20–26.

[38] S. Kaur, M. Kotaki, Z. Ma, R. Gopal, S. Ramakrishna and S. C. Ng, Oligosaccharide functionalized nanofibrous membrane, Int. J. Nanosci., 5(2006) 1–11.

[39] N. L. Lala, R. Ramaseshan, B. Li, S. Sundarrajan, R. S. Barhate,Y.-J. Liu and S. Ramakrishna, Fabrication of nanofibers with antimicrobial functionality used as filters: protection against bacterial contaminants. Biotechnol. Bioeng. 97(2007)1357–1365.

Chapter 3.
Experimental Part

Chapter 3. Experimental Part

3.1 Materials

Polyethersulfone (PES) Ultrason E6020P (M_w= 58000 and density of 1.37 g/cm^3) was purchased from BASF (Germany). As the sub layer of the membrane a technical poly(ethylene terephthalate) (PET) non-woven was used. The chemical structure of PES and PET is shown in figure 3.1. The solvents *N,N*-dimethylformamide (DMF) and *N,N*-dimethylacetamide (DMAc) were obtained from Merck (Germany). Zirconium oxide (zirconia) powder with the average particle size of 29–68 nm was supplied from Nanoamor Co.(USA). Trifluoroacetic acid (TFA) and tetra-n-butyl titanate (TBT) (titania precursor) were also obtained from Aldrich chemical co. (USA). All materials were used as received.

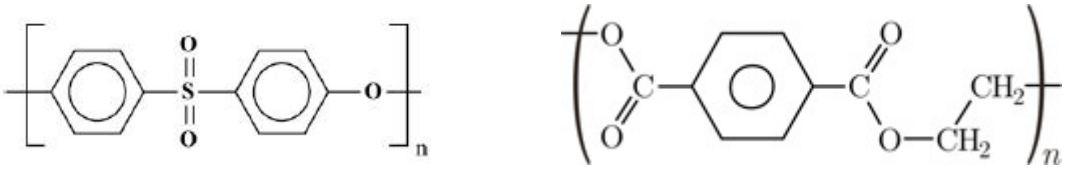

(A) (B)

Figure 3.1: Chemical structure of PES (A) and PET(B)

3.2 Preparation of samples

All the samples prepared and studied in the current PhD research can be categorized as two classes of neat PES and modified PES electrsopun nanofibrous membranes. The latter group consists of the heat treated and composite nanofibrous membranes.

3.2.1 PES nanofibrous membrane

PES nanofibrous membranes were produced by electrospinning. Briefly, prepared PES solution (20 wt%) in DMF was fed with a constant rate of 0.5 ml/h into a needle by using a syringe pump (Harvard Apparatus, USA). By applying a 20 kV voltage (Heinzinger Electronic GmbH, Germany) PES was electrospun on Aluminum foil (as the control substrate) and PET non-woven. The latter substrate was used as a support for the nanofibrous membrane and to facilitate the handling issue. The schematic diagram of the composite membrane is illustrated in figure 3.2. The

electrospinning conditions are tabulated in table 3.1. Furthermore, the electrospinning set-up is shown in figure 3.3.

3.2.2 Heat treated PES nanofibrous membrane

The PES nanofibrous membranes prepared as above mentioned, after peeling off the sub layer were heated in the oven (Heraeus Vacutherm, max T=200°C) at the temperature of 190 °C for 6 hours in air and then were slowly cooled in the oven. The selected temperature is above the boiling point of the solvent (T_B(DMF)=153 °C) and below the glass transition temperature of PES (225 °C).

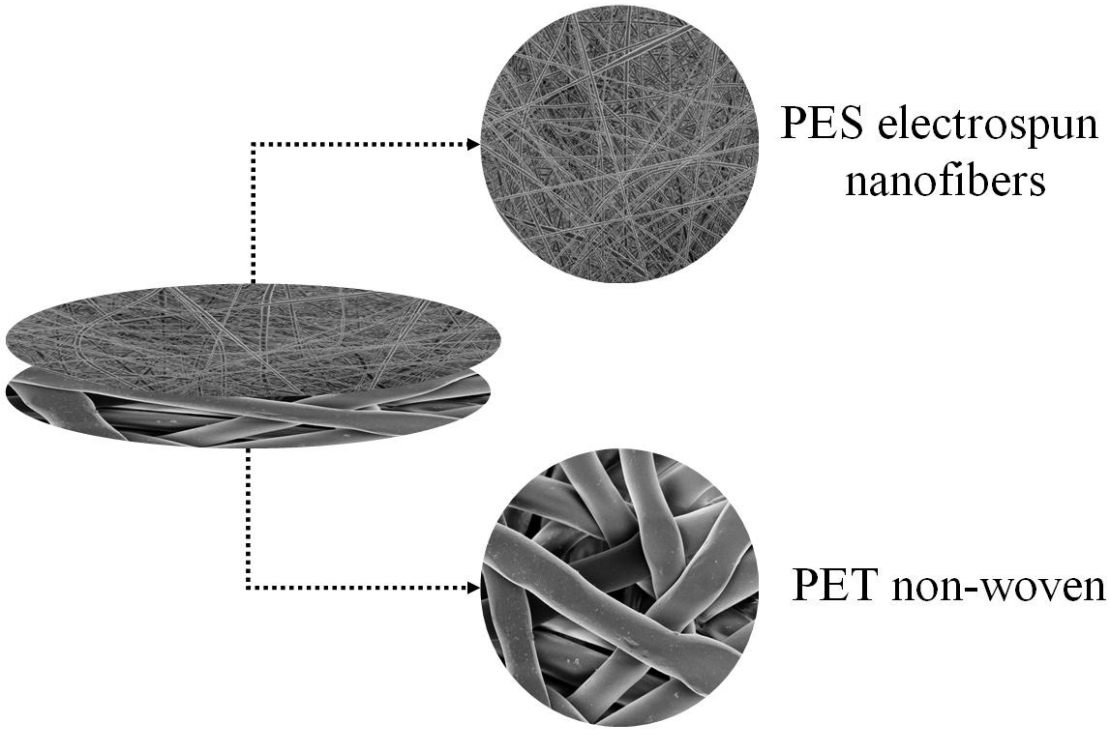

Figure 3.2: Structure of the PES/PET composite membrane

Table 3.1: Electrospinning conditions

	PES nanofibrous membrane	**ZrO_2/PES nanofibrous membrane**	**TiO_2/PES nanofibrous membrane**
PES Concentration	20 wt%	20 wt%	20 wt%
Applied voltage	20 kV	20-25 kV	19-23 kV
Feed rate	0.5 mL/h	0.5 mL/h	0.3-0.5 mL/h
Spinning distance	25 cm	25 cm	25 cm
Collection time	8 h	8 h	8 h
Inner diameter of the needle	0.8 mm	0.8 mm	0.8 mm

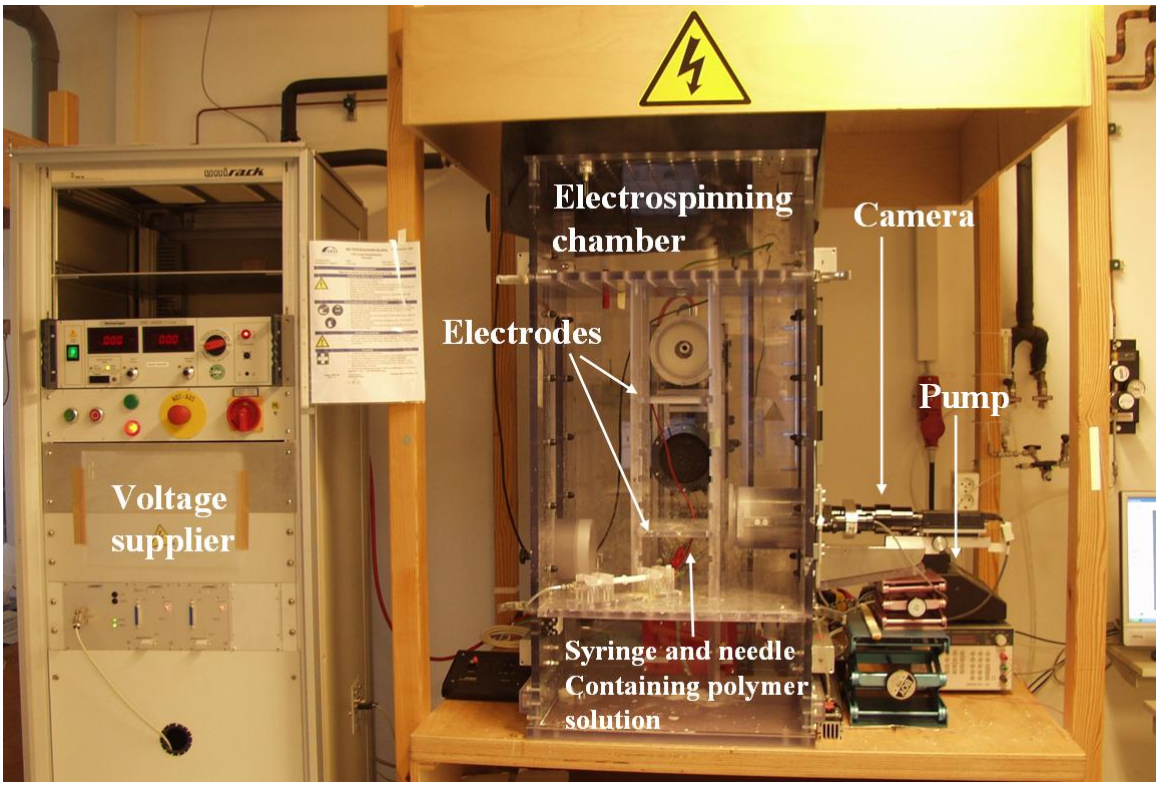

Figure 3.3: Electrospinning set-up

3.2.3 Zirconia nanoparticle doped PES nanofibrous membrane

The PES solutions containing zirconia nanoparticles were prepared through a two-step method. Initially the nano-zirconia (ZrO_2) (1.0, 5.0, 7.0 wt.%) was dispersed in DMF by magnetic stirring and ultrasonicated at room temperature for 105 min to disrupt possible agglomerates.

In the second step, the appropriate weight of PES flakes was added to the ZrO_2/DMF dispersion. This was followed by magnetic stirring until the polymer dissolved completely.

ZrO_2/PES nanofibrous mats were produced by electrospinning of the prepared solution on an Aluminum foil under the given conditions as tabulated in table 3.1. The schematic of the preparation process is shown in figure 3.4.

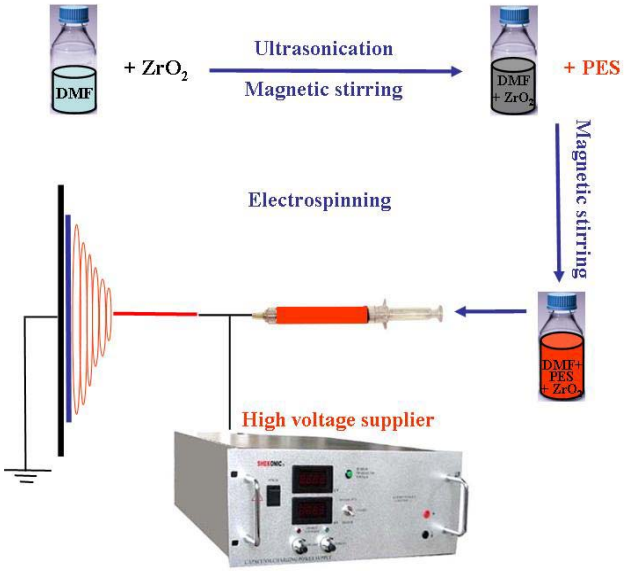

Figure 3.4: Schematic of the preparation process of ZrO_2/PES electrospun nanofibrous membranes (the colours are not meaningful)

3.2.4 Titania nanoparticle doped PES nanofibrous membrane

PES solution with a concentration of 20 wt% was prepared by dissolving PES flakes in DMAc and acidized with special amount of TFA. Simultaneously, to get titanium precursor sol-solution, TBT was hydrolyzed with TFA for 6 hours at special molar ratio (TFA/TBT) of ≈ 4, then added to PES solution. The amount of TBT was somehow selected to obtain 5 and 8 wt% TiO_2 in the final composite nanofibers. The TFA added had two important roles including: 1) acting as a hydrolysis/condensation catalyst 2) reacting with the alkoxide forming reasonable complexes thereby hampering hydrolysis during sol synthesis and inhibiting precipitation [1,2,3]. The progressive formation of the microstructure would be in a more controlled manner if the hydrolysis and condensation steps are separated and tempered e.g. by using an acid catalyst like TFA.[2]

The final solution was stirred overnight to obtain a clear homogenous solution for electrospinning. Briefly, for electrospinning the prepared solution was fed with a constant rate of 0.3-0.5 ml/h (depending on the viscosity) into a needle by using a syringe pump (Harvard Apparatus, USA). By applying a 19-23 kV voltage (Heinzinger Electronic GmbH, Germany) electrospinning was done on an Aluminum foil. The electrospinning conditions are tabulated in table 3.1. To accomplish the hydrolysis, the electrospun nanofibers were left (aged) in air overnight.[3]

After electrospinning, in order to in-situ generation of titania nanoparticles a hydrothermal treatment was performed. Through hydrothermal treatment, condensation reaction of the titania precursor occurs and generates TiO_2 nanoparticles.[4] For this reason, the electrospun nanofibers were peeled off from Aluminum foil and immersed in a hot water bath (75 °C) for 10 hrs. Subsequently, the nanofibers were left to be dried in air overnight. At last, the nanofibrous mat was anealed in oven at 100 °C for 6 hrs in order to avoid the agglomeration of the TiO_2 nanoparticles[5,6,7] and partially crystallize the amorphous titania formed through sol-gel to obtain anatase with a higher hydrophilicity effect.

The schematic of the preparation process of the TiO_2/PES electrospun nanofibrous membranes is shown in figure 3.5.

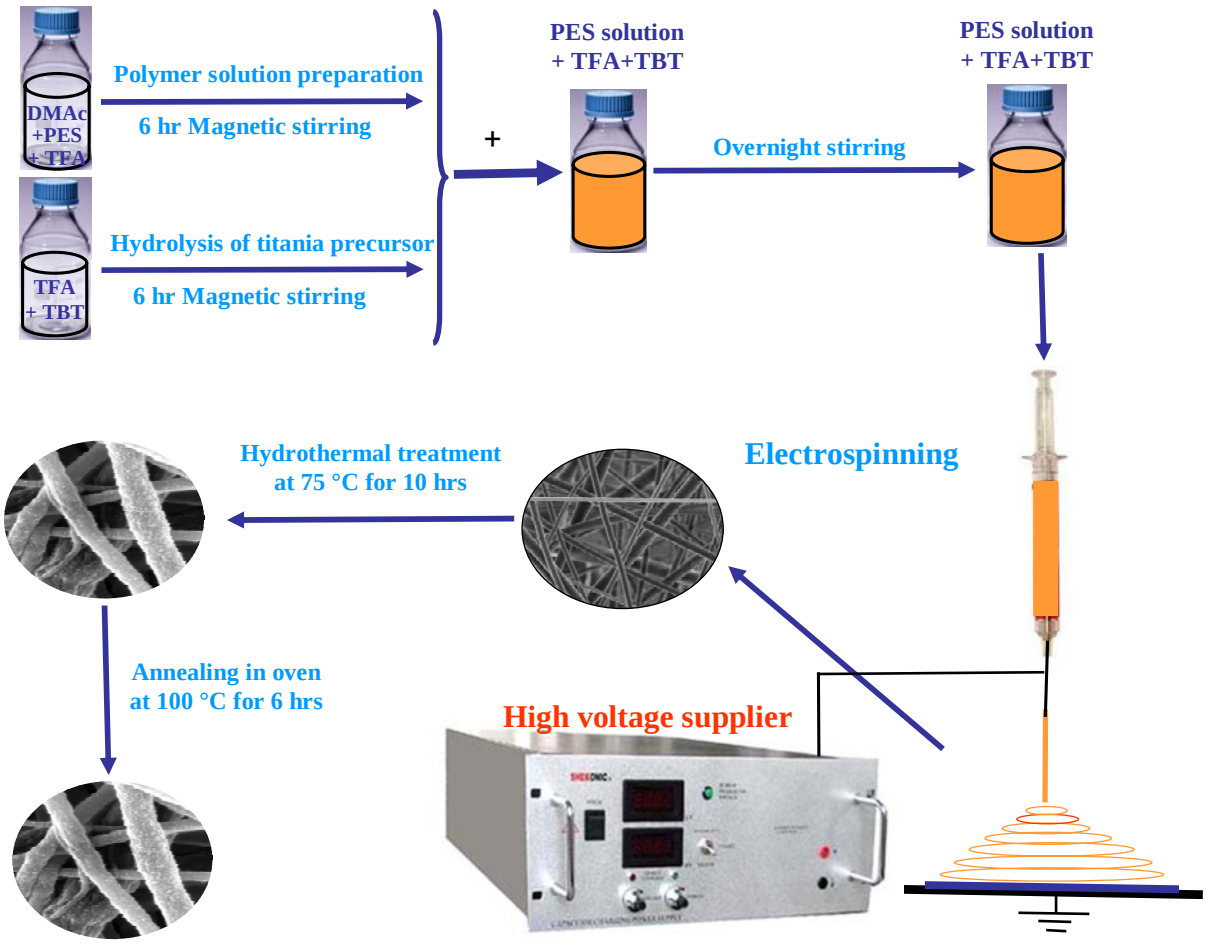

Figure 3.5: Schematic of the preparation process of TiO_2/PES electrospun nanofibrous membranes

3.3 Characterization tests

Characterization of elelctrospun nanofibrous mats has its own complexities, however successful integration of such materials into a specific technology will require their precise evaluation at the level of surface, bulk and architecture. In fact, characterization of electrospun nanofibrous membranes comprises two main aspects of microstructure (internal structure or material properties) and macrostructure (external structure or membrane properties). Microstructure is completely dependent to membrane material properties such as molecular weight, chemical property and crystallinity. On the other hand, macrostructure relies on structural properties of the membrane including porosity, fiber density, fiber diameter, pore size, specific surface area and fiber surface morphology (roughness). These parameters are interrelated and influence on the resultant properties of the electrospun nanofibrous membrane.

3.3.1 Characterization of membrane properties

3.3.1.1 Permeability test

The permeability and structural stability (integration) of the electrospun nanofibrous membranes (ENMs) are studied by water flux measurements as a dead-end operating mode.

Circular ENMs 46 mm in diameter as un- and heat treated in two arrangements of a single layer and 5 layers were used for flux measurements. The latter arrangement is later in the text (chapter 4) referred to as multi layer. It was seen as a model for cartridge filters acting under a higher feed pressure. In fact, this new system reflects the performance of the PES ENM at harsher conditions in term of higher mechanical stresses. A custom-built dead-end filtration set-up was designed for permeability also retention measurements which is shown in figure 3.6. The dried membrane was placed in the membrane cell and the water in the reservoir (500 ml distilled water) was circulated by a pump through the membrane cell. The flux measurements were performed at special time intervals including 0, 1, 3, 5, 7 and 24 hours. At the time intervals also the pressure difference (ΔP) between up and down stream side of the membrane was recorded. To measure the water flux the time needed to permeate 200 ml water through the membranes was recorded and the flux was calculated by equation 3.1:

$$J = \frac{Q}{A.\Delta t} \qquad \text{Eq. 3.1}$$

where J is the permeation flux (l/m^2.h), Q is the permeated volume (l) of water, A is the effective area of the membranes (m^2), and Δt is the sampling time (h). The flux measurement tests were repeated three times.

To see the effect of addition of inorganic nanoparticles such as zirconia and titania (mechanical reinforcement) on permeability of PES electrospun nanofibrous membranes water flux measurement was done using another set-up shown in figure 3.7. The time of permeation of 300 ml water through the membranes with the effective area of 2 cm^2 was recorded and according to equation 3.1 was converted to the flux. The possibility of applying a higher primary feed pressure is the main difference of this new set-up with the previous one, while long term water flux measurement is not feasible with this new set-up.

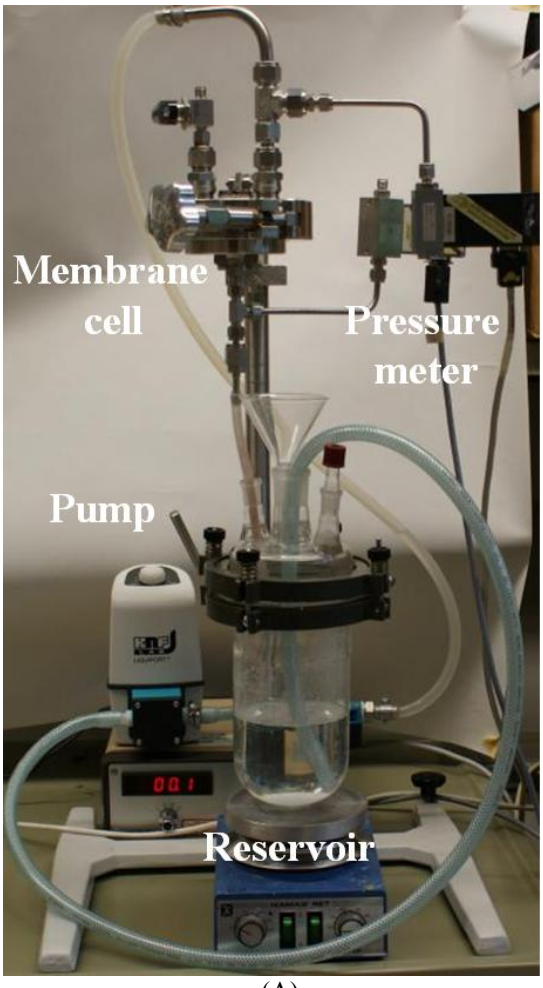

(A)

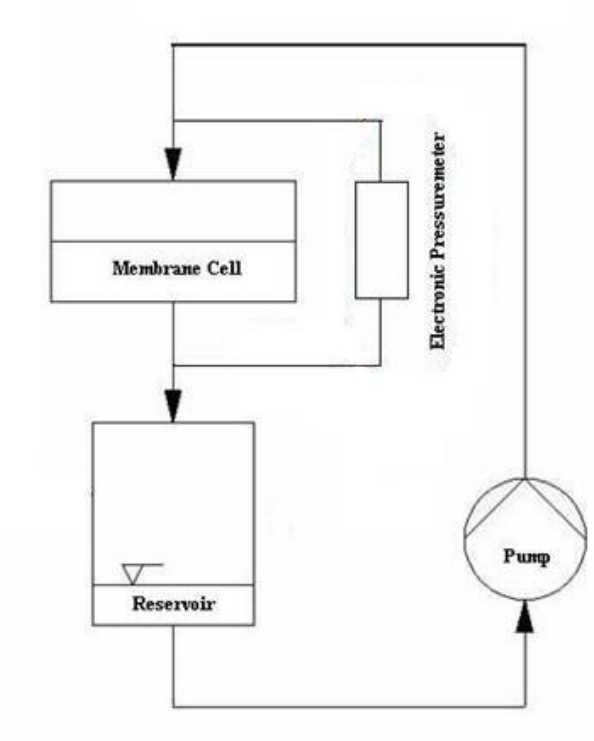

(B)

Figure 3.6: Permeation set-up used for flux and retention tests

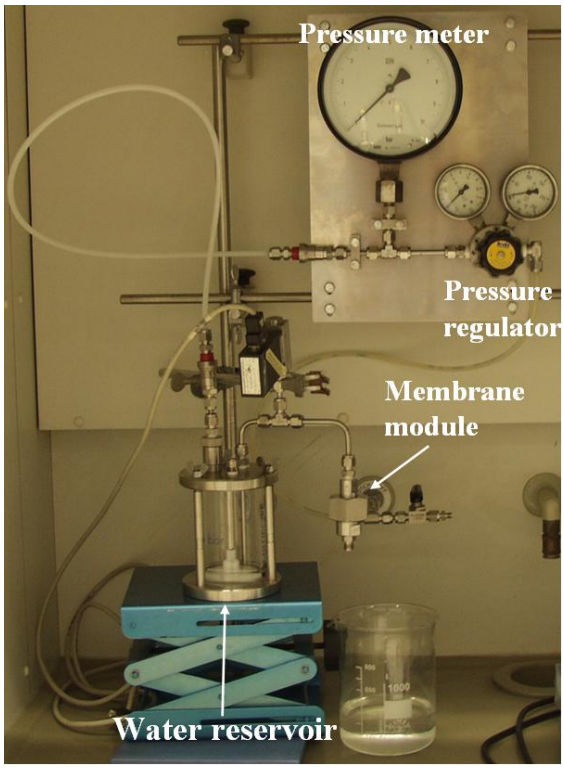

Figure 3.7: Permeation set-up with controllable applied feed pressure

3.3.1.2 Retention test with particle suspension

The retention capability of the PES/PET ENMs was determined using Polystyrene suspensions in two ranges of particle size (micron and sub-micron).

3.3.1.2.1 Preparation of the particle suspensions

As feed system for the retention tests, aqueous suspensions containing Polystyrene (PS) particles were prepared via nano-precipitation technique.[8]

The nanoprecipitation is in fact a preparation method of polymer colloids based on a phase separation process. Addition of a rather diluted polymer solution to a non-solvent for the polymer leads to a phase separation thereby spontaneously formation of the polymer particles. In the next step, the polymer solvent is separated from the obtained colloidal dispersion through heating and subsequent evaporation. To facilitate the process, usually a water-miscible solvent (such as acetone, tetrahydrofuran, etc.) is used for the phase separation.[9]

Two types of suspensions were prepared containing particles with an average particle size below and above 1 μm, respectively. For the preparation of the

nanoparticles a technical approach patented by Ebert et al. [10] was used. Polystyrene (Mw=100k) (Avocado Research Chemicals Ltd., UK) (0.1 wt%) was dissolved in tetrahydrofuran (THF) (Merck, Germany) and as the surfactant solution, Pluronic F-68 (2.5 g/l) (Sigma, USA) was dissolved in water. By mixing the two solutions PS particles precipitate in water and the surfactant inhibits growth and agglomeration of the particles. THF is removed from the suspension in a rotational evaporator (rotavapor BÜCHI 461, Switzerland). The average size of the particles in the suspensions was varied by variation of the evaporation times. Schematic of the preparation process of the PS nanoparticles is shown in figure 3.8.

The particle size distribution was determined by using a particle size analyzer (Delsa C ™ Nano particle size analyzer, Beckman Coulter, USA). The principle of this technique will be elaborated later in this chapter.

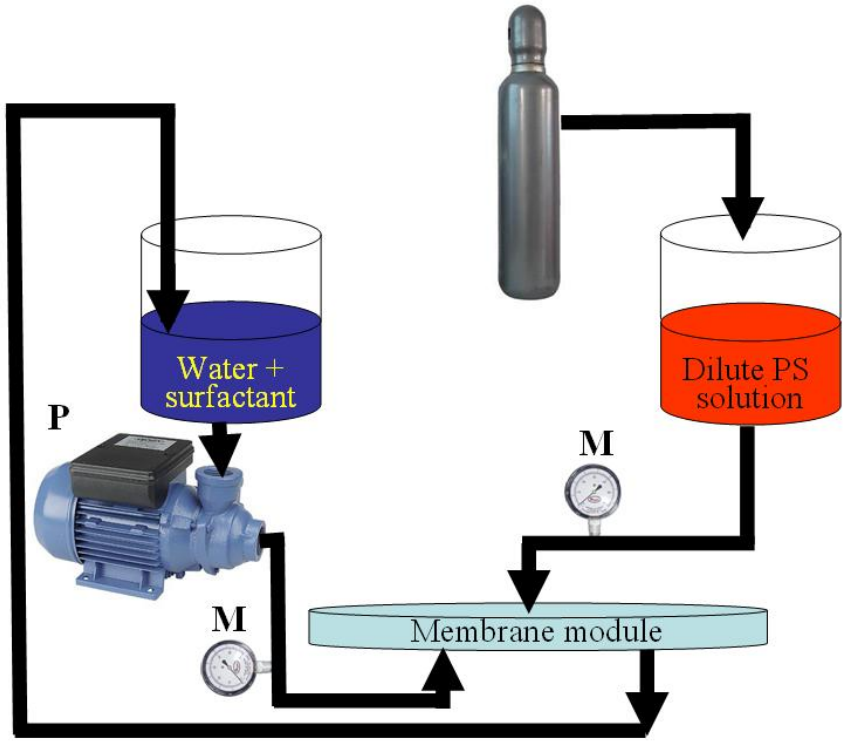

Figure 3.8: Experimental set-up used for the preparation of nanoparticles. M: manometer; P: pump

3.3.1.2.2 Retention test

The potential of the electrospun nanofibrous membranes in particulate removal as a water pre-treatment step is evaluated through a retention test using a Polystyrene (PS) model suspension.

The retention performance of the electrospun nanofibrou membranes is determined at different time intervals (0, 1, 3, 5, 7 and 24 hours). The reservoir of the custom-built set-up shown in figure 3.6 was filled with 500 ml PS suspension (0.35 g/l) as the feed in a dead-end operating mode. At the mentioned intervals, 100 ml permeate is taken to be analyzed by the particle size analyzer (PCS). As a measure for the retention ability the d90 is chosen. The d90 is the value of the particle size distribution representing the 90 % of the particles which may pass the membrane according to their particle size. Besides, the time required for permeation also the pressure difference (ΔP) are recorded. The retention test was repeated three times using new PS suspensions with similar d90s (below and above 1 μm).

3.3.1.3 Capillary flow porometry (Bubble point test)

Capillary flow porometry is used for measuring the pore size distribution of electrospun nanofibrous membranes based on a liquid extrusion method. Primarily, all pores should be completely wetted with a special liquid, which is then as shown in figure 3.9 forced out of the pores by an inert gas. The energy required for replacement of liquid with gas is equal to the surface free energy when the sample–liquid interface is converted to the sample–gas interface (equation 3.2):

$$pdV = (\gamma_{s/g} - \gamma_{s/l})dS \qquad \text{Eq. 3.2}$$

where p is the pressure applied; dV is the displaced volume of liquid by gas; $\gamma_{s/g}$ and $\gamma_{s/l}$ are the surface free energies of solid–gas and solid–liquid; dS is the increase of solid–gas surface area. In case of combination of equation 3.2 with the Young's equation (equation 3.3), and by replacing the pore cross-section area with the equal area circle, the final working equation (equation 3.4) would be as:

$$\gamma_{s/g} - \gamma_{s/l} = \gamma_{l/g} Cos\theta \qquad \text{Eq. 3.3}$$

$$p = \frac{4\gamma_{l/g} Cos\theta}{d} \qquad \text{Eq. 3.4}$$

where $\gamma_{l/g}$ is the liquid surface tension; d is the pore diameter and θ the wetting angle.[11,12]

The smaller the pore size, the higher capillary attraction will be, hence a higher pressure is required for opening up. The largest pore is opened up by gas at a point called "bubble point". Besides, the mean flow pore diameter is the pore diameter at which 50% of flow passes through the pores larger and the rest through the pores smaller than it.[13]

3.3.1.3.1 Pore size measurement of PES electrospun nanofibrous membranes

Average pore size of the electrospun nanofibrous membranes was measured using an automated capillary flow porometer from Porous Materials Inc.(PMI,USA). The stamps of the PES/PET nanofibrous membranes were immersed in the wetting fluid Porewick® from PMI (surface tension = 16×10^{-5} J/cm=16 dyn/cm) for 10 min and then transferred to the test cell (effective area ~ 4.9 cm^2). Through an automated procedure and using nitrogen as pressurizing gas, a gradually rising pressure is applied across the nanofibrous membranes. When the applied N_2 pressure exceeds the capillary attraction of the liquid in the pores, gas will pass through the sample. At each pressure the corresponding bubble (gas) flow rate is measured. The relationship between the pore size and the corresponding pressure is given by the equation 3.4.

The measurements were repeated three times using new samples. Sample to sample mass variation was less than 10%.

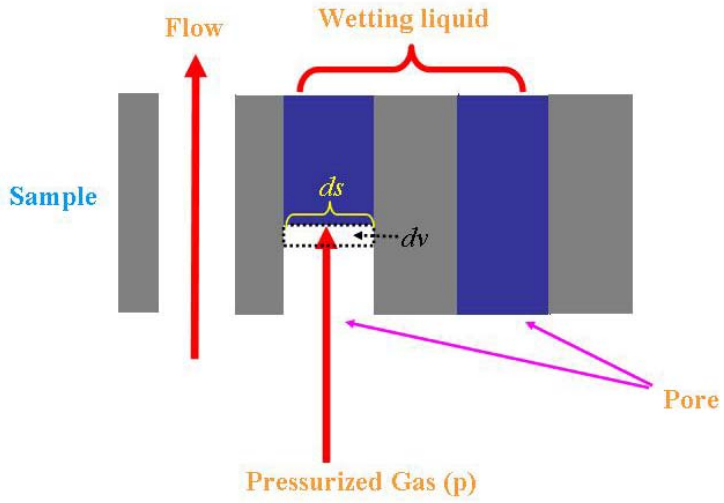

Figure 3.9: Principle of flow porometry [12]

3.3.2 Morphological properties

3.3.2.1 Scanning Electron Microscopy (SEM)

Scanning electron microscopy is a useful instrument for imaging topographies of specimens at very high magnifications using electrons instead of light.

Compared to traditional optical microscopes, the scanning electron microscope possesses many advantages. For instance, the SEM has a larger depth of field (up to 100 times), permitting more of a specimen to be in focus at one time. Additionally, very high resolution of SEM allows the specimens which are very close to each other, to be detected and magnified at much higher levels (>100,000x). Utilizing electromagnets rather than lenses in the SEM facilitates a much more control in the degree of magnification. In addition to the mentioned advantages, the scanning electron microscope provides considerably clear images, giving rise to a high efficiency for various research areas.[14,15]

While SEM inspection, a spot volume of the specimen is electron bombarded by an electron beam produced at the top of the microscope by an electron gun which is a thermal emission source, such as a heated tungsten filament or a field emission cathode. Depending on the inspection purpose, the incident electrons' energy varies from as low as 100 eV to as high as 30 keV. As shown in figure 3.10 A, the electron beam travels vertically (top to bottom) through the microscope and under vacuum. The electromagnetic fields and lenses present on the SEM column focus the beam down toward the sample. Finally, the scanning coils located near to the end of the column are responsible for positioning and directing the focused electron beam onto the sample surface. To image topography, the electron beam is scanned in a raster pattern over the surface.[14]

As seen in figure 3.10 B, the bombarding electrons, also known as primary electrons, force out the electrons of the specimen due to elastic and inelastic scattering events occurring at the surface and near-surface of the sample. The high-energy electrons dislodged by an elastic collision of an incident electron with a sample atom's nucleus are called backscattered electrons. This kind of electrons are as energetic as the incident electrons and in number are a function of the specimen's atomic number. Hence, the backscattered electron imaging could be useful in distinguishing one material from another with atomic number difference of at least 3.[14,16]

The low energy (50 eV or less) electrons emitted by the inelastic scattering of incident electrons are called secondary electrons. In fact, secondary electrons are either those incident electrons that after collisions with the nucleus lose their energy significantly or those loosely bound electrons that eject from the sample atoms. A positively biased grid or detector collects the secondary electrons and subsequently translates them into a signal. Sweeping the electron beam across the area to be inspected results in production of many such signals which are subsequently amplified, analyzed, and translated into images of the evaluated topography.[16]

As seen in figure 3.10 A, generally two types of electron detector are utilized for SEM imaging: 1) Scintillator type detectors (for secondary and backscattered electron imaging) which are positively charged to attract electrons thereby improve signal to noise ratio and 2) solid-state detectors only for backscattered electrons.[14]

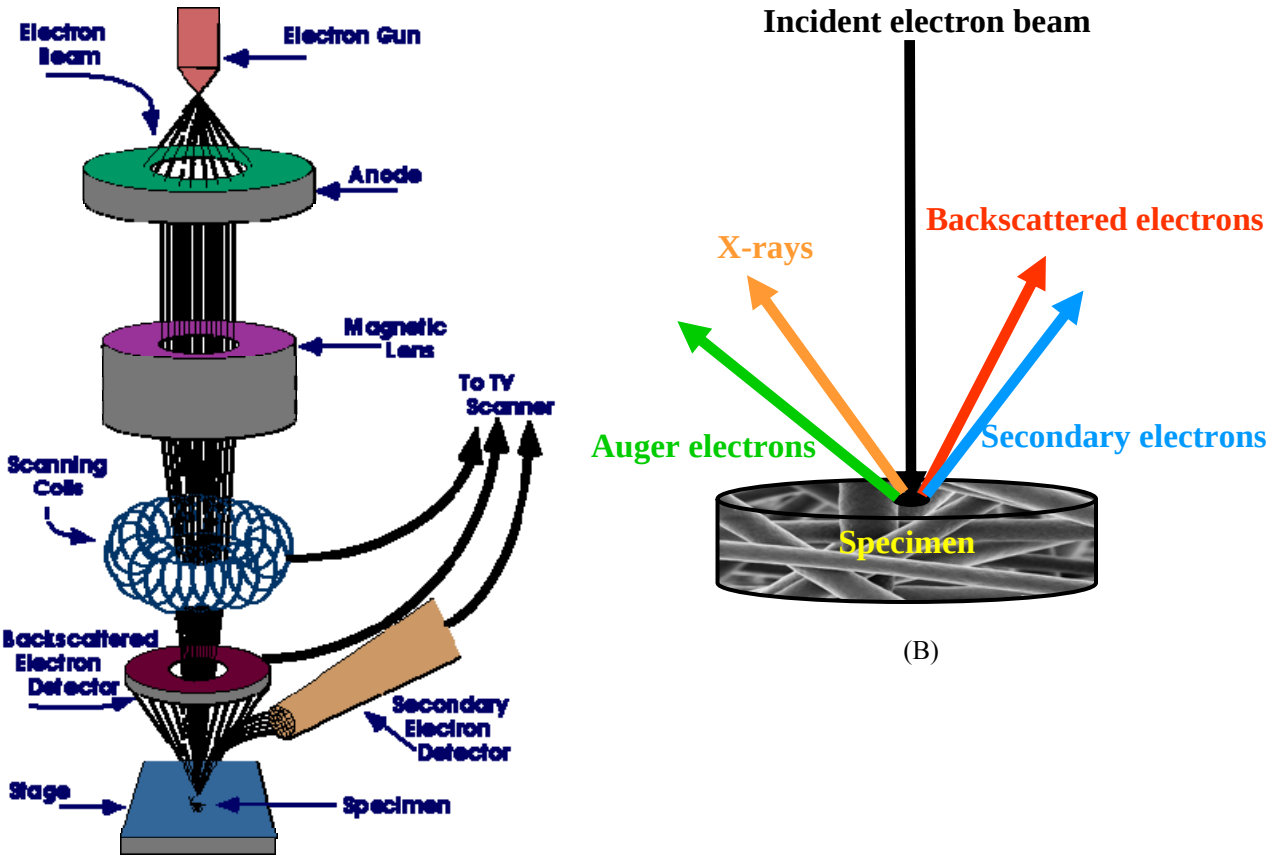

Figure 3.10: A) Schematic of the SEM and B) electron beam-specimen interaction [14]

As illustrated in figure 3.10 B, other sorts of signals produced by the interaction of the primary electron beam with the specimen are characteristic X-rays and auger electrons. When an incident electron dislodges an electron from an inner atomic shell, a vacancy is formed in that electron shell. The vacancy could be filled by an electron from an outer shell to balance the atomic orbitals following an ionization event. During this process, the filling electron loses energy as X-rays. The released characteristic X-rays are usually utilized for energy dispersive X-ray analysis.

Auger electrons are released when an outer shell electron replaces an inner shell electron already dislodged by a primary or backscattered electron and fills the respective vacancy. This replacement is accompanied with release of excess energy which could be carried away by an Auger electron. Owing to the equality of the energy of Auger electrons with the energy difference between the two shells, similar to X-rays an Auger electron can represent the type of element from which it was released and its respective shell energy. Auger Electron Spectroscopy (AES) for analysis of surface chemistry is based on discriminating between Auger electrons of various energies. Auger electrons due to their low energy level can be emitted only from near the surface. Possessing an escape depth of 0.5 to 2 nm, these electrons show a good potential spatial resolution close to that of the primary beam diameter.[17]

3.3.2.1.1 SEM on PES electrospun nanofibrous membranes

In the current PhD study, the morphology of the PES electrospun nanofibers as neat and as doped with inorganic nanoparticles was analyzed with a scanning electron microscope (SEM) (LEO 1550VP Gemini from Carl ZEISS) after a gold coating. Additionally, the diameter of the electrospun nanofibers and approximate particle size of the inorganic nanoparticles were determined from the SEM images using the Adobe Acrobat v.07 software.

3.3.2.2 Transmission Electron Microscopy (TEM)

Through Transmission Electron Microscopy (TEM) technique, different features of a sample including the morphology, crystallographic structure and even composition can be analyzed. Compared to SEM, TEM using electron beam energies of 60 to 350 keV, provides a much higher spatial resolution and possibility of easier analysis of features at atomic scale (as small as a few nanometers).

The other main difference between SEM and TEM reverts to their operation principle. While in SEM, imaging is based on dislodged or reflected electrons from the specimen, in TEM the electrons transmitted through the specimen are collected and used for imaging. Similar to SEM, in TEM the primary electron beam is made by an electron gun. The electron beam is then focused by lenses and apertures giving rise to a very thin, coherent beam controllable to strike the specimen. TEM image forms on the basis of collection and processing of the transmitted portion of the beam to the other side of the specimen.[16] The schematic of TEM instrument is shown in figure 3.11.

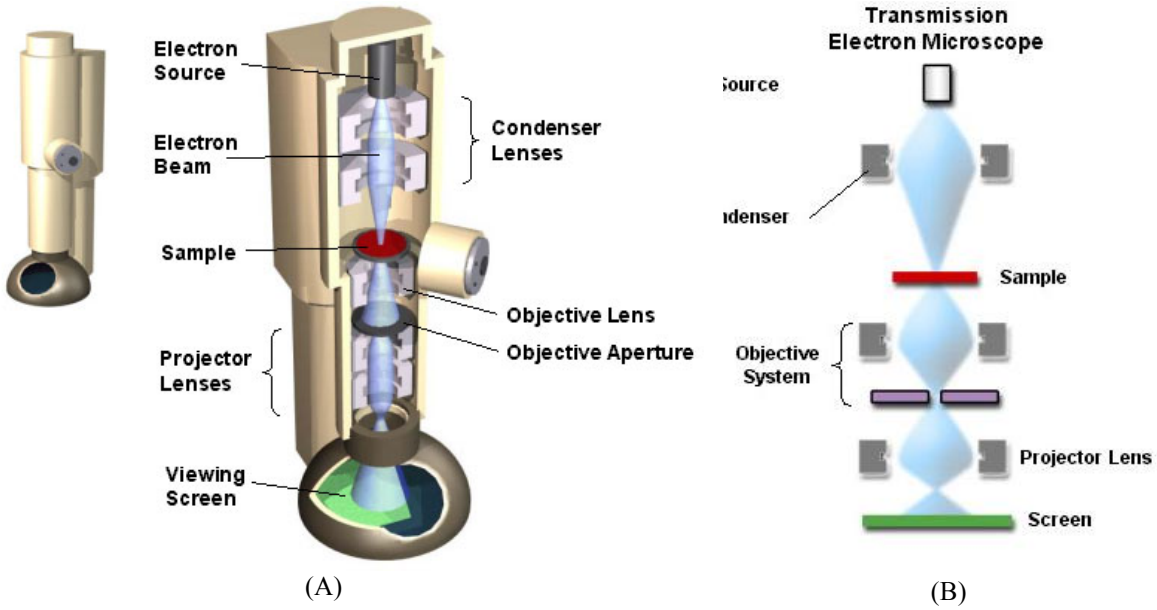

Figure 3.11: Schematic of TEM [18]

Considering the short mean free path of an electron in a solid, for an effcicient transmission, the samples to be studied by TEM analysis should be as thin as <300 nm. The exact thickness of the sample is determined according to the parameters such as

sample density and the electron accelerating voltage (variable from 100 to 300 kV). ‘‘Parallel beam’’ operation mode is infact the most conventional operation mode of TEMs. In such a mode, a defocused electron beam several microns wide is utilized to strike and pass through the sample. The defocused beam is replaced with a scanned focused beam less than 10 nm wide in a more advanced operation mode called scanned beam mode used in new TEMs. In this mode, the focused beam is scanned over the desired area in a similar way to other scanning microscopes. One very intersting feature of most TEMs is their ability to resolve details of <0.5 nm such as lattice fringes and rows of atoms on almost every kind of specimen. TEMs may also be equipped with a diverse range of supplementary techniques such as EDS, selected area electron diffraction (SAED) and electron energy loss spectroscopy (EELS). The EDS provides elemental information from X-rays. EELS is based on measurement of the loss in kinetic energy of an ejected electron from the sample. Accordingly, EELS is able to determine the elemental concentration and even the valance state of the parent atom. SAED is another technique which can represent crystallographic information according to diffraction patterns.[19]

3.3.2.2.1 TEM on PES electrospun nanofibrous membranes

In the current PhD study, the presence, morphology, distribution mode and approximate particle size of the inorganic nanoparticles incorporated into the PES electrospun nanofibers were investigated through transmission electron microscopy (TEM) (Tecnai G2 F20 field emission at an acceleration voltage of 200kV).

3.3.3 Mechanical properties

3.3.3.1 Nanoindentation

Indentation tests are probably the most common technique for mechanical testing of materials. This test is accomplished via pressing a hard tip, normally a diamond, into the sample with a given load. After removal of the load the area of the residual indentation is measured. The ratio of the maximum applied load to the residual indentation area represents the hardness of the sample.[20]

In such a test, in case of using a very sharp tip, the contact area between the sample and the tip thereby the volume of material being tested will be very small. This reality was the origin of the nanoindentation idea. In fact, creation of such small indentation hardly visible without a powerful microscope is not a challenge.[20] However, determining the indentation area can be problematic. Hence, depth sensing indentation methods were developed to circumvent this problem. In this method, benefiting high resolution sensors and actuators the load and displacement of the indenter are recorded during the indentation process and these data are analyzed to obtain the contact area, and thereby mechanical properties such as hardness and elastic modulus, without having to see the indentations.[20, 21] Schematically a nanoindentation set-up is shown in figure 3.12.

For nanoindentation, depending on the objective of characterization, different kinds of indenter or probes are utilized [22]:

• Three-sided pyramidal probes (see figure 3.13 A)

• Cono-spherical probes (see figure 3.13 B)

• Specialty probes (see figure 3.13 C)

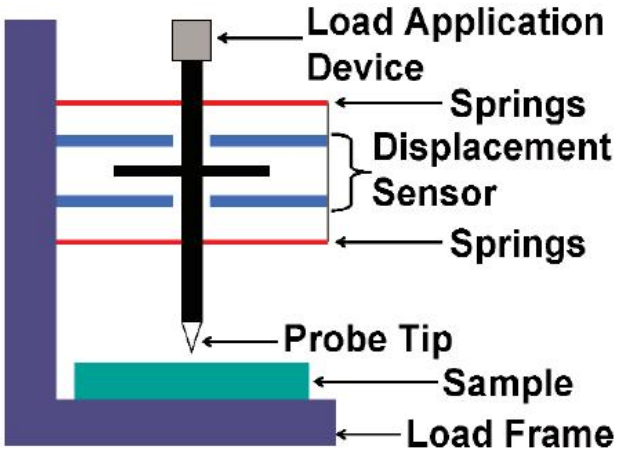

Figure 3.12: Schematic of a nanoindentation set-up [23]

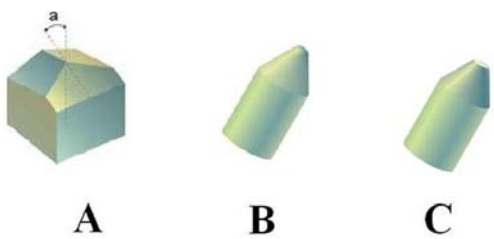

Figure 3.13: Schematic of the nanoindentation probes A) Three-sided pyramidal probes B) Cono-spherical probes C) Flat ended probes [22]

The standard three-sided pyramidal probe is the Berkovich probe. The most important structural features of the Berkovich probe are: a total included angle (plane to edge) of 142.3°, an aspect ratio of 1:8 and an average radius of curvature of about 150 nm. This probe is usually used for bulk materials, hard polymers and thin films thicker than 100 nm.[22]

Cono-Spherical probes are conical shaped probes with a spherical end. Because of their exclusive geometry, attaining the small radius of curvature similar to that obtained with the Berkovich probe is very difficult. Cono-Spherical probes can be classified as two groups: Imaging and Non-Imaging cono-Spherical probes. The main differentiating property of these probes is their radius [R] which is below and above 10 μm for imaging and non-imaging cono-Spherical probes, respectively. Typically, imaging cono-spherical probes are used for nanoindentation on soft materials and nanoscratch testing and non-imaging probes for very soft polymer or biological samples. Both kind of cono-Spherical probes are available in an array of available cone angles [a] with the standards being 60°, 90° and 120°. [22]

Specialty probes such as flat ended probes are available in two different types. The first is a flat punch, which is in fact a cylindrical shaped probe with a flat end, whereas the second one is a 60 degree cone with a flat end. Since it is very difficult to align the probe perfectly parallel to the sample, such kind of probes are usually only used with very soft samples, with which it is possible to load the probe enough to get the full contact area.

In order to characterize the viscoelastic behavior, none of the tip geometries provides the most optimum solution. Pyramids, i.e. the Berkovich, are used extensively for various applications. The main reason is that the sharp geometry of such tips grants a high degree of spatial resolution and induces plasticity at a shallow depth.

Despite successful implementation of this tip geometry in characterizing viscoelastic solids by numerous researchers, others have shown that the strain imposed by the Berkovich (pyramids and cones), which because of geometric similarity is constant with depth, can exceed the small strain assumptions of linear viscoelasticity. In contrary, cono spherical probes with a spherical tip geometry can generate data consistent with the assumptions of linear viscoelasticity. Yet, to accurately manufacture small radii spheres is complicated. Additionally, due to the transient behavior, the contact area is continuously changing and this prevents

fulfilling the conditions of steady-state harmonic motion and a given contact area, as two main criteria required for experiments performed in the frequency domain. The flat punch indenter geometry is able to address all the previously mentioned difficulties. For example, the contact area can be directly measured and it is not affected by transient behavior or thermal drift. However, the flat punch is not also a perfect solution. The main drawback of such tip geometry is that the punch cannot be mounted perfectly normal to the test surface. There is always a small angle between the face of the punch and the surface of the sample which necessitates a robust means of identifying the point at which the face of the punch is in full contact with the surface of the sample.[22]

3.3.3.1.1 Nanoindentation on PES electrospun nanofibrous membranes

The possibility of evaluation of the mean pressure (hardness) of specific areas of an electrospun nanofibrous membrane with very fine spatial resolution and with minimal preparation are the advantages which have made nanoindentation as an important mechanical characterization technique used for this kind of membranes.[11]

To investigate the compressive mechanical performance of the PES electrospun nanofibrous mats, nanoindentation testing was performed. Indentation tests were conducted using a Nanoindenter XP (MTS system Co., MN, USA) with a continuous stiffness measurement (CSM) technique. A conical diamond flat punch indenter with diameter of 50 μm and angle of 60° was used for the tests.

All nanoindentation tests were performed at room temperature. The tests start as soon as achieving a thermal equilibrium state and the drift of the indenter tip decreases to below a set value (0.5 nm/s). After the first contact between the indenter tip and the specimen surface, the indentation load is gradually applied to the surface of the specimen.

The CSM technique is carried out by introduction of a small, sinusoidal varying force on top of the applied linear force driving the motion of the indenter. Subsequently, the displacement response of the indenter to the sinusoidal force at the excitation frequency (45 Hz in this study) is measured continuously versus the indentation depth.[24,25] Accordingly, the dynamic mechanical properties as a function of indentation depth are achieved.

The nanoindentation tests were carried out as follows: a displacement rate of 100 nm/s was maintained constant during the increment of load until the indenter reached 10,000 nm deep into the surface. After that, the load was kept at maximum value for 10 s to inhibit the effect of creep on the unloading behavior.[26] The indenter was then withdrawn from the surface at the unloading rate of 0.1 mN/s until 10% of the maximum load at which the probability of the relaxation of the sample and/or thermal stability of the instrument was inspected.[24] Finally, the indenter was completely removed from the material. At least 10 indents were performed on each sample and the distance between the indentations was 200 μm to avoid interaction. The collected data were processes by TestWorks 4 (MTS Systems Corporation) as the proprietary software of the nanoindentation instrument and used for construction of load-displacement curves. After all, the mechanical properties were calculated according to the Oliver and Pharr method.[25]

3.3.3.1.2 Measurement of mean pressure and elastic modulus

Figure 3.14 represents a typical load-displacement graph of the nanoindentation test. The maximum indentation load (P_{max}) and the slope of the initial portion of the unloading curve (indicating stiffness) are of the most important characteristics of the curves by which the mean pressure, $\overline{P}$, and the storage modulus, E', of the electrospun nanofibrous membranes are calculated.

The mean pressure, $\overline{P}$, is determined from the maximum indentation load, P_{max}, divided by the contact area, A (equation 3.5) [24]:

$$\overline{P} = \frac{P_{max}}{A} \qquad \text{Eq. 3.5}$$

The storage modulus (E') of the electrospun nanofibrous mats can be inferred from the initial unloading contact stiffness (S), i.e. the slope of the initial portion of the unloading curve by following the equation 3.6 [21,26,27]:

$$E' = \frac{\sqrt{\pi}}{2\beta}\frac{S}{\sqrt{A}} \qquad \text{Eq. 3.6}$$

where β is a constant that depends on the geometry of the indenter (β = 1 for a flat punch indenter).

Besides, h_{max} and h_f represent the displacements at peak load and after complete unloading, respectively.[21] The recovery index of the PES ENMs which shows the reciprocal magnitude of compaction of the electrospun membranes can be defined by equation 3.7:

$$I_r = \frac{(h_{max} - h_f)}{h_{max}} \times 100\,\% \qquad \text{Eq. 3.7}$$

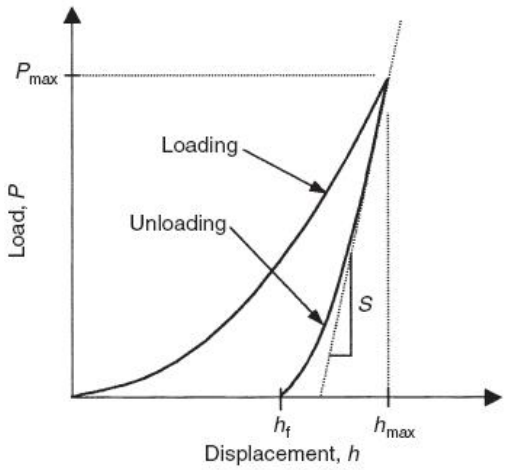

Figure 3.14: Schematic representation of indentation load-displacement data during one complete cycle [21]

The hold time at the maximum load can show the creep effect of the electrospun nanofibrous mats, that is, increase of displacement (indentation depth) at the maximum load.

3.3.3.2 Dynamic mechanical analysis (DMA)

This technique - also called as dynamic mechanical thermal analysis (DMTA)- is a very versatile, convenient, rapid and sensitive test for characterization of thermo-mechanical properties of polymers as a function of frequency, temperature or time.[28,29] The measurements can be conducted in different ways as: 1) by applying a small oscillating displacement to a sample to measure the resulting force or 2) by applying a sinusoidal load to measure the resulting deformation or 3) by applying a constant load (or a displacement) to obtain creep (or relaxation) data. The diverse material properties which can be obtained by DMA are: 1) the glass transition temperature (T_g), 2) the coefficient of thermal expansion (CTE) and 3) viscoelastic properties such as the storage (elastic) modulus, the loss (viscous) modulus and

damping. Depending on the property to be tested, various fixtures are used such as single/dual-cantilever, three point bend, tension/compression and shear sandwich. The loading mode determines the type of elastic modulus including shear, tensile or flexural modulus.[28]

As the standard mode which is shown in figure 3.15, DMA is usually performed by applying a sinusoidal force to a sample and subsequent examining the respective material's response. From the obtained response and based on the phase lag and sample recovery, properties like the tendency to flow (viscosity) and the stiffness (modulus) can be calculated. Such properties can be depicted in another way including the ability to release heat (damping) and the ability to recover from deformation (elasticity). Two main descriptions for such changes in the sample are based on the relaxation of the polymer chains and the changes in the free volume of the polymer.[29]

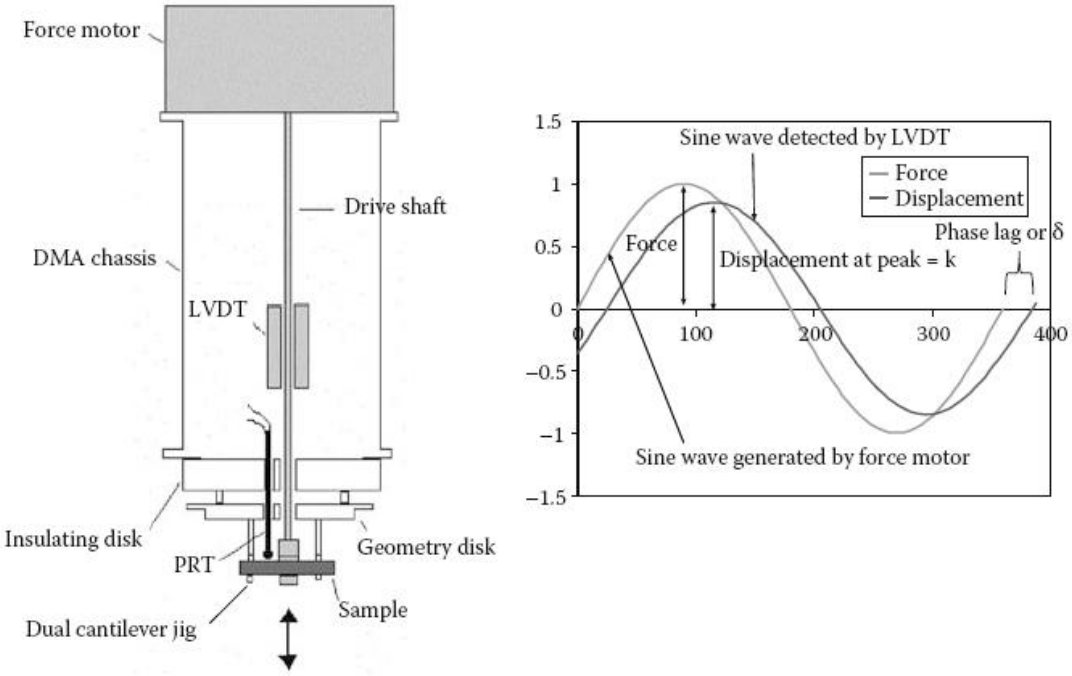

Figure 3.15: Schematic of a DMA set-up; The oscillatory force and as a result the sinusoidal stress applied by DMA generates a sinusoidal strain. The phase lage between the stress-strain sine waves and the displacement measured at the peak of the sine wave are extracted from the obtained curves and used for calculation of quantities like the modulus, the viscosity, and the damping [29]

DMA can be advantageous in terms of obtaining a modulus each time when a sinusoidal force is imposed, i.e. the possibility of tracking variations of modulus within a temperature or frequency range. Hence, if an experiment is to run at the given frequency of 1 hertz (Hz) or 1 cycle/second, in every second a modulus value can be measured. This measurements can be performed while slowly varying temperature at a rate like 5–10°C/min, that is, not obvious change of the temperature per cycle. This means that while a DMA recording the modulus versus temperature over a 200°C range takes 20–40 minutes. Similarly, with a heating rate of 2°C/min, a broad range of frequency or shear rate of e.g. 0.01 to 300 Hz can be scanned in less than 2 hours.[29]

Different with the Young's modulus of the classic stress–strain curve which is the slope of the initial linear region of the curve, in DMA, based on the response of the sample to the sine wave, a complex modulus (E*) composed of an elastic modulus (E′) and a loss modulus (E″) is calculated. Such diverse range of moduli gives a better idea about characterization of the material. Using such an approach, the ability of the material to return energy (E′), to lose energy (E″), and the damping as the ratio of these effects (tan delta) can be readily evaluated.[29]

3.3.3.2.1 DMA on PES electrospun nanofibrous membranes

The frequency and temperature-dependant elastic moduli of the PES electrospun nanofibrous mats as neat and reinforced with inorganic nanoparticles were measured using a dynamic mechanical analyser (RSA II, Rheometrics Co.) equipped with a tensile film fixture.

The electrospun nanofibrous samples were cut as 23 mm x 3.9 mm with a thickness of 130 μm.

Briefly, to characterize temperature-dependent mechanical properties, DMA test was performed at the excitation frequency of 6.28 rad/s (1Hz) and deformation amplitude of 0.5%. The temperature range studied was from 25 to 270 ◦C with a heating rate of 2 ◦C/min under air atmosphere.

Additionally, frequency-dependent mechanical properties were investigated at the ambient temperature, with a frequency sweep from 0.005 to 100 rad/s using a deformation amplitude of 0.5%.

3.3.3.3 Tensile test

This test is a destructive mechanical test and as shown in figure 3.16A is conducted by applying a gradually increasing tensile force to the sample being evaluated uniaxially along the long axis of the sample until a plastic deformation and then a rupture happens.[30]

Two ends of the specimen whose cross section is circular or rectangular are placed and secured inside the holding grips of the testing apparatus as depicted in figure 3.16 B. Then the specimen is elongated at a constant rate and the instantaneous applied load and the respective elongations are successively and simultaneously measured by a load cell and an extensometer, respectively. The obtained result are depicted by a computer as the graph of load versus elongation.

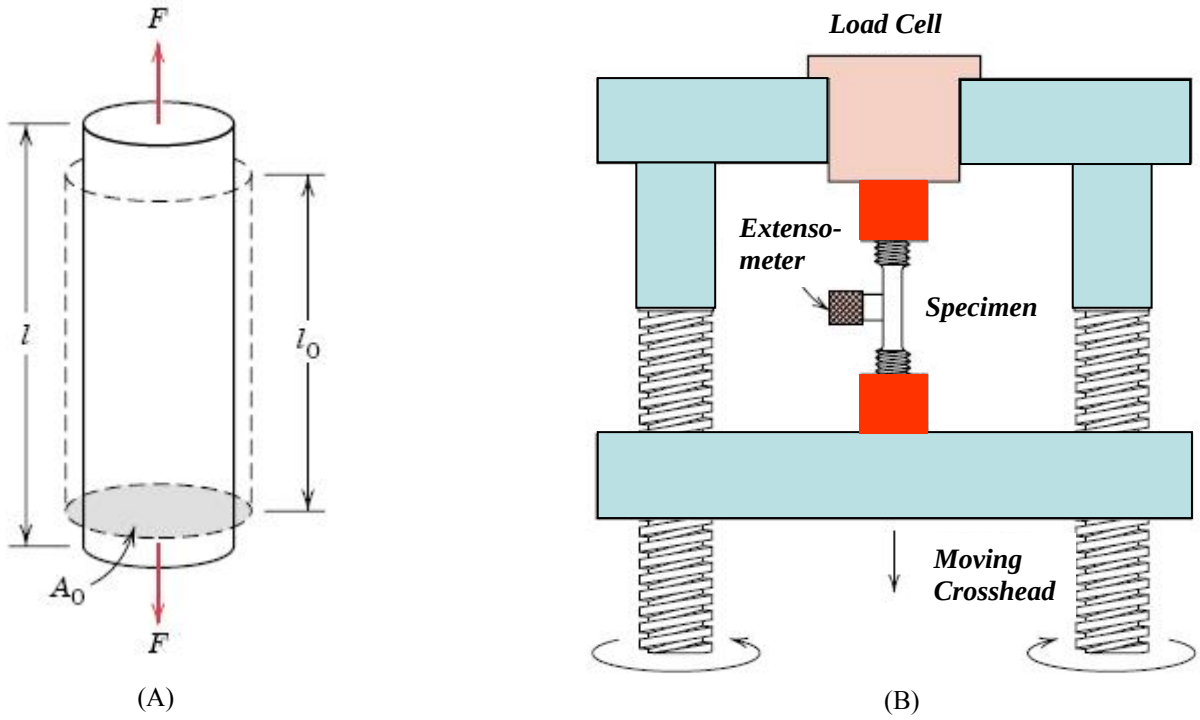

Figure 3.16: Schematic illustration of A) a tensile test ; the dashed lines represent the shape of the specimen before deformation and B) the tensile testing machine [30]

For every sample, the load–deformation characteristics are a function of its size. This means that if sample B has a double size cross section area compared to sample A, it will require twice the load to produce the same elongation. Such geometrical interventions should be removed through normalizing load and elongation

to the respective parameters of engineering stress (σ) and engineering strain (ε) which are accordingly defined as equations 3.8 and 3.9 [30]:

$$\sigma = \frac{F}{A_0} \qquad \text{Eq. 3.8}$$

where F is the load applied (N), A_0 is the initial cross sectional area (m^2) and σ is the engineering stress (MPa).

$$\varepsilon = \frac{l_i - l_0}{l_0} = \frac{\Delta l}{l_0} \qquad \text{Eq. 3.9}$$

where l_0 and l_i are the initial and instantaneous lengths when F = 0 and F_i , respectively. Engineering strain (ε) is unitless, but meters per meter are frequently used. In case of multiplying the strain value by 100, the strain can be also expressed as a percentage.

3.3.3.3.1 Tensile test on PES electrospun nanofibrous membranes

The testing process for electrospun nanofibrous mats needs to special grips, load cell and extensometer different with those used for other kind of materials and conventional samples. The load cell is a finely calibrated transducer able to record the applied load very precisely. In addition, smallest elongations are also accurately measured using a calibrated extensometer. The resultant stress vs. strain plot (obtained from load-elongation data) is used for determination of mechanical properties.

The PES nanofibrous mats as neat and reinforced with zirconia and titania nanoparticles were carefully cut into rectangular stripes with dimensions of 10 mm x 80 mm and thickness of 60-140μm. The tensile properties were characterized by a tensile machine (Zwick/Roell Z020-20KN, Germany) equipped with a 20-N load-cell at ambient temperature. The cross-head speed was 2 mm/min and the gauge length was 20 mm. The reported tensile moduli, tensile strengths and elongations represented average results of ten tests.

3.3.4 Thermal properties

3.3.4.1 Differential Scanning Calorimetry (DSC)

Differential Scanning Calorimetry (DSC) is a thermal analysis technique used to study the thermal behavior of polymers when heated. As shown in figure 3.17, in DSC, the temperature of an empty, reference sample pan and a polymer sample pan

mounted on separate heating blocks is monitored by using thermocouples. Both the samples should be in thermal equilibrium. Any thermal event occurring in the polymeric sample changes this thermal balance. The amount of energy required to keep this equilibrium gives an insight to the thermal events in progress.[31,32,33]

In fact, DSC measures a specimen's heat capacity (C_p) at constant pressure based on the temperature difference (ΔT) of the reference and polymer sample pans. Heat capacity is the amount of energy (heat) required (ΔH) to increase the temperature of the sample 1 ºC at constant pressure and can be calculated according to equation 3.10:

$$C_p = \frac{\Delta H}{\Delta T} \qquad \text{Eq. 3.10}$$

Heat capacity is usually normalized and converted to specific heat by its dividing by the number of grams of the specimen. In other words, specific heat is the heat required to increase the temperature of one gram of specimen by one degree Celsius. Thus, specific heat varies according to different polymer characteristics. The variations of specific heat of the polymer sample pan versus the reference one can be depicted as a plot.[31,32,33]

The polymer characteristics usually analyzed by DSC include: 1) the glass transition temperature (T_g), 2) melting temperature (T_m) and 3) crystallization temperature (T_c). In a typical DSC plot (C_p-T) e.g. that given in figure 3.18 for a semicrystalline polymer, the first temperature is shown as a discrete change in C_p but the two latter ones as a single peak.

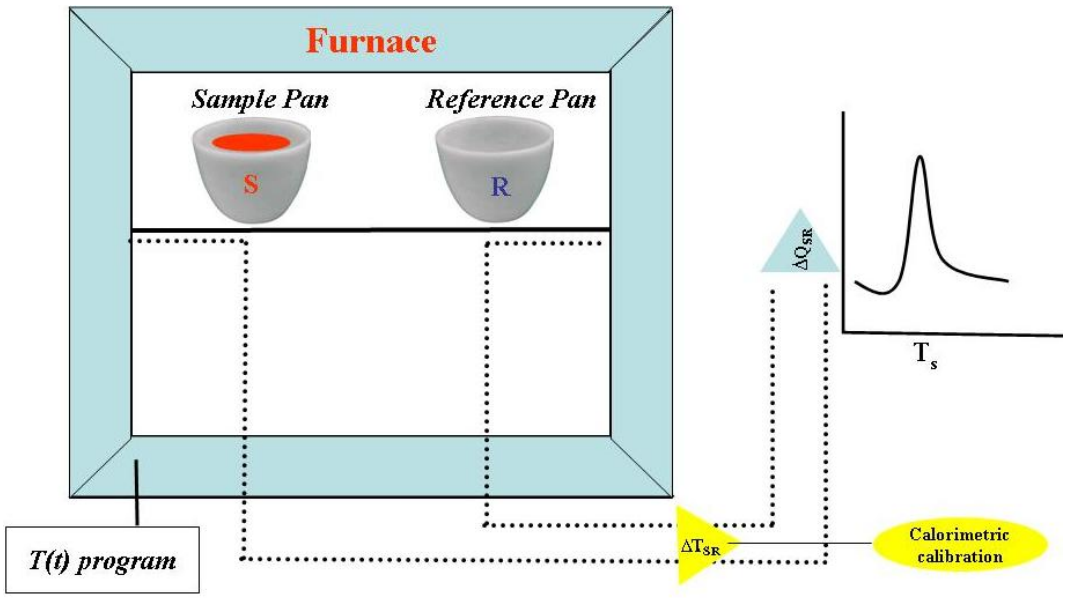

Figure 3.17: Schematic illustration of a DSC measurement [34]

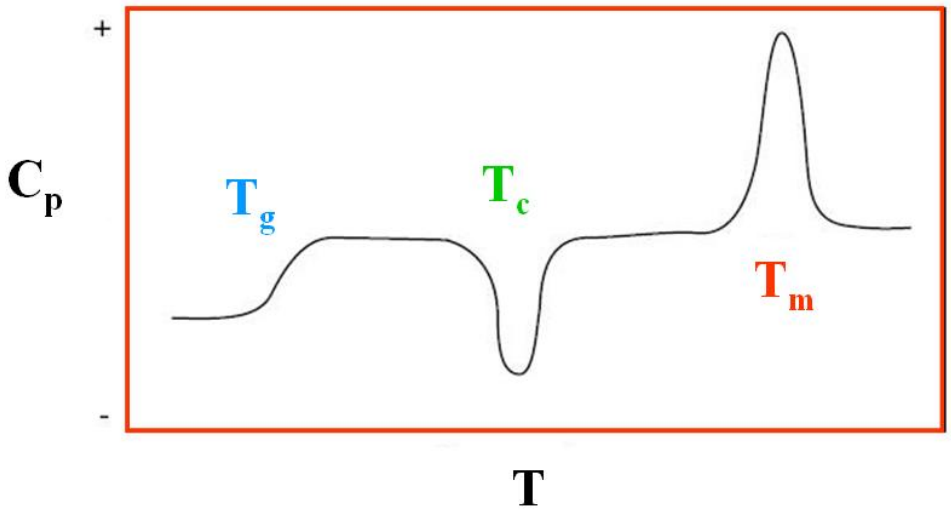

Figure 3.18: A typical DSC graph obtained while heating a semi crystalline polymer containing the low temperature second order transition of glass transition, exothermic transition of crystallization and endothermic transition of melting [33]

3.3.4.1.1 DSC on PES electrospun nanofibrous membranes

In DSC measurement (Netzsch DSC 204 Phoenix), the electrospun nanofibrous membranes were first heated to 300 °C at a speed of 10 °C/min followed by keeping the samples for 5 min under nitrogen atmosphere to remove the effect of the thermal history. Subsequently, the samples were cooled down to 100 °C and the second scan started from 100 °C to 300 °C. The glass transition temperature (T_g) was the temperature specified at the onset of the transition in the heat capacity.

3.3.4.2 Thermogravimetric analysis (TGA)

TGA analysis offers a tremendous potential for characterizing thermal stability of polymers and fibers. This technique not only provides qualitative and quantitative data for kinetics of thermal degradation thereby weight losses of the samples, but also it can characterize the effect of additives and chemical modification on fibers and textile materials and the behavior of copolymer or polymer blends.

Thermogravimetric analysis (TGA) is conducted by heating a sample to a certain temperature and then monitoring variation of its weight versus time. Weight alteration represents polymer degradation or removal of residual solvent. To monitor degradation under different conditions (e.g. an oxidative atmosphere or under dry nitrogen), the sample chamber's environment should be tunable.

The most optimum TGA experiments are performed at a given temperature and with monitoring weight variations as a function of time. Useful quantitative information about the rate of degradation at that temperature could be extracted from the results obtained. However, repetition of the experiment for several temperatures to get an idea about the practical temperature range without degradation of the polymer can be time-consuming. Hence, as shown schematically in figure 3.19, usually most TGAs are based on monitoring weight while scanning temperature.[33,34]

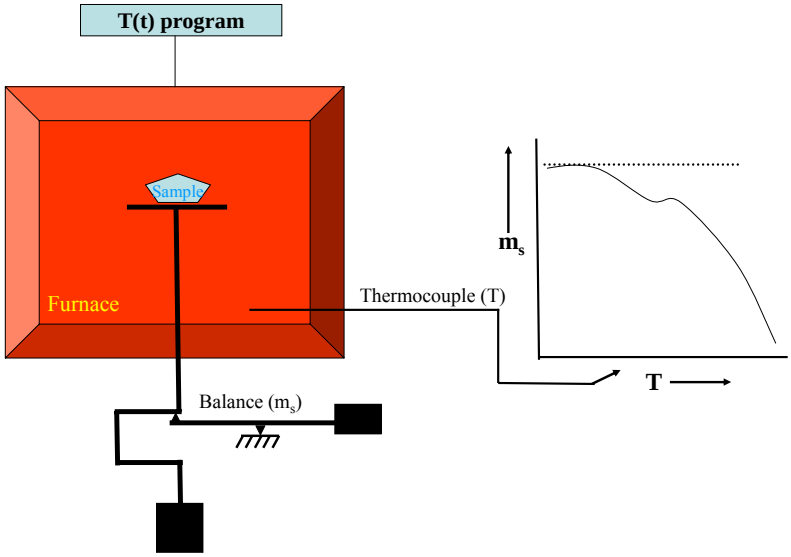

Figure 3.19: Schematic of a TGA experiment [34]

3.3.4.2.1 TGA on PES electrospun nanofibrous membranes

Thermal gravitational analysis (TGA) were used to investigate the thermal property of the ENMs. The thermal stability of the PES ENMs was evaluated by TGA using a thermogravimetric analyzer of Netzsch 209 TG. TGA analysis was performed at 25–600 ◦C with a heating rate of 10 ◦C/min under Argon. The decomposition temperature (T_d) was defined as the temperature at 5% weight loss.

3.3.5 Photon Correlation Spectroscopy (PCS)

Photon Correlation Spectroscopy (PCS) commonly referred to as dynamic light scattering (DLS) is one of the most known methods for particle size measurement. In this technique, as shown in figure 3.20, a monochromatic light beam,

such as a laser, is shined onto a solution containing tiny spherical particles in Brownian motion. When the incoming light hits the moving particle, its wavelength (and intensity) changes. This change so called "Doppler Shift" is related to the size of the particle.[35]

In such a technique, particle size distribution is measured according to the change in scattered light intensity collected over different time intervals. These data are described using an electric field correlation function (CF), for which the decay rate (Γ) is defined through equation 3.11 [35,36,37]:

$$\Gamma = q^2.D_m \qquad \text{Eq. 3.11}$$

In which D_m is the mutual diffusion coefficient and q is the scattering vector magnitude, defined as equation 3.12:

$$q = \frac{4n\pi \sin\frac{\theta}{2}}{\lambda_0} \qquad \text{Eq. 3.12}$$

where n is the refractive index of the solution, θ is the scattering angle, and λ_0 is the laser wavelength. If we assume that the particles are in Brownian motion (as a dilute solution) and possess a spherical shape with a small diameter compared to the molecular dimensions, then D_m is approximately equal to the diffusion coefficient extrapolated to infinite dilution (D_0). Accordingly, Stoke-Einsteins' Law (equation 3.13) can be used to calculate the effective hydrodynamic radius (r) of a particle:

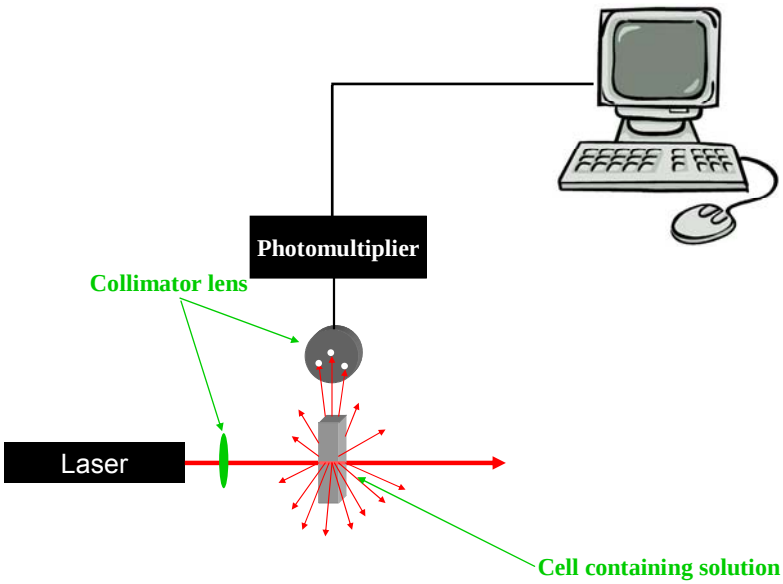

Figure 3.20: Schematic of a PCS set-up [35]

$$r = \frac{k_b T}{6\pi\mu D_0} \qquad \text{Eq. 3.13}$$

where k_b is the Boltzmann constant, T is the temperature in Kelvin degrees and η is the viscosity of the solvent.[37]

The set-up: The PCS set up, illustrated as figure 3.20, emits a laser beam passing through a collimator lens and hitting the cell containing the solution. The laser beam which has already been focused by the collimator lens, after collision to the particles present in the solution is scattered and detected by a photomultiplier that transforms a change of intensity of the laser into a change of voltage. The other collimating lens before the photomultiplier is used to get a proper amount of scattered light. After all, the signal created by the photomultiplier is quickly preamplified and transferred to the computer where the voltage is elaborated through a program in Labview.[35]

3.3.6 Attenuated total reflection Fourier transform infrared spectroscopy (ATR-FTIR)

Attenuated total reflection infrared (ATR-IR) spectroscopy is a powerful technique used for surface chemical analysis of materials. The basis of the technique is on passing IR radiation through a crystal made of a high refractive index IR transmitting material and its subsequent total reflection within the crystal. Outcome of the total internal reflection occurred is an evanescent wave extends beyond the surface of the crystal. Measurement of the changes occurring when a totally, internally reflected infrared beam hits the sample is the principle of ATR spectroscopy. Hence, the sample to be subjected to the evanescent wave should be kept in intimate physical contact with the ATR crystal. The wave after contact with the sample will be attenuated in spectral regions where the sample absorbs energy thereby a spectrum yields. As shown in figure 3.21, to maximize the interaction with the sample, the IR light is reflected several times inside the crystal.[38]

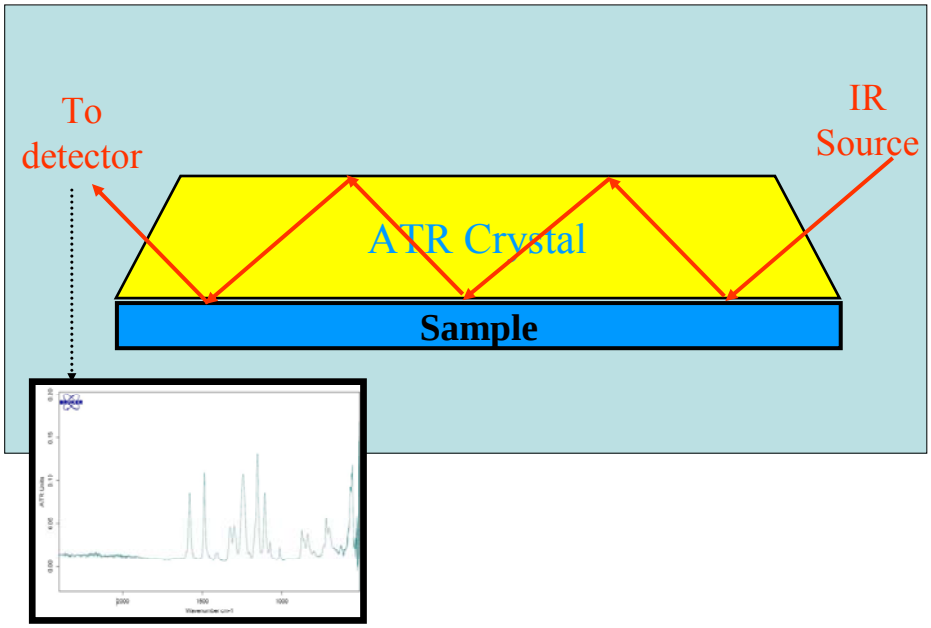

Figure 3.21: Schematic of ATR-FTIR

This technique is a vibrational spectroscopic technique in which IR radiation interacts with molecules by exciting their bond vibration modes. Consequently, a chemical functional group adsorbs IR radiation in a specific wavenumber range regardless of the structure of the rest of the molecule. The correlation of the band wave number position with the chemical structure is used to identify a functional group in a sample. [39]

Advantages such as ease of use and very little sample preparation required has led to an extensive application for ATR compared to the other available reflection methods. Through ATR technique, characterization of either thick or highly absorbing materials which are not easily analyzed by transmission spectroscopy is possible. For the bulk material or thick film, no sample preparation is required for ATR analysis. [38]

3.3.6.1 ATR-FTIR on PES electrospun nanofibrous membranes

Chemical surface analysis of the neat PES and TiO_2/PES electrospun nanofibrous membranes was performed by Fourier Transform Infra Red Spectrometry (FTIR). Attenuated total reflection Fourier transform infrared (ATR-FTIR) spectra were recorded using a Bruker Equinox55 spectrometer.

3.3.7 Water contact angle measurement

Water contact angle measurement or the sessile drop technique is a method of characterization of solid surface energies. This technique is based on measurement of the contact angle between a liquid (water) drop with known surface energy and its substrate surface. The measurement is extremely sensitive and dependent to the changes in surface physicochemical conditions associated to surface energy, polarity thereby hydrophilicity of the outermost surface of the solid. The method is performed by placing a drop of water or other liquid onto the surface to be studied followed by measuring the respective angle of contact according to the Young's equation (equation 3.3).[11,40]

One important prerequisite of contact angle method is smoothness of the surface being evaluated. In contrast, an electrospun nanofibrous membrane due to its high porosity has a surface of nano or micro-scale roughness preventing a full contact between liquid drops and the surface. Hence, in such a case contact angle measurements are with some errors and not able to show the degree of hydrophilicity of the polymer accurately.[11]

Several contact angle models have been proposed for correlation of contact angle of rough surfaces to the normal smooth ones, of which the best known is the Cassie's model. In. the Cassie's model, the assumption is that when measuring contact angle on a highly rough surface such as a hydrophobic electrospun nanofibrous membrane, the liquid drop is mounted on a composite surface consisting of the polymer fibers and air pockets (see figure 3.22). This situation can be described by the following equation (equation 3.14):

$$\cos\theta_a = f_1 \cos\theta_1 - f_2 \qquad \text{Eq. 3.14}$$

where f_1 is the fraction of the surface in contact with liquid; f_2 is the fraction without any contact with the surface. This model has been shown to possess a very good applicablility for superhydrophobic and hydrophobic surfaces such as hydrophobic non-woven polymer materials.[11]

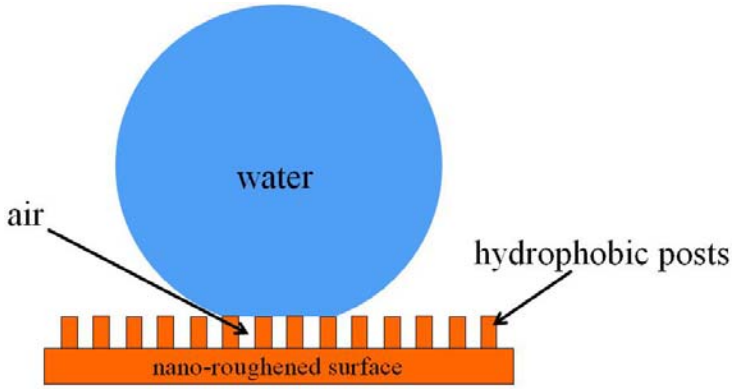

Figure 3.22: Simple schematic of the Cassie's model

3.3.7.1 Water contact angle measurement of PES electrospun nanofibrous membranes

The static water contact angle of the neat PES, ZrO_2/PES and TiO_2/PES electrospun nanofibrous membranes was measured using a contact angle analysis system (Kruess DSA 100, Germany). A 0.5µl droplet was dispensed on the membrane and the resultant angle measured.

3.3.8 X-ray diffraction analysis (XRD)

X-ray diffraction analysis (XRD) is a rapid analytical technique which is usually benefited for phase characterization of crystalline materials. The basis of the method is on constructive interference of monochromatic X-rays and a crystalline sample. The sequences of production of such monochromatic X-rays include: 1)X-Ray production by a cathode ray tube, 2) filtering to get monochromatic radiation, 3) collimation to concentrate and finally direction toward the specimen.[41] As shown in figure 3.23, the X-ray waves interact with the sample giving rise to a constructive interference and a diffracted ray when conditions satisfy Bragg's Law (equation 3.15) [42]:

$$n\lambda = 2d \sin\theta \qquad \text{Eq. 3.15}$$

where n is an integer number representing the order of the diffraction peak; λ is the wavelength (Å); d is interatomic spacing (Å) and θ is the diffraction angle (^{o}).

According to this law, the wavelength of X-ray radiation is associated to the diffraction angle and the lattice spacing. Typically, the sample (especially powdered samples with diverse orientation) is scanned through a range of 2θ angles and all

possible diffraction directions (correlated to diffraction peaks) of the lattice is obtained. Since every crystalline material has its own proprietary set of d-spacings, through conversion of the diffraction peaks to d-spacings and subsequent comparison of d-spacings with standard reference patterns, the mineral is identified.[41]

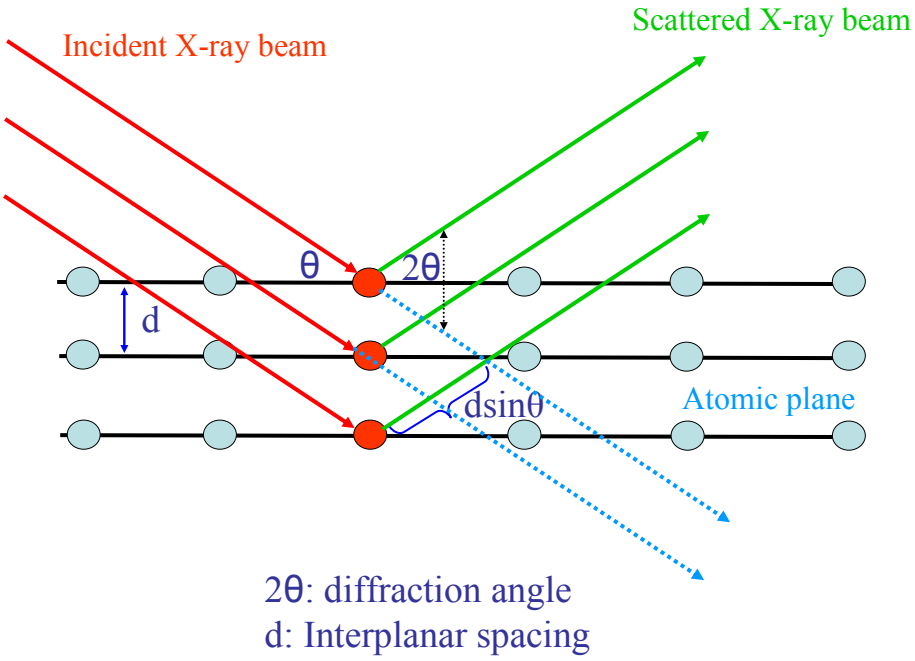

Figure 3.23: Schematic of the basis of XRD according to the Bragg's law

3.3.8.1 XRD analysis on titania nanoparticle containing PES electrospun nanofibrous membranes

Structural analyses of the neat PES and TiO_2/PES ENMs (5 wt%) were carried out at room temperature using a X-ray diffractometer (Bruker D5000) with Cu- Kα radiation. The composite ENMs also were heated up to 500 °C in air atmosphere for pyrolysis of the polymeric matrix and investigation of the structural properties of the TiO_2 nanoparticles.

3.4 References

[1] P. Viswanathamurthi, N. Bhattarai, H.Y. Kim, D.R. Lee, S.R. Kim, M.A. Morris, Preparation and morphology of niobium oxide fibres by electrospinning, Chemical Physics Letters 374 (2003) 79–84.

[2] O. Carp, C.L. Huisman, A. Reller, Photoinduced reactivity of titanium dioxide, Progress in Solid State Chemistry 32 (2004) 33–177.

[3] Dan Li and Younan Xia, Fabrication of Titania Nanofibers by Electrospinning, Nano Lett., 3(4)(2003) 555-560.

[4] Xiangfu Meng, Nan Luo, Shengli Cao, Shimin Zhang, Mingshu Yang, Xiao Hu, In-situ growth of titania nanoparticles in electrospun polymer nanofibers at low temperature, Materials Letters 63 (2009) 1401–1403.

[5] Xiaobo Chen and Samuel S. Mao, Titanium Dioxide Nanomaterials: Synthesis, Properties, Modifications, and Applications,Chem. Rev. 107(2007) 2891-2959.

[6] Y Li, T.J White, S.H Lim. Low-temperature synthesis and microstructural control of titania nano-particles. J. Solid State Chem. 177(2004) 1372-1381.

[7] Naofumi Uekawa, Jyunichi Kajiwara, Kazuyuki Kakegawa, Yoshinori Sasaki. Low Temperature Synthesis and Characterization of Porous Anatase TiO_2 Nanoparticles. J. Colloid Interface Sci. 250(2002) 285-290.

[8] H. Fessi, F. Puisiex, J. P. Devissaguet, J. P. Ammoury and S. Betina, Nanocapsule formation by interfacial polymer deposition following solvent displacement, Int. J. Pharm., 55 (1989) R1-R4.

[9] GG. Yordanov, CD Dushkin, Preparation of poly(butylcyanoacrylate) drug carriers by nanoprecipitation using a pre-synthesized polymer and different colloidal stabilizers, Colloid and Polymer science 288(9)(2010) 1019-1026.

[10] K.Ebert, B.Maltzahn, R.Just, Verfahren zur Herstellung von Nanopartikeln unter Verwendung poröser Membranen. Deutsches Patent DE 10 2005 025 057

[11] David R. Nisbet, Andrew E. Rodda, David I. Finkelstein, Malcolm K. Horne, John S. Forsythe,Wei Shen, Surface and bulk characterisation of electrospun membranes: Problems and improvements, Colloids and Surfaces B: Biointerfaces 71 (2009) 1–12.

[12] Porous Materials, Inc website: www.pmiapp.com

[13] R. Gopal, S. Kaur, C.Y. Feng, C. Chan, S. Ramakrishna, S. Tabe, T.Matsuura, Electrospun nanofibrous polysulfone membranes as pre-filers:particulate removal, J. Membrane Sci. 289 (2007) 210–219.

[14] http://mee-inc.com/sem.html

[15] www.purdue.edu/rem/rs/sem.htm

[16] http://www.siliconfareast.com/SEMTEM.htm

[17] Mady Elbahri, Unconventional nanomanufacturing on a substrate, CAU Kiel, January 2007, PhD Dissertation.

[18] barrett-group.mcgill.ca

[19] Raymond Eller Kirk, Donald Frederick Othmer, Kirk-Othmer encyclopedia of chemical technology John Wiley & Sons, 1996

[20] http://www.nanoindentation.cornell.edu/

[21] G.M. Pharr, Measurement of mechanical properties by ultra-low load indentation, Materials Science and Engineering A253 (1998) 151–159.

[22] http://www.hysitron.com

[23] MR. Van Landingham, Review of instrumented indentation, J. Res. Natl. Inst. Stand. Technol. 108 (2003) 249-265.

[24] Xiaodong Li, Bharat Bhushan, A review of nanoindentation continuous stiffness measurement technique and its applications, Materials Characterization 48 (2002) 11 – 36.

[25] W.C. Oliver, G.M. Pharr, An improved technique for determining hardness and elastic modulus using load and displacement sensing indentation experiments, J. Mater. Res. 7 (1992) 1564.

[26] B J Briscoey, L Fiori and E Pelillo,Nanoindentation of polymeric surfaces, J. Phys. D: Appl. Phys. 31 (1998) 2395–2405.

[27] G.M.Odegard, T.S. Gates, H.M. Herring, Characterization of viscoelastic properties of polymeric materials through nanoindentation, Experimental mechanics 45(2)(2005)130-136.

[28] Shiqiang Deng, Meng Hou, Lin Ye, Temperature-dependent elastic moduli of epoxies measured by DMA and their correlations to mechanical testing data, Polymer Testing 26 (2007) 803–813.

[29] Kevin P. Menard, Dynamic mechanical analysis; a practical introduction, 2nd edition, CRC Press, 2008.

[30] William D. Callister, Fundamentals of Materials Science and Engineering, John Wiley&Sons, 2001.

[31] Rodriguez, F., C. Choen, C. K. Ober, and L. A. Archer, Principles of Polymer Systems. 5th ed. 2003, New York, NY: Taylor & Francis Books, Inc. 760.

[32] Erin Lynn Camponeschi, Dispersion and alignment of carbon nanotubes in polymer based composites, Georgia Institute of Technology, December 2007, PhD Dissertation.

[33] J. Nairn, Polymer Characterization, MSE 5473 Class Notes, University of Utah (2005).

[34] Michael E.Brown, Handbook of thermal analysis and calorimetry, vol.1, 2nd edition, Elsevier science, 1998.

[35]M. Sartor, Dynamic light scattering;
http://www.physics.ucsd.edu/neurophysics/courses/physics_173_273/dynamic_light_scattering_03.pdf

[36] Y Harada and T Asakura, Dynamics and dynamic light-scattering properties of Brownian particles under laser radiation pressure, Pure Appl. Opt. 7 (1998) 1001–1012.

[37] Delsa Nano Submicron Particle Size and Zeta Potential, Particle Analyzer, User's manual, Beckman Coulter.

[38] https://scholarbank.nus.edu.sg/bitstream/handle/10635/14901/06chp2.pdf?sequence=6

[39] http://www.nuance.northwestern.edu/keckii/ftir2.asp

[40] Donald F Weirauch, Roger L Strong, Robert M Wallace and Dipankar Chandra, An evaluation of the sessile drop technique for the study of (Hg, Cd)Te surfaces, Semicond. Sci. Technoi. 8 (1993)'916-921.

[41] http://serc.carleton.edu/research_education/geochemsheets/techniques/XRD.html

[42] http://web.pdx.edu/~pmoeck/phy381/Topic5a-XRD.pdf

Chapter 4.

PES/PET electrospun nanofibrous composite membrane for pre-treatment of water - evaluation of the filtration potential

Chapter 4.

PES/PET electrospun nanofibrous composite membrane for pre-treatment of water - evaluation of the filtration potential

4.1 Introduction

Application of membrane technology in (drinking) water treatment is worldwide increasing steadily. Advantages such as simplicity in concept and operation, not involving any phase changes or chemical additives, being modular and easy to scale up, low energy consumption, greater efficiency for raw materials use and potential for recycling of by-products also need to equipments small in size tempt industry to benefit membranes for industrial processes. All of these advantages translate into cost savings and more environmentally sustainable processes.[1]

Despite such significant advantages, for water filtration conventional porous polymeric membranes suffer from various shortcomings including low-flux and high-fouling tendency. Primarily, such drawbacks are due to the geometrical structure of pores, the pore size distribution [2] and unwanted macro-void formation throughout the membrane thickness. [3] It appears that the electrospun nanofibrous membranes possessing several promising filtration features including high porosity, interconnectivity of the pores and tunable small pore size can overcome some of these limitations. [4, 5] For instance, Yoon et al. [5] and Wang et al. [6] have shown that electrospun nanofibrous membranes can replace low permeable asymmetric ultrafiltration membranes. Additionally, the interconnected pores are assumed to offer a lower fouling tendency to the membranes and small pore size of the nanofibrous non-wovens results in a higher retention.[4]

In the current study a PES electrospun nanofibrous mat was evaluated for applicability in the pre-filtration of waste water streams. In filtration pre-filters are used to remove coarser particles from the feed water. Hence, the performance of the down stream membrane such as reverse osmosis (RO) and nanofiltration (NF) membranes is preserved for a longer duration before cleaning and/or replacement.[7] Implementation of pre-filters prevents different problems including fouling thereby loss of capacity and lowers cleaning and replacement costs.[8]

Compared to the conventional fibrous pre-filters the nanofibrous ones can offer very small pore sizes at comparable areal density thus allowing a higher retention. Recently, Aussawasathien et al. [7] and Gopal et al. [9,10] have explored the viability of developing nylon-6, polyvinylidene fluoride and polysulfone pre-filters via the electrospinning process. Their applicability in particulate removal from monodisperse suspensions has been demonstrated. Such electrospun membranes have been successful in eliminating more than 90% of the micro-particles from suspension.[7]

In the current study, a PES electrospun membrane is made and its potential as a water pre-filter is evaluated. PES was selected as the membrane material due to its high thermal and chemical resistance also its appropriate mechanical properties. Besides, to alleviate the handling issue of the highly electrostatic charged electrospun mat, a PET technical non-woven is employed as a sub layer. To prevent delamination, a heat treatment approach is adopted which could be influential on filtration performance of the membranes as well.

Different with similar researches and as a novel approach, PES/PET ENM is investigated through a retention test in more realistic conditions for a long time i.e. 24 hours and using a heterodisperse aqueous suspension mimicing real water feeds. Previously mentioned similar researches are based on a very short filtration time and utilizing monodisperse suspensions. Moreover, to predict performance of the membrane at eventual higher feed pressures at industrial scale, the PES/PET ENM is characterized in term of water flux in two arrangements of single and multi layer. Multi layer membrane as a cartridge filter could elaborate the filtration performance of the ENM under higher pressures.

4.2 Results and Discussion

4.2.1 Characterization of the PES nanofibrous mats

The morphology of the electrospun nanofibers is shown in figure 4.1. The surface of the nanofibers is relatively smooth and no beads and droplets can be observed within the area inspected by SEM. Other properties of the PES nanofibrous mat are tabulated in table 4.1. The thickness of the PES nanofibrous mats was measured using a digital micrometer (Deltascope® MP2C from Fischer).

4.2.2 Heat treatment

The main concern in preparation of the composite membranes is creating a stable interface between the supporting and the nanofibrous layers. Hence, in this study a heat treatment approach was adopted to enhance the interfacial stability of the ENMs. Continuous heating results in diffusion of the solvent to the surface of the nanofibers. In this way local re-dissolution of the PES occurs which obviously leads to better contact between the PES nanofibers and the fibers of the PET non-woven by simply sticking them together. As shown in figure 4.2, the improved adhesion at the interface is clearly seen in SEM pictures (figures 4.2B and 4.2C for the heat treated membrane in comparison to figure 4.2A for the untreated one).

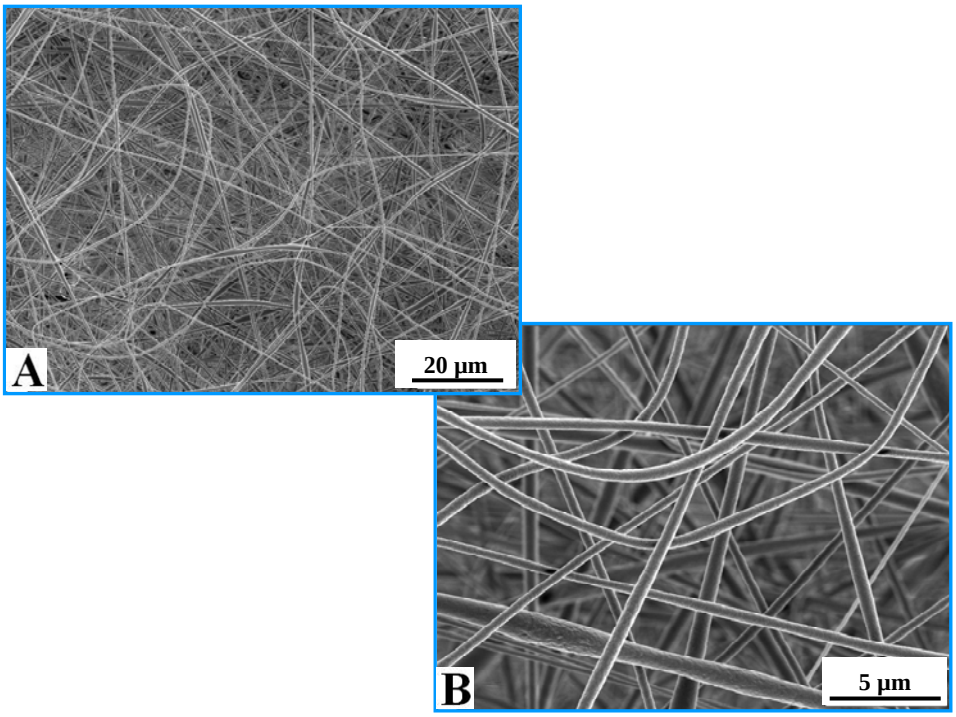

Figure 4.1: SEM micrographs showing the morphology of the PES electrospun nanofibers

Table 4.1: PES nanofiber mat properties

Morphology of the nanofibers	Smooth surface, no beads and droplets
Diameter of the nanofibers	260 ±110 nm
The thickness of the PES nanofibrous mat	100 ±30 µm

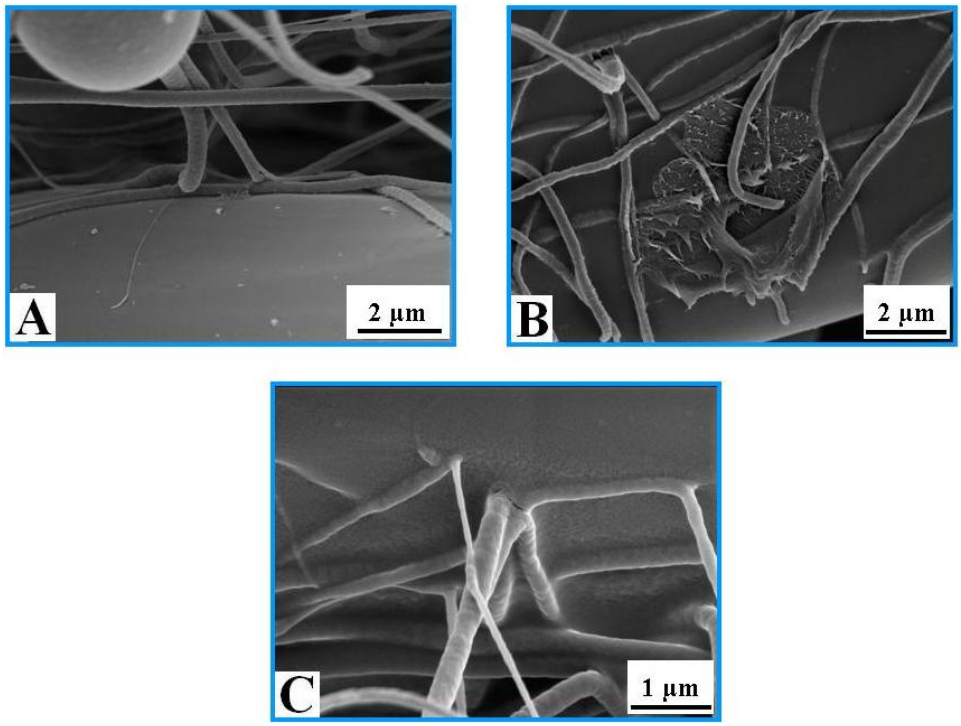

Figure 4.2: SEM micrographs showing the adhesion of the PES nanofibers to the PET non-woven; A) Untreated B&C) Heat treated

The ATR-FTIR spectra of the PES nanofibers before and after heat treatment are shown in figure 4.3. The band assignments for the infrared spectrum of PES are listed in table 4.2. As can be seen in figure 4.3 no obvious difference between the spectra of the PES nanofibers heat treated in air and untreated is observed. This means that heat treatment in air can not oxidize the nanofibers. Considering the difficulties and expenses of heat treatment under vacuum, this result can be very promising for application of such membranes on industrial scale.

As can be seen in figure 4.3, the only difference between the spectra of the heat- and untreated nanofibers is the peak appearing at 1671 cm^{-1} for the untreated nanofibers. This peak which disappears after the heat treatment is related to carbonyl vibration of N-C=O group caused by the remaining solvent DMF.[11] The FTIR results imply that the surface chemistry of the nanofibers does not change significantly by the applied heat treatment.

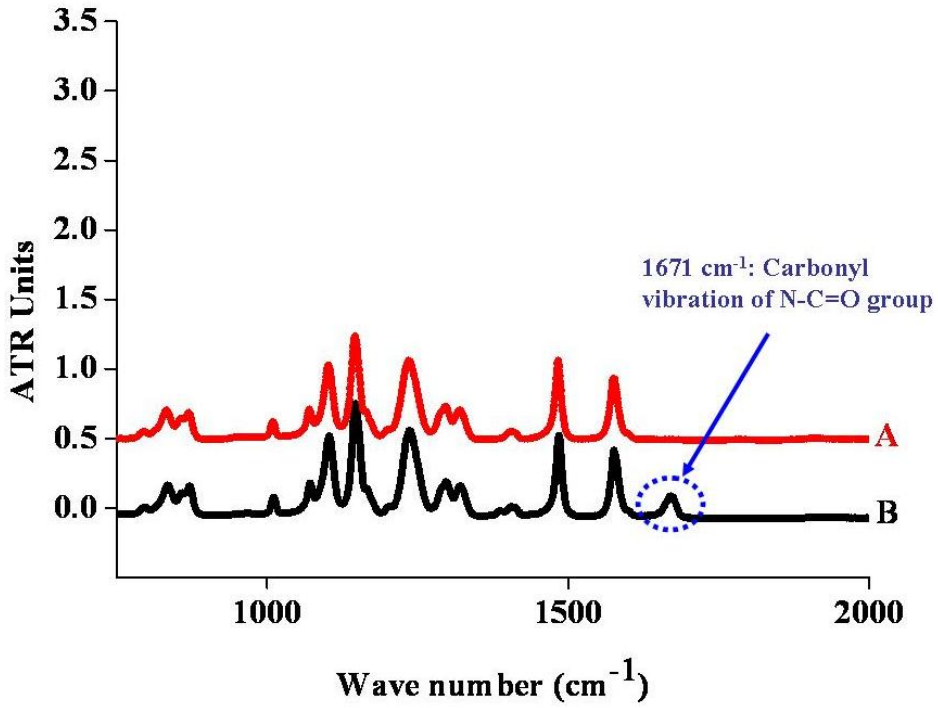

Figure 4.3: ATR-FTIR spectra of A) the heat treated PES nanofibers in air B) the untreated PES nanofibers

Table 4.2: Band assignments for the infrared spectrum of PES [12]

Wavenumber (cm^{-1})	***Assignment***
3095	aromatic C-H vibration
1575,1483	aromatic band (C=C ring)
1404	CH_2 bond
1320	asymmetric vibrations of the SO_2 group
1296	Vibrations of the SO_2 group
1234	C–O ether
1145	Symmetric vibrations of the SO_2 group
1101	aromatic ring
1070	Symmetric vibrations of SO_3^-
1010	Un-known
870,832,797,698	C-H
	bending vibrations
717	CH_2 bond

Based on the TGA curves, as shown in figure 4.4, the weight loss starts at 120°C and at the maximum heat treatment temperature (190°C) weight reduction of the untreated PES nanofibers is around 2.5%. This amount for the as-received PES and the heat treated PES nanofibers are 0.6% and 0.8%, respectively. Evaporation of DMF is the main reason for loss of weight in the untreated nanofibers within the studied range of temperature.

4.2.3 Membrane characterization

Different characteristics of the PES/PET nanofibrous membranes are tabulated in table 4.3.

4.2.3.1 Pore size distribution

Based on the gas-liquid displacement measurements, the bubble point, i. e. the biggest pore of the ENMs, was detected at 0.1 bar corresponding to 5 µm pore size as calculated using equation 3.4. A mean flow pore diameter of 2 µm was determined from the measurements. This range of pore size in the PES nanofiber mats is comparable with typical characteristics of microfiltration (MF) membranes.[13]

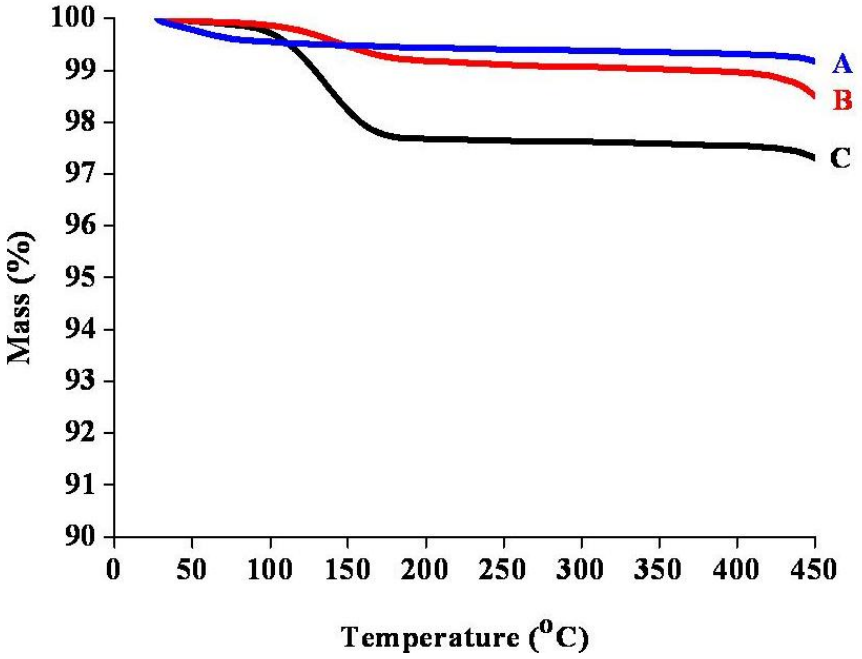

Figure 4.4: Thermogravimetric analysis (TGA) curves of A) as-received PES B) heat treated PES nanofibers and C) untreated PES nanofibers (All TGA measurements were performed in Argon atmosphere)

Table 4.3 : PES/PET composite membrane properties

Thickness	200 µm
Areal density	0.2-0.3 g/cm^2
Active filtration area	≈0.001 m^2
Mean flow pore diameter	2 µm
Bubble point pore diameter	5 µm

4.2.3.2 Permeability

Pure water flux measurements were performed to study the permeability and structural stability of the PES/PET ENMs as single and multi (5) layer.

As can be seen in figure 4.5A the pure water fluxes measured for both, the single layer un- and heat treated PES/PET membranes are high and comparable with the primary feed rate (≈60x10^3 l/h.m^2) at the onset of the experiment (t = 0). In both cases the fluxes were practically constant during the tests.

From figure 4.5B it can be seen that the pressure differences (ΔP) for the single layer un- and heat treated PES/PET membranes are very low (≈50-170 mbar at the start and the end of measurements, respectively) and virtually steady until the end of measurements.

According to the Darcy's law [14,15,16], the flux through a MF membrane can be expressed as follows (equation 4.1):

$$J = \frac{\varepsilon r^2}{8\mu\tau}\frac{\Delta P}{\Delta x} = \frac{k\Delta P}{\mu\Delta x} \qquad \text{Eq. 4.1}$$

where J is the water flux (m^3/s), ε the porosity (-), r the pore radius (m), τ the tortuosity (-), k the permeability coefficient (m^2), ΔP the pressure difference across the membrane (Pa) (1 Pa=10^{-5} bar), µ the dynamic viscosity (Pa s) and Δx the membrane thickness (m).

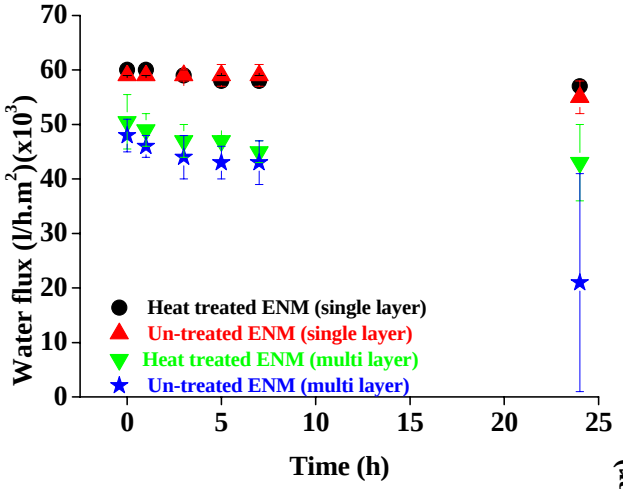

(A)

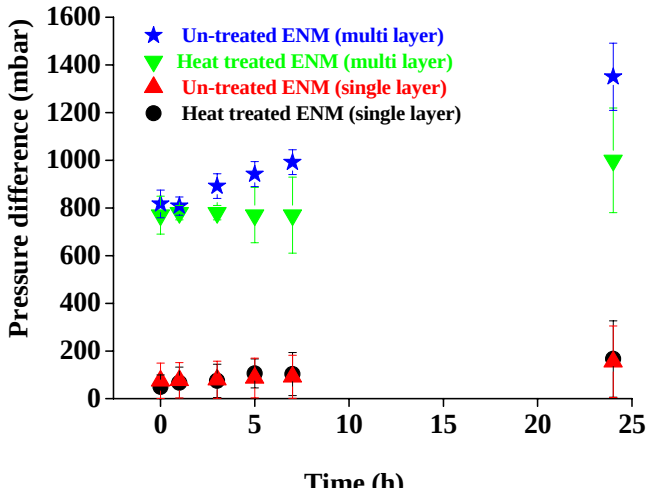

(B)

Figure 4.5: Permeation performance of the PES/PET membranes A) Pure water flux and ; B) Pressure difference over the membranes

The practically constant fluxes determined for the single layer ENMs, either untreated or heat treated, indicate that the pore size, the porosity and the tortuosity, did not change if constant thickness of the mats is assumed. For the multi-layer ENMs, either untreated or heat treated, the fluxes decreased with time. Within 8 hours of filtration the rate of decrease is comparable. The fluxes measured after 24 hours filtration, however, revealed significant differences. While for the heat-treated ENMs only a slight decrease in flux and correspondingly a low pressure increase across the membrane, was determined. The decrease in flux was significantly for the untreated ENM's. Correspondingly, as shown in figure 4.5B, the pressure increase across the membrane rises from about 820 mbar at the start of the experiment to approximately 1350 mbar after 24 hours filtration. The results show that the applied heat-treatment can preserve the structural integrity of the fibrous mats due to the interfiber sticking.

The higher thickness of the multi layer membranes compared to the single layer membranes results in a higher pressure increase (ΔP) across the membrane. The high ΔP leads to higher compressive and shear forces on the nanofibrous layer applied by water flow and consequently, in its deformation at surface and bulk (compaction). The deformation reduces the interconnectivity of the pores, clogs the pores, decreases the effective porosity and as a consequence, the flux of the membrane. The deformation happens only on the uppermost nanofibrous layer of the untreated ENMs as can be seen from figures 4.6A-C. Different patterns of water flow on the uppermost layer compared to the other next layers are most probably the main reason for occurrence of deformation only on this layer. In addition, the uppermost layer acts as a damping layer for the next layers via absorption of the main mechanical stress applied by water flow.

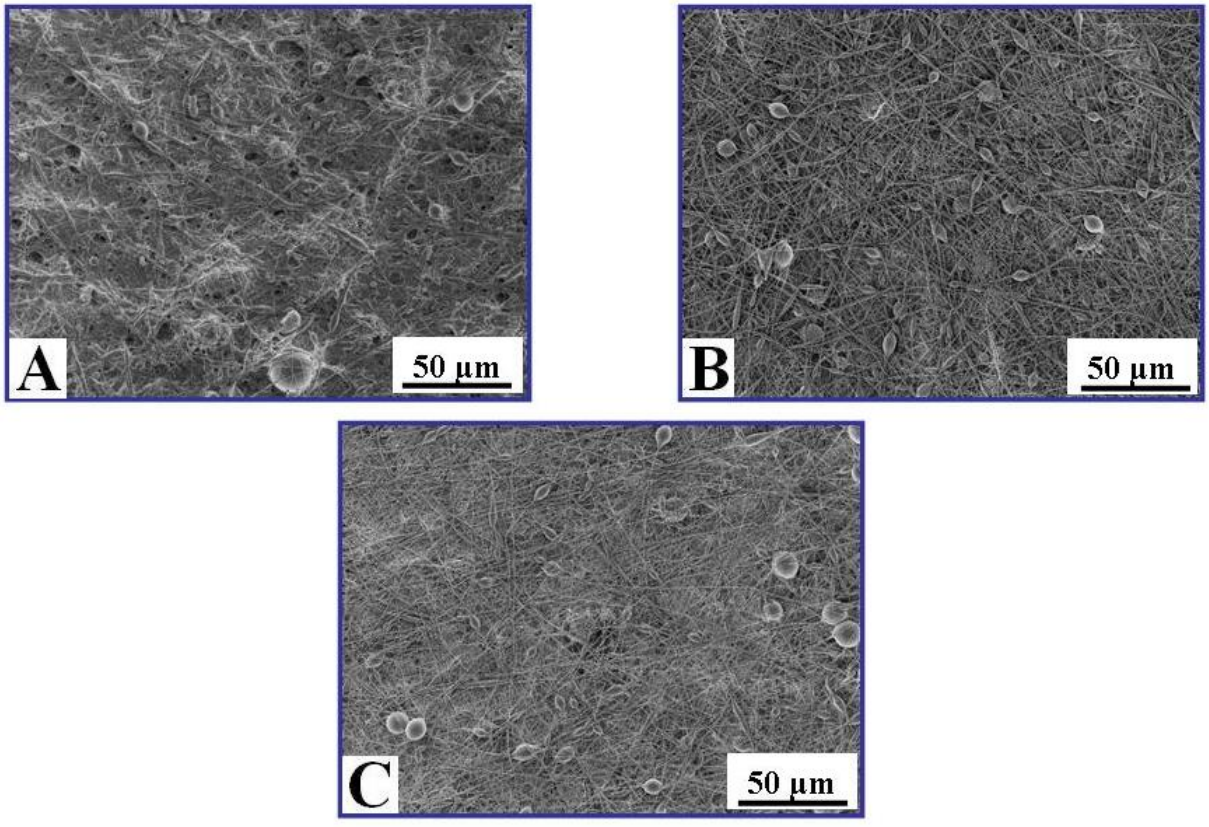

Figure 4.6: The surface of three consecutive layers of an untreated multi layer PES/PET membrane after filtration A) the uppermost layer B) the second layer C) the third layer

In contrast to the untreated PES/PET membranes, the heat treated ones maintain their steady trend of water flux and ΔP throughout the measurements. This shows that heat treatment can preserve the fibrous media and prevent its deformation.

Similar to the mechanism involved in improvement of the interfacial stability the re-dissolution of the PES upon heat induced out-diffusion of solvent as seen in figure 4.7 may stick the PES nanofibers to each other. The interfiber adhesion makes the nanofibrous layer more resistant against compressive and shear stresses applied by water flow during filtration and as a result the deformation is limited or even prevented. After 24 hours filtration the surface and bulk deformation (compaction) could not be observed for the heat treated ENMs (figures 4.8B and 4.8D). As can be seen in figure 4.8A and 4.8C, the untreated membrane undergoes a compaction, i.e. a change in membrane thickness, of about 48% compared to the heat treated one.

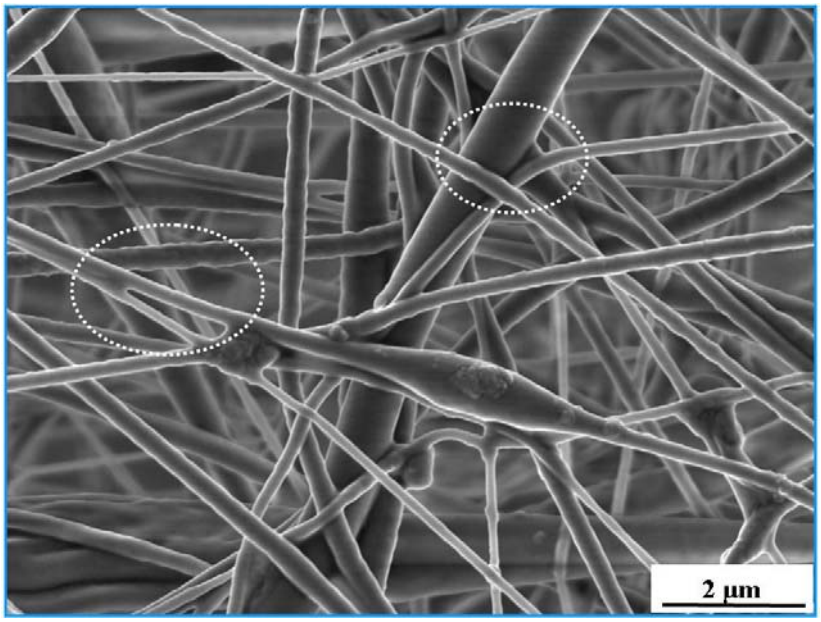

Figure 4.7: Interfiber adhesion of PES nanofibers after the heat treatment

4.2.3.3 Retention tests with particle suspensions

The filtration performance of the PES/PET ENMs as single layer was investigated using a simple model based on aqueous PS suspensions. Retentions, pressure differences and fluxes were determined for the different ENMs.

As mentioned earlier (chapter 3), d90 was taken as a measure of retention performance of the ENMs. The d90 is the value of the particle size distribution representing the 90 % of the particles which may pass the membrane according to their particle size. It should be noted that the polydispersity index (PI) values of all the primary suspensions used as feeds varied between 0.2 and 0.5 representing a broad dispersion of particle size.[17] The particle size distribution of all the feed and permeate suspensions containing nano- and microparticles are shown in figure 4.9.

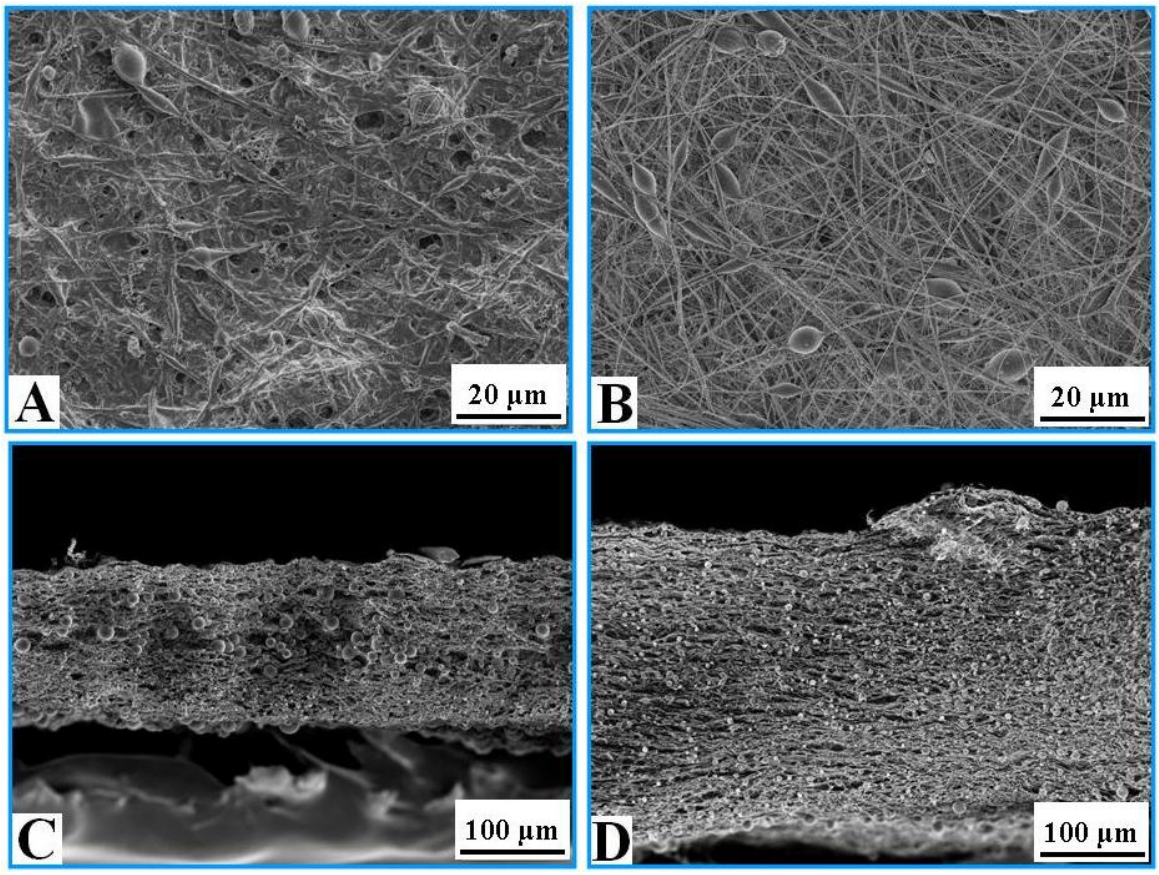

Figure 4.8: SEM micrographs showing A) surface of the uppermost layer of the untreated PES/PET membrane after filtration B) surface of the uppermost layer of the heat treated PES/PET membrane after filtration C) cross section of the uppermost layer of the untreated PES/PET membrane after filtration D) cross section of the uppermost layer of the heat treated PES/PET membrane after filtration

As can be seen in figures 4.9 and 4.10, the retention performance of the untreated ENMs is strongly dependent on the size distribution (d90) of the particles suspended in the feed. When d90 is closer to the average pore size of the ENMs and over 1 µm, the membranes were able to reject the particles based on their size after 1 hour. As seen in figures 4.9 B and 4.10 A, the d90 of the particles in the primary feed is 1140 nm but after 1 hour in the first permeate this size decreases to approximately 600 nm. The rejection is not completed even after 24 hours and still there are particles present in the permeate with a d90 close to the d90 of the first permeate. This means that the bigger particles are rejected by size exclusion without blocking the pores of the ENMs. The smaller particles can pass the ENMs and are circulating in the filtration loop. It is observed from the figures 4.10 B and 4.10 C, respectively, that this rejection performance is along with a high permeate flux and very low pressure difference. This behavior can be very promising, if we consider the PES ENMs as a pre-filter.

In contrast to that, retention measurements with suspensions containing particles with a d90 below 1 µm revealed a different trend. As shown in figures 4.9 A and 4.10 A, the d90 dropped from an initial value of 560 nm to about 200 nm after 1 hour. The results illustrated in figures 4.10 B and 4.10 C, demonstrate that this retention is accompanied by a significant decrease in flux and correspondingly, a dramatic rise in pressure increase. After 5 hours of filtration the ENMs were almost completely blocked. Practically no flux could be detected.

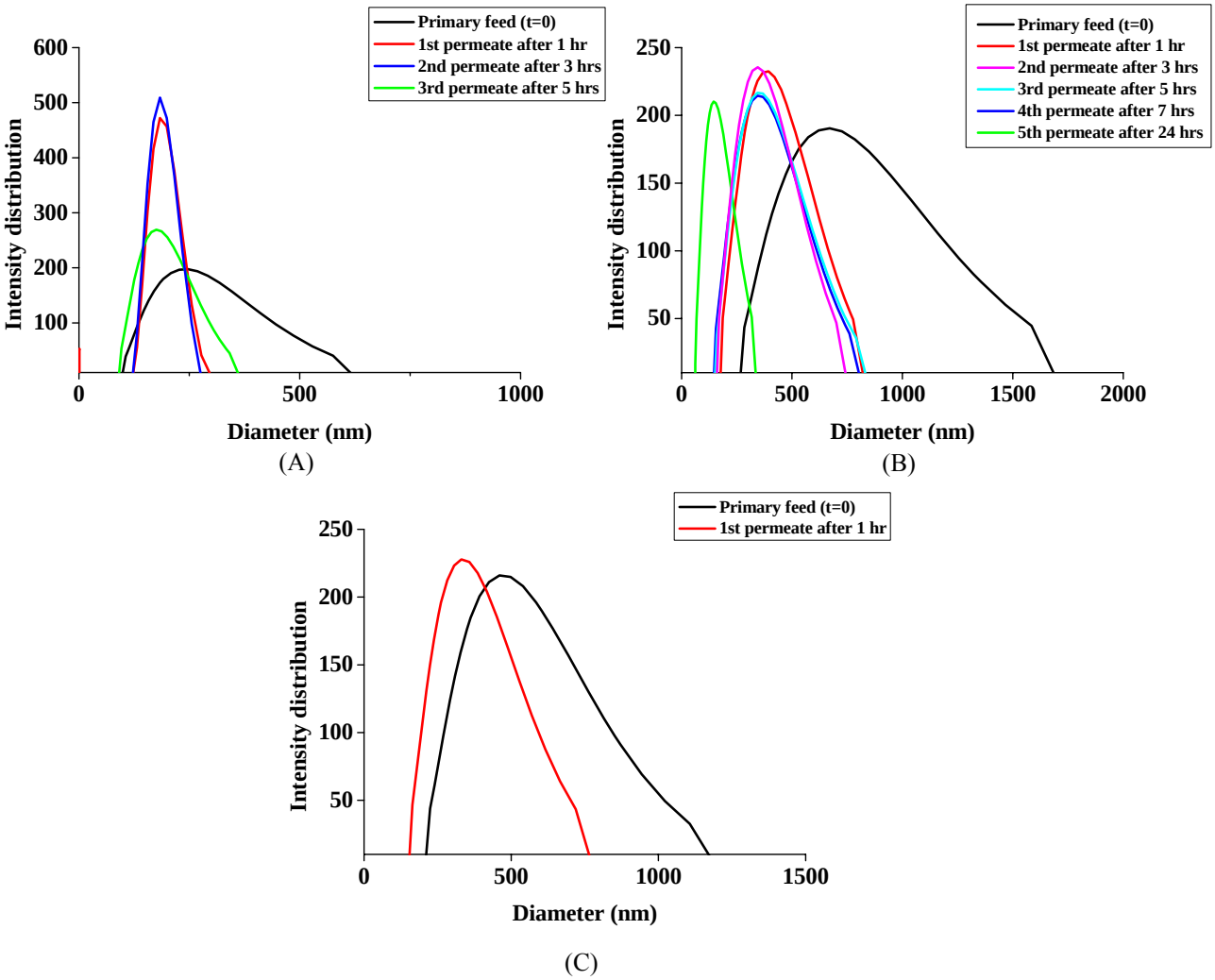

Figure 4.9: Particle size distribution of the feed and permeate suspensions; A) retention test using the untreated ENM with a feed suspension of d90 below 1µm B) retention test using the untreated ENM with a feed suspension of d90 over 1µm C) retention test using the heat treated ENM with a feed suspension of d90 below 1µm

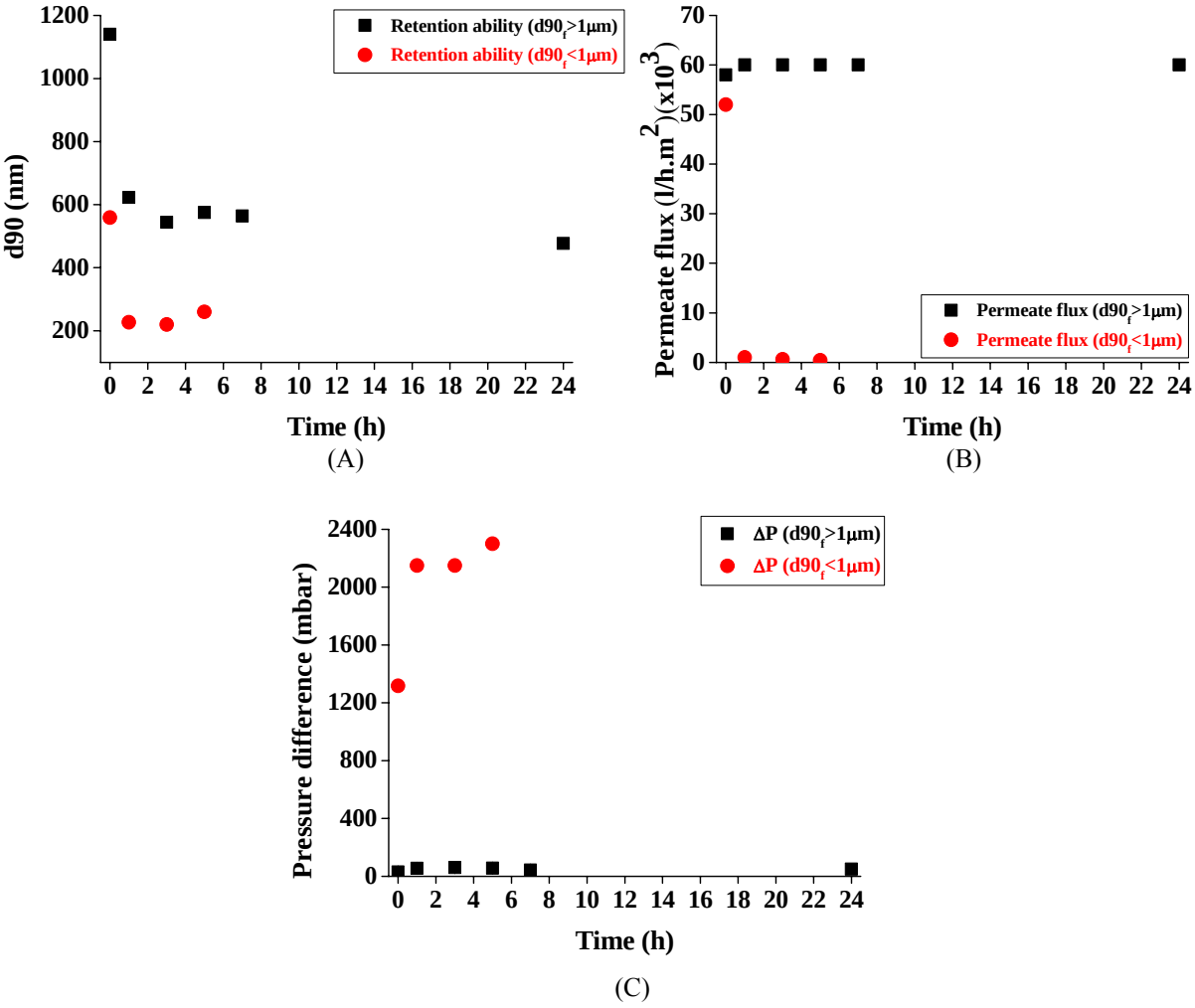

Figure 4.10: The retention performance of the untreated PES/PET ENMs A) d90 of the permeate suspension B) flux of the membranes; C) pressure difference over the membranes ($d90_f$: d90 of the primary feed)

The flux and retention results are supported by the optical analyses of the ENMs after the filtration experiments.

The retention results are in good agreement with the results published by Gopal et al. [9] for monodisperse suspensions. They studied the retention performance of polyvinylidene fluoride electrospun membranes with an average pore size of 4 to 10 µm. For a monodisperse suspension of 10 µm particles a retention of 96 % was determined. The measured fluxes indicated that there was no permanent fouling of the electrospun filters. The filtration of monodisperse suspensions with 1 µm particles revealed that these particles can obviously closely pack together and block the pores. The retentions of particles were 98 % with instantaneous onset of flux reduction.

After the filtration run with the suspension containing particles with a d90 below 1 µm, as seen in figures 4.11 A and B, the surface of the untreated ENMs is

covered by a relatively dense cake layer which was already described by Gopal et al. [9,10]. The PS nanoparticles are captured by the nanofibers (physical trapping) accompanied by the already described structural change of the nanofibrous layer under the filtration conditions.

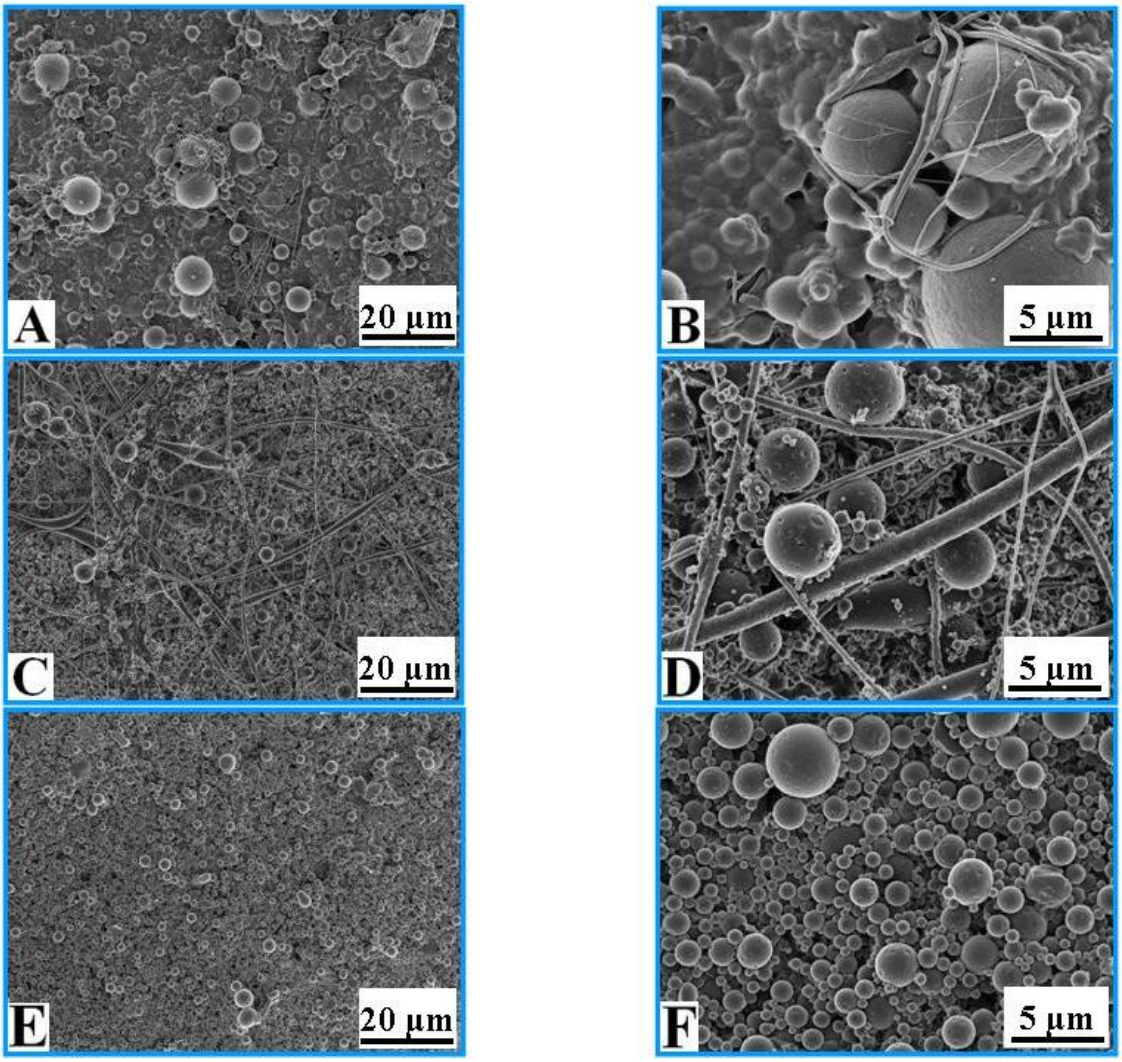

Figure 4.11: The cake layer formed at the surface of the A,B) untreated PES/PET membranes (feed suspension: d90<1µm) C,D) untreated PES/PET membranes (feed suspension: d90>1µm) E,F) heat treated PES/PET membranes (feed suspension: d90<1µm)

The cake layer clogs the pores of the ENMs significantly at the surface. It is assumed that immediately at the start of the experiment the nanoparticles are trapped by the nanofibers and act as the initiation points for cake layer formation. Noteworthy, when the particle size is in sub-micron range (0.1-1 µm), due to the superimposition of brownian diffusion, lateral migration and shear induced diffusion, the escape velocity of particle from the surface of the membrane reaches its minimum.[18] This theory explains the severe particle deposition observed in the ENMs when the particle

size drops below 1µm. As shown in figures 4.11 C and D, in case of the suspensions characterized by a d90 above 1 µm no such cake layer can be observed on the surface of the untreated ENMs. Obviously, the bigger particles prevent the formation of a closely packed particle layer. Interestingly, as seen in figures 4.11 E and F, the cake layer observed after the filtration of particle suspensions below 1 µm through heat-treated PES nanofibrous mats was composed of closely packed but discrete particles. It can only be speculated whether the broad particle size distribution in combination with the structural integrity of these heat-treated ENMs is responsible for this behaviour.

Direct comparison of the flux and retention behaviour of untreated and heat-treated PES electrospun membranes with particle suspensions below 1 µm revealed no significant difference. As seen in figures 4.9 A&C and 4.12 A, the d90 of the suspensions decreased immediately. Correspondingly, as illustrated in figures 4.12 B&C the permeate flux decreased drastically while the pressure across the membranes increased significantly.

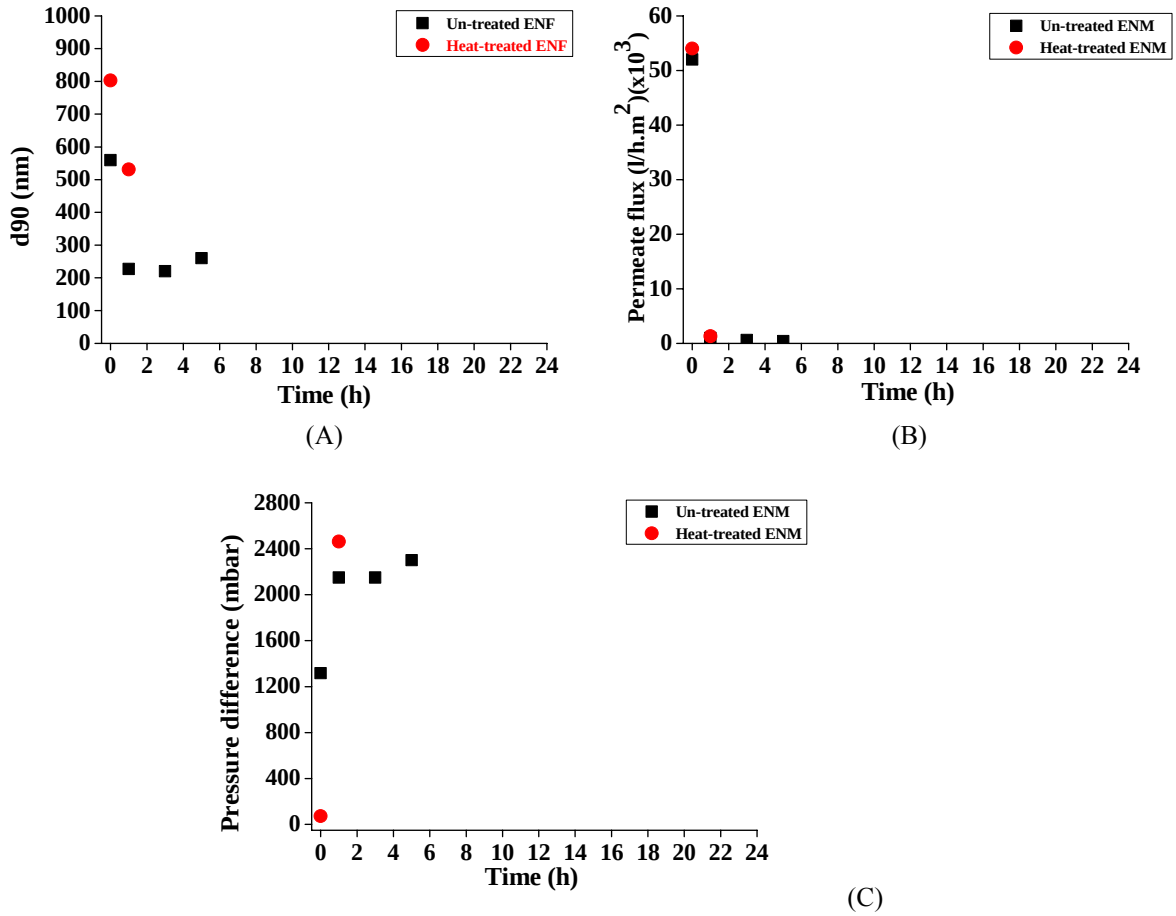

Figure 4.12: Results of retention performance of the PES/PET ENMs A) d90 of permeate suspensions; B) flux of the membranes; C) pressure difference over the membranes

It should be noted that the turbidity of permeated suspension decreases significantly with time. Most probably bigger agglomerates are formed due to instability of the surfactant layer around the particles under flow conditions. These agglomerates, clearly seen in figures 4.11 A to D, are rejected and do not take part in the filtration process any more. Consequently, the particle loading of the permeating suspension decreases.

4.3 Conclusion

Electrospun nanofibrous nonwovens due to their special structural features can be considered for filtration application. In the current study, applicability of PES electrospun nanofibrous mat supported by a PET sublayer for liquid filtration was investigated. Pure water flux measurements demonstrated the high permeability of this nanofibrous composite membrane. Moreover, in a particle challenge test based on particulate aqueous suspensions, this nanofibrous composite membrane showed a high permeability while rejecting microparticles efficiently. However, in the case of nanoparticles much smaller than the average pore size, formation of a dense cake layer declined the permeability drastically. Considering the characteristics of real particulate suspensions in water treatment, containing a mixture of micro- and nanoparticles, this electrospun nanofibrous membrane has the potential to be used in pre-treatment of water, one step before ultra- and nanofiltration membranes.

Despite promising filtration ability, at high feed pressures (here simulated by the cartridge filter i.e. multi layer configuration) the PES nanofibrous layer is deformed i.e. compacted. This failure leads to loss of water permeability which occurs for both the un- and heat treated ENMs but with a much less extent for the latter group. Such a failure necessitates structural modification of the ENM under investigation to preserve the high porosity and interconnectivity of the pores thereby permeability. Next chapters deal with such modifications according to an accurate determination of mechanical performance of the ENM at different filtration modes.

4.4 References

[1] R.W. Baker, E.L. Cussler, W. Eykamp, W.J. Koros, R.L. Riley, H. Strathmann, Membrane separation systems : recent developments and future, Noyes Data Corporation, 1991.

[2] W.J. Wrasidlo, K.J. Mysels, The structure and some properties of graded highly asymmetrical porous membranes. J. Parenteral Sci Technol 38(1984) 24-31.

[3] F.G. Paulsen, S.S. Shojaie, W.B. Krantz, Effect of evaporation step on macrovoid formation in wet-cast polymeric membranes, J Membrane Sci. 91 (1994) 265-282.

[4] C. Burger, B. S. Hsiao, and B.Chu, Nanofibrous materials and their applications, Annu. Rev. Mater. Res. 36 (2006) 333–368.

[5] Kyunghwan Yoon, Kwangsok Kim, Xuefen Wang, Dufei Fang, Benjamin S. Hsiao, Benjamin Chu, High flux ultrafiltration membranes based on electrospun nanofibrous PAN scaffolds and chitosan coating, Polymer 47 (2006) 2434–2441.

[6] X. Wang, X. Chen, K. Yoon, D. Fang, B.S. Hsiao, B. Chu, High flux filtration medium based on nanofibrous substrate with hydrophilic nanocomposite coating, Environ. Sci. Technol. 39 (2005) 7684–7691.

[7] D. Aussawasathien, C. Teerawattananon, A. Vongachariya, Separation of micron to sub-micron particles from water: Electrospun nylon-6 nanofibrous membranes as pre-filters, J. Membrane Sci. 315 (2008) 11–19.

[8] Michelle Chapman-Wilbert, The desalting and water treatment membrane manual; A guide to membranes for municipal water treatment, U.S. Department of the interior, Water Treatment Technology Program Report No. 1, September 1993.

[9] R. Gopal, S. Kaur, Z. Ma, C. Chan, S. Ramakrishna, T. Matsuura, Electrospun nanofibrous filtration membrane, J. Membrane Sci. 281 (2006) 581–586.

[10] R. Gopal, S. Kaur, C.Y. Feng, C. Chan, S. Ramakrishna, S. Tabe, T.Matsuura, Electrospun nanofibrous polysulfone membranes as pre-filers:particulate removal, J. Membrane Sci. 289 (2007) 210–219.

[11] Meng Wang, Li-Guang Wu, Xing-Cun Zheng, Jian-Xiong Mo, Cong-Jie Gao, Surface modification of phenolphthalein poly(ether sulfone) ultrafiltration membranes by blending with acrylonitrile-based copolymer containing ionic groups for imparting surface electrical properties, J. Colloid and Interface Sci. 300 (2006) 286–292.

[12] S. Belfer, R. Fainchtain, Y. Purinson, O. Kedem, Surface characterization by FTIR-ATR spectroscopy of polyethersulfone membranes-unmodified, modified and protein fouled, J. Membrane Sci. 172 (2000) 113–124.

[13] M. Mulder, Basic Principles of Membrane Technology, 2nd ed., Kluwer Academic, Boston, 1996.

[14] Zhan Wang, Dezhong Liu, Wenjuan Wu, Mei Liu, Study of dead-end microfiltration flux variety law, Desalination 201 (2006) 175–184.

[15] Phillip Gibson, Heidi Schreuder-Gibson, Donald Rivin, Transport properties of porous membranes based on electrospun nanofibers, Colloids and Surfaces A: Physicochemical and Engineering Aspects 187–188 (2001) 469–481.

[16] Ingmar H. Huisman, Benoît Dutrê, Kenneth M. Persson, Gun Trägårdh, Water permeability in ultrafiltration and microfiltration:Viscous and electroviscous effects, Desalination 113 (1997) 95-103.

[17] M. Nidhin, R. Indumathy, K. J. Sreeram and Balachandran Unni Nair, Synthesis of iron oxide nanoparticles of narrow size distribution on polysaccharide templates, Bull. Mater. Sci., 31(1) (2008) 93–96.

[18] J.R. Alvarez, Pressure driven membrane processes, in: J. Coca, S. Luque (Eds.), Membrane Applications in the Food and Dairy Industry, University of Oviedo, Spain, 1999, pp. 23–42.

Chapter 5.

Evaluation of the mechanical properties of polyethersulfone electrospun nanofibrous membranes

Chapter 5.

Evaluation of the mechanical properties of polyethersulfone electrospun nanofibrous membranes

5.1 Introduction

In separation technology, application of electrospun nanofibrous mats can be classified as three major areas: gas, liquid and molecular filtration. As air filters, electrospun nanofibrous non-wovens have been used commercially over the last 20 years.[1] However, in other filtration areas the research is extensively being done to meet the requirements for industrialization of such nanofibrous filters.

To benefit this novel classs of membranes for a specific technology, the fibres' surface, bulk and architectural properties should be thoroughly understood. Similar to the major influence of the material properties of polymeric membranes on their performance and interaction with their surrounding environment, development of electrospun nanofibrous membranes for industrial applications certainly require their accurate characterization.Although being very important, detailed characterization of these properties is frequently overlooked.[2]

Mechanical characterization of the electrospun nanofibrous membranes can be considered as one of the very important evaluations which rarely has been done. Despite promising filtration features, however, an electrospun membrane which is exposed to various stresses applied by fluid flow should also possess sufficient mechanical strength. Indeed, for air or liquid filtration applications, besides chemical stability a membrane needs to be mechanically strong enough in order to efficiently separate particulates from fluid streams such as air, water, hydraulic fluids, lubricant oils or fuels.[3]

In the previous study, the filtration performance of polyethersulfone (PES) electrospun nanofibrous membrane (PES) was evaluated through water flux measurement and retention test.[4] The results showed promising filtration abilities of this membrane for pre-treatment of water, however simulation of high pressure applications by a cartridge filter configuration revealed loss of permeability after sometime. This observation necessitates mechanical modification of the ENM. But

beforehand, we should be aware of the mechanical performance and stability of the membranes during different filtration modes.

Similar to microfiltration membranes, the PES ENMs with equal characteristics, e.g. pore size [4], can be operated in two ways: 1) as a straight-through filter i.e. dead-end filtration in which all of the feed liquid is passed through the membrane by applying a given pressure, or 2) in cross flow mode, that is, pumping the feed liquid across the membrane parallel to its surface.[5]

Depending on the filtration mode including dead-end or cross flow, the membrane should be mechanically stable under different kinds of applied stresses including shear, compressive and tensile ones.

In the current study, mechanical performance of the PES ENM is characterized under different mechanical conditions of compressive and tensile forces. Additionally, the efficiency of heat treatment as a strengthening mechanism for the electrospun nanofibrous membrane will be investigated.

The compressive mechanical properties of the PES ENM are evaluated through nanoindentation tests. Ultra-low load indentation, or nanoindentation, is a technique with around two decades history and especially developed for exploring the mechanical properties of materials at very small scales.[6] Nanoindentation owing to the possibility of evaluation of the hardness (mean pressure) of specific areas of an electrospun nanofibrous membrane with very fine spatial resolution and with minimal preparation is considered as an important mechanical characterization technique for this kind of membrane.[2]

In addition to the compressive mechanical properties, the tensile mechanical performance of the PES ENM is evaluated via a tensile test statically at ambient temperature. However, depending on the filtration application, a membrane can also be exposed to a broad range of temperature and dynamic forces. In order to characterize the dynamic tensile mechanical behavior of the PES ENMs under a range of temperatures a Dynamic Mechanical Analysis (DMA) was performed.

5.2 Results and Discussion

5.2.1 Morphological characterization of PES nanofibrous mat

The un- and heat treated PES electrospun nanofibrous membranes (prepared as described in chapter 3) were characterized morphologically to see the eventual effect of heat treatment. The morphology of the electrospun nanofibers is shown in figure 5.1. The surface of the nanofibers is relatively smooth and no beads and droplets are observed in the nanofibrous mat within the area inspected by SEM. The PES nanofibers had a diameter of approximately 200± 60 nm.

From SEM images of the electrospun PES nanofibers (shown in figures 5.2 A and B), the fiber junctions in the heat treated nanofibrous mat seem to be closely jointed or even slightly fused together, as compared to those in the untreated membranes. The selected temperature for the heat treatment (190 °C) is above the boiling point of the solvent (T_b(DMF)=153 °C) and below the glass transition temperature of PES (225 °C). The residual solvent in the nanofibers can partially re-dissolve PES by heating. Continuous heating results in diffusion of the solution outward of the nanofibers to the interface with the other nanofibers. By evaporation of the solvent at the interface, the nanofibers stick to each other firmly. A previous ATR-FTIR characterization demonstrated that this process does no lead to oxidation of the PES nanofibers.[4]

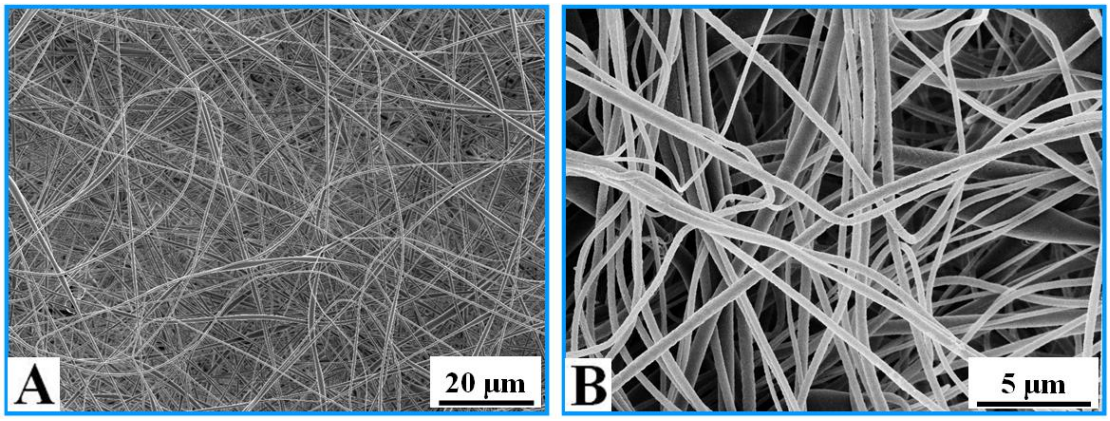

Figure 5.1: SEM micrographs showing morphology of the PES electrospun nanofibers

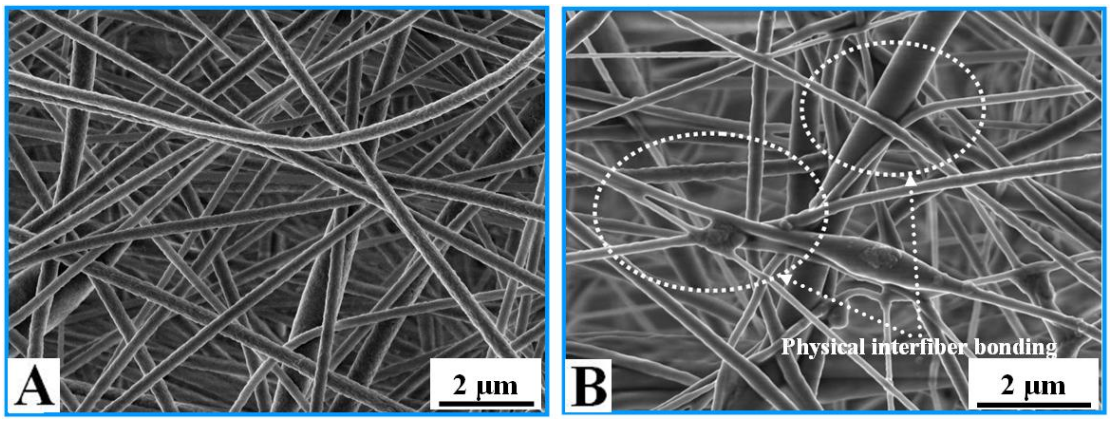

Figure 5.2: SEM micrographs showing formation of physical interfiber bondings after heat treatment A) untreated nanofibers B) heat treated nanofibers

5.2.2 Nanoindentation

Mechanical performance of the PES ENMs under compressive forces applied while filtration were evaluated via Nanoindentation test. This test is especially useful to demonstrate compaction behaviour of the ENMs.

Figure 5.3 represents the typical nanoindentation load-displacement graph obtained for the PES electrospun nanofibrous mats.

The mean pressure, $\overline{P}$, was determined from the maximum indentation load, P_{max}, divided by the contact area, A (equation 5.1) [7,8]:

$$\overline{P} = \frac{P_{max}}{A} \qquad \text{Eq. 5.1}$$

According to the load-displacement graph (see figure 5.3), considering a constant contact area (A) for a 50 µm flat punch, a higher P_{max} for the untreated nanofibrous mat implies a higher $\overline{P}$ as compared to the heat treated one.

The calculated values of $\overline{P}$ for the un- and heat treated ENMs are presented in table 5.1. Figure 5.4 represents the $\overline{P}$ data as a function of indentation depth for the PES electrospun nanofibrous mats. For both the ENMs there is an ascending trend of mean pressure versus indentation depth however with a higher rate for the untreated ENM. This ascending trend is attributed to compaction of electrospun nanofibrous mats which lowers porosity and strengthens the mat. The lower rate for the heat treated membrane means that it is compacted after experiencing a higher load level. In other words, it shows a higher resistance to compaction and preserves a higher

amount of porosity. This reality can be quantified according to the recovery index equation (equation 3.7) and presented as table 5.2.

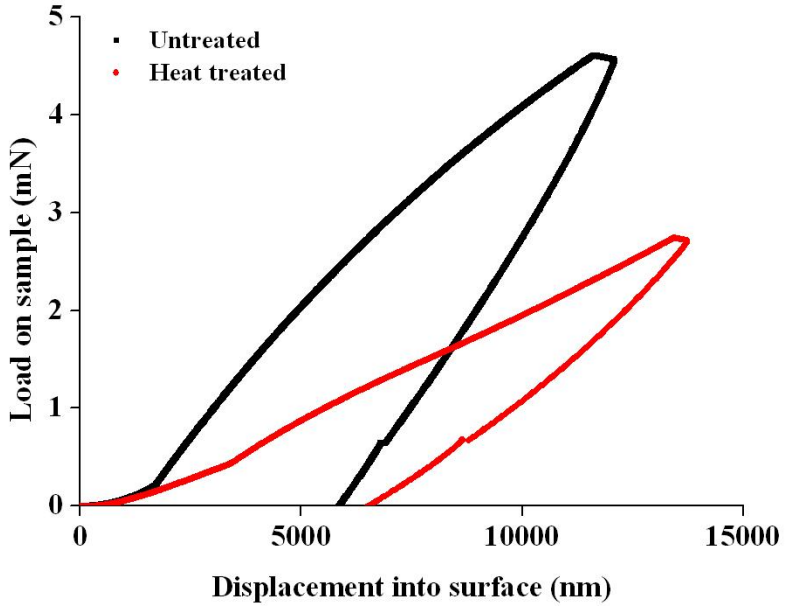

Figure 5.3: The load-displacement curve obtained by nanoindentation test for the PES electrospun nanofibrous mats

Table 5.1: Mechanical properties of the PES electrospun nanofibrous mats obtained through nanoindentation test

	Untreated electrospun nanofibers	**Heat treated electrospun nanofibers**
Mean pressure (MPa)	2.15 ± 0.25	1.3 ± 0.2
Stiffness (N/m)	964 ± 300	500± 140
Storage modulus(MPa)	19.3 ± 6	10± 3

Table 5.2: Recovery index of the PES nanofibrous mats

	Recovery index (%)
Untreated electrospun nanofibers	48 ± 6
Heat treated electrospun nanofibers	53 ± 2

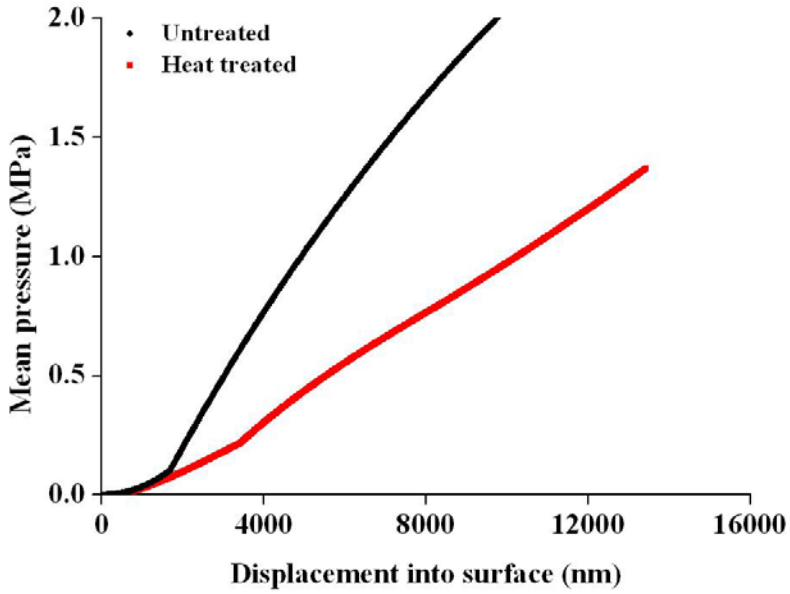

Figure 5.4: Mean pressure versus displacement profiles into surfaces of the PES electrospun nanofibrous mats

In addition to mean pressure, the storage modulus (E') was determined through the nanoindentation test. The storage modulus i.e. the energy stored elastically while deformation is directly correlated to the stiffness of the electrospun mat.[9,10]

The storage modulus (E') of the electrospun nanofibrous mats can be inferred from the initial unloading contact stiffness (S) , i.e. the slope of the initial portion of the unloading curve by following the equation 5.2 [11]:

$$E' = \frac{\sqrt{\pi}}{2\beta}\frac{S}{\sqrt{A}} \qquad \text{Eq. 5.2}$$

where β is a constant that depends on the geometry of the indenter (β = 1 for a flat punch indenter). The calculated values of E' for the untreated and heat treated ENMs are presented in table 5.1. The assumption for measuring storage modulus as above (Oliver-Pharr method) is based on the concept that primary unloading should be prevailed by the linear elastic recovery. To meet this condition i.e. minimizing the viscoelasticity effect, the load should be kept constant at the end of the loading part for a short given time (holding time) or a high loading/unloading rate is implemented. Otherwise even during the unloading part, there would be some continued deformation (often identified as a "nose" in the force curve) i.e. the penetration depth is still increasing while the load is decreasing. This assumption is one of the major drawbacks of this method for the evaluation of elastic modulus for polymeric

materials.[12] Therefore, the presented results (values) cannot be accurate and show only the general trends.

On the whole, surprisingly, a higher elastic modulus is observed for the untreated membranes as compared to the heat treated ones. The probable reasons should be sought in the following instances:

1- Pore collapse and compaction during loading on the electrospun nanofibrous membrane which results in a higher density and lower porosity. Similar behavior has been reported by Kucheyev et al. [13].

According to Lu et al. [14] and Pal [15], the effective elastic modulus for a highly porous structure such as an electrospun nanofibrous membrane can be expressed by equation 5.3:

$$E = E_m(1-\phi)^2 \qquad \text{Eq. 5.3}$$

Where E and E_m stand for the effective elastic modulus of the porous (with porosity of ϕ) and bulk material, respectively. Decrease of porosity through applied load and compaction of the nanofibrous layer results in a higher elastic modulus in the membranes. Heat treatment preserves more porosity as compared to the untreated membranes and this is why the elastic modulus of the heat treated sample is lower than that of the untreated one.

Additionally for the low density solids with relative densities ρ*<= 10%, the elastic modulus follows the equation $E \approx (\rho^*)^m$, in which depending on the composition and morphology m ≈ 3–4.[13] Hence, E increases very rapidly (superlinearly) with compaction and increase of relative density.

2- Van der Waals interaction of high aspect-ratio nanofibers (nanofiber sliding) during deformation.[13] Higher movement of untreated nanofibers results in their higher interactions and consequently a higher resistance to penetration of indenter.
3- Dissipative movement of air filling the pore volume [13]
4- Indenter friction with sliding nanofibers [13]

The energy dissipation during loading-unloading can be estimated by measuring the area confined between load-unload curves.[11] Based on our measurements, plastic work for the untreated and heat treated ENMs are 13.5 and 9 nN.m, respectively. These values show the untreated ENM undergoes a higher plastic deformation. Kucheyev et al. [13] state that two possible mechanisms for energy

dissipation in highly porous solids can be (i) van der Waals interaction of high aspect-ratio nanoligaments (nanofibers in the current study) due to their sliding during deformation and (ii) dissipative movement of air filling the pore volume.

The hold time at the maximum load was used to show the creep effect of the electrospun nanofibrous mats. Increase of displacement (indentation depth) at the maximum load represents the creep. As can be seen in figure 5.5, the creep effect was more apparent in the case of the untreated nanofibrous mats. In polymeric materials, cross linking of the polymer chains decreases the creep.[16] Similarly, the physical interfiber bonding of the nanofibers lowers creep of the heat treated nanofibrous mats.

5.2.3 Tensile test

Other than compressive stresses, the PES ENMs are also subjected to tension stresses. Hence, mechanical performance of the PES ENMs should be also evaluated through tensile test whether statically or dynamically (DMA). The value of tensile mechanical properties of the electrospun nanofibrous mats are presented in table 5.3. Also, the typical tensile stress-strain curves for these nanofibrous mats are shown in figure 5.6.

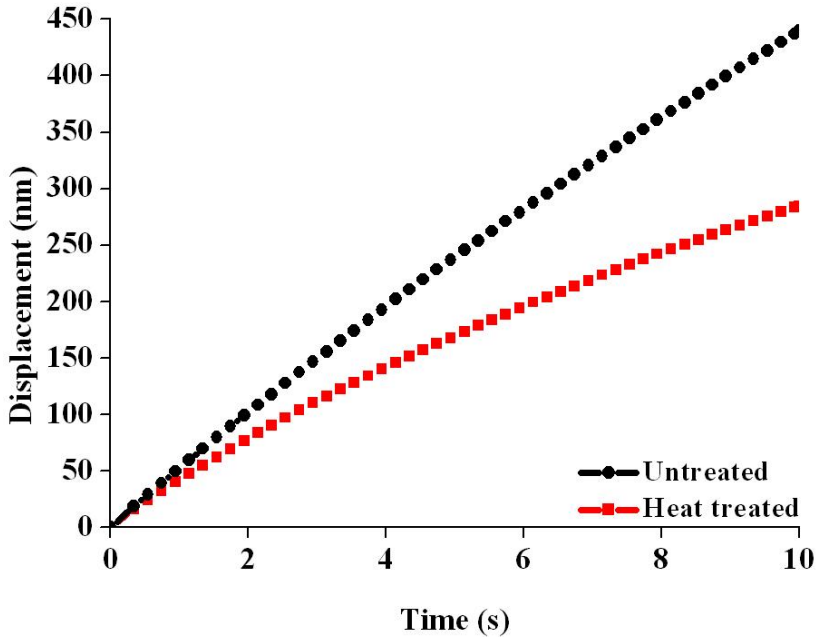

Figure 5.5: Variation of displacement at hold segment of load representative of creep of the PES electrospun nanofibrous mats

Table 5.3: Tensile properties of the PES electrospun nanofibrous mats

Sample	Tensile modulus (MPa)	Tensile strength (MPa)	Elongation at break (%)
Untreated	16 ±3	0.6 ±0.1	22 ±7.5
Heat treated	21 ± 8	0.9 ±0.3	13.5 ± 5

As can be seen in figure 5.6, for the untreated nanofibrous mat, stress increases gradually up to the peak and then decreases with a similar trend. In contrary, stress variation versus strain results in a steep slope for the heat treated ENM indicating an increase in the tensile modulus and strength with a concurrent decrease of the elongation to break. This behavior can be explained as follows: the untreated nanofibers can easily slide by one another during tensile deformation, resulting in low tensile strength and high elongation. However, for the heat treated nanofibrous mats, the nanofibers firmly adhered to each other can not slide freely. In other words, the interfiber bonding limits the stretchability of the membrane and makes the nanofibrous mat more rigid. Therefore, the heat treated nanofibrous mat had higher tensile modulus and strength and lower elongation at break.

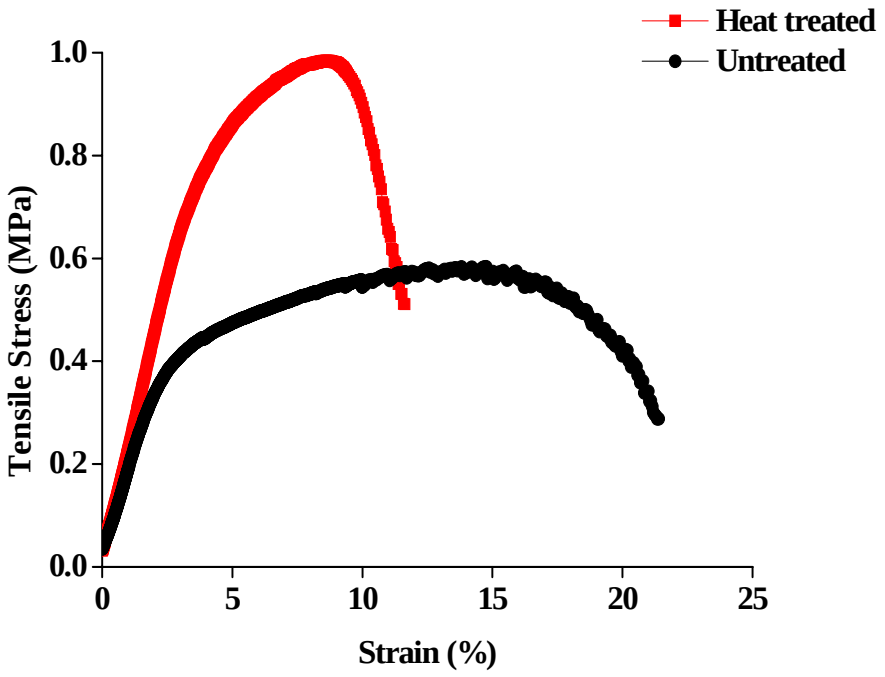

Figure 5.6: Stress- strain curves for the PES electrospun nanofibrous mats

Similarly, such a performance has been reported by other researchers.[17,18] In such studies based on a different principle with our residual solvent based approach, the mat is heated up to a temperature above glass transition temperature and just below melting point. This temperature may be even lower than T_b of the residual solvent (e.g. in the case of PVDF nanofibrous mat with DMAc solvent [19]). Through fusing the nanofibers to each other the nanofibrous web becomes rigid and mechanically stronger.

5.2.4 DMA (Dynamic tensile mechanical properties)

Dynamic mechanical analysis (DMA) results measured for the PES electrospun nanofibrous mats are shown in figure 5.7.

As can be seen in this figure, at the glass transition in the region between 220 and 240 ºC, loss modulus (E") and loss factor (tan δ) which are representative of damping exhibit their maximum. Below the glass transition temperature (T_g), the storage modulus of both the electrospun nanofibrous mats shows a decreasing trend, while the loss modulus is constant throughout the temperature sweep up to T_g. The decline of the storage modulus with temperature shows that the filtration performance of the electrospun mats is affected by temperature. This finding can be very important for the applications in which repeated cleaning of the membrane with hot water or sterilization with steam (autoclave) will be necessary.

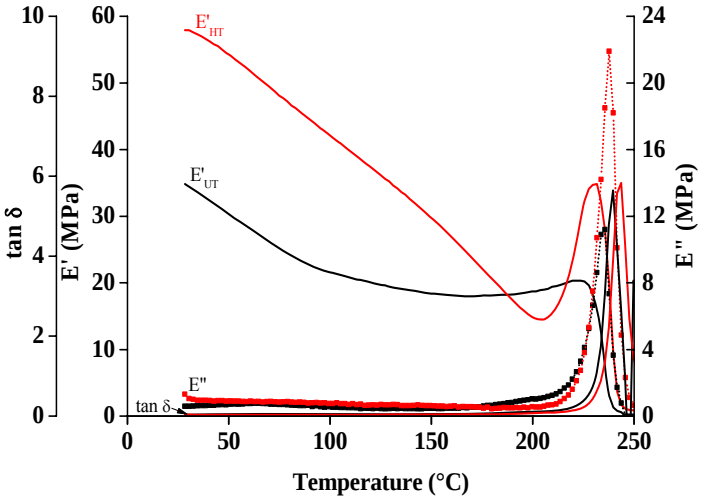

Figure 5.7: DMA results including E', E"and tanδ for the PES electrospun nanofibrous mats (UT: untreated and HT: heat treated represented as black and red colored lines, respectively)

The decreasing trend of the storage modulus can be attributed to the microstructure of the PES nanofibers. The heating while the DMA test results in expansion thereby increase of the free volume of the chain segment of the polymer and its freedom of motion. With a further increase of temperature localized bond movements occur giving rise to a decrease in storage modulus. This decline continues at higher temperatures mainly due to start of movement of the segment, whole side chains or whole main chains in the amorphous regions of the polymer.[20]

Different from the PES electrospun nanofibers, bulk PES in another study [21] has shown a plateau in the temperature range between ambient temperature up to T_g. However, at T_g a rapid decrease in the modulus occurs which is attributed to the α-transition or the onset of segmental motion in the polymer chains. This comparison shows that in addition to the microstructure, the macrostructure of the electrospun nanofibrous mats is also influential on alteration of their mechanical behavior with temperature. The high surface area of the nanofibers make them more sensitive to temperature and subsequently rapid loss of storage modulus.

As can be seen in figure 5.7, the heat treated electrospun nanofibrous mats show a higher storage modulus as compared to the untreated ones in most of the temperature sweep. This behavior is attributed to the presence of physical interfiber bonding in the heat treated electrospun nanofibrous membranes. However, a similar damping behavior (E" and tan δ) for both the electrospun nanofibrous mats is observed.

5.2.5 A comparison between the elastic moduli obtained through different mechanical characterization tests

By comparing the moduli obtained from the indentation and tensile tests, as well as dynamic mechanical analysis (DMA) (tabulated in table 5.4) some discrepancy appear. The probable reasons could be:

1- The difference of loading direction (compressive force for nanoindentation versus tensile one for tensile test and DMA) applied during the mechanical tests.[22]

2- The different states of stress in the tensile test versus the DMA (static versus dynamic), depending on the test geometries and magnitudes of the applied force amplitude.

3- In addition, usually it is seen that the elastic moduli measured by DMA are not in a good agreement with those obtained by other mechanical tests[23,24], although in principle they should be the same.

4- Nanoindentation results are indeed the mechanical properties that measured for electrospun fibers at nanoscale (in the current study microscale) and naturally could be tremendously different from the bulk mechanical properties (tensile) obtained at macroscale. The reason reverts to this reality that the bulk tensile properties of the electrospun nanofibrous mats depend to their porosity, total fiber content and orientation of fibers with respect to the direction of application of tensile force. Therefore, it is assumed that between the local elastic modulus and mean pressure values obtained through nanoindentation and the macroscopic mechanical properties a significant difference should be seen, especially for porous materials.[24]

Table 5.4: Elastic moduli obtained for the untreated and heat treated PES electrospun nanofibrous mats through different mechanical tests

Sample	**Elastic modulus (MPa) by nanoindentation**	**Elastic modulus (MPa) by tensile test**	**Elastic modulus (MPa) by DMA (at the ambient measurement)**
Untreated	19.3 ± 6	16 ± 3	35.5 ± 2
Heat treated	10 ± 3	21 ± 8	55.5 ± 2

5.3 Conclusion

Effective electrospun nanofibrous membranes should be mechanically stable during different modes of filtration such as dead-end and cross flow. Any kind of compaction and disintegration results in loss of efficiency and even in their failure.

In this study the mechanical performance of this type of membranes under tensile and compressive stresses which are applied during dead-end and cross flow filtrations was investigated. The results show that compaction occurs under compressive stresses which can be somewhat decreased through heat treatment of the ENM. Moreover, the heat treated electrospun nanofibrous mats show better tensile

mechanical properties (static and dynamic) and resist more against tensile disintegration.

On the whole, the obtained results indicate how the PES ENMs behave mechanically during an actual filtration when facing different kind of stresses including static or dynamic tensile or compressive stresses. These findings can help us in proper adjustment of the filtration elements including feed rate and pressure differences to prevent any failure in the membranes. Subsequently, reinforcement of the ENMs to overcome their failure or to increase their longevity can be a strategy to expand their application range. Heat treatment as a modification approach was not that efficient to prevent compaction considerably. In next chapters, other modification solutions i.e. nanocomposite strategy will be emphasized.

5.4 References

[1] C. Burger, B. S. Hsiao, and B.Chu, Nanofibrous materials and their applications, Annu. Rev. Mater. Res. 36(2006) 333–68.

[2] David R. Nisbet, Andrew E. Rodda, David I. Finkelstein, Malcolm K. Horne, John S. Forsythe,Wei Shen, Surface and bulk characterisation of electrospun membranes: Problems and improvements, Colloids and Surfaces B: Biointerfaces 71 (2009) 1–12.

[3] Kyunghwan Yoon, Benjamin S. Hsiao, Benjamin Chu, Formation of functional polyethersulfone electrospun membrane for water purification by mixed solvent and oxidation processes, Polymer (2009) 1–7.

[4] S.Sh.Homaeigohar, K. Buhr, K.Ebert, Polyethersulfone electrospun nanofibrous composite membrane for liquid filtration, Journal of membrane science 365(2010)68-77.

[5] R.W. Baker, E.L. Cussler, W. Eykamp, W.J. Koros, R.L. Riley, H. Strathmann, Membrane Separation Systems; Recent Developments and Future Directions, Noyes Data Corporation, 1991.

[6] G.M. Pharr, Measurement of mechanical properties by ultra-low load indentation, Materials Science and Engineering A253 (1998) 151–159.

[7] W.C. Oliver, G.M. Pharr, An improved technique for determining hardness and elastic modulus using load and displacement sensing indentation experiments, J. Mater. Res. 7 (1992) 1564.

[8] Xiaodong Li, Bharat Bhushan, A review of nanoindentation continuous stiffness measurement technique and its applications, Materials Characterization 48 (2002) 11– 36.

[9] W.J. Sichina, Prediction of polymer damping properties using the diamond DMA and master curves, Perkin Elmer Instruments, application note.

[10] L. Cheng, X. Xia, L.E. Scriven, W.W. Gerberich, Spherical-tip indentation of viscoelastic material, Mechanics of Materials 37 (2005) 213–226.

[11] B J Briscoey, L Fiori and E Pelillo, Nanoindentation of polymeric surfaces, J. Phys. D: Appl. Phys. 31 (1998) 2395–2405.

[12] Davide Tranchida, Stefano Piccarolo, Joachim Loos, and Alexander Alexeev, Mechanical characterization of polymers on a nanometer scale through nanoindentation. A study on pile-up and viscoelasticity, Macromolecules 40(2007) 1259-1267.

[13] S.O. Kucheyev, A.V. Hamza, J.H. Satcher Jr, M.A. Worsley, Depth-sensing indentation of low – density brittle nanoporous solids, Acta Materialia 57 (2009) 3472-3480.

[14] G. Lu, G.Q. (Max) Lu, Z.M. Xiao, Mechanical properties of porous materials, Journal of Porous materials 6 (1999) 359-368.

[15] Rajinder Pal, Porosity-dependence of Effective Mechanical Properties of Pore-solid Composite Materials, Journal of Composite Materials 39(2005) 1147.

[16] Lawrence, E. N. and Robert, F. L., Mechanical Properties of Polymers and Composites (2nd ed.). Marcel Dekker, 1994.

[17] Sung-Seen Choi, Seung Goo Lee, Chang Whan Joo, Seung Soon Im, Seong Hun Kim, Formation of interfiber bonding in electrospun poly(etherimide) nanofiber web**,** Journal of Materials Science 39 (2004) 1511–1513.

[18] Zuwei Ma, M. Kotaki, S. Ramakrishna, Surface modified nonwoven polysulphone (PSU) fiber mesh by electrospinning: A novel affinity membrane, Journal of Membrane Science 272(2006) 179–187.

[19] Renuga Gopal, Satinderpal Kaur, Zuwei Ma, Casey Chan, Seeram Ramakrishna, Takeshi Matsuura, Electrospun nanofibrous filtration membrane, Journal of Membrane Science 281(2006) 581–586.

[20] P. Yucheng, SQ Sheldon, KG Moon, Effect of temperature on the dynamic mechanical properties of resin film and wood, Forest product journal, 58(12)(2008) 191954516.

[21] A.A. Mehmet-Alkan, F. Biddlestone, J.N. Hay, The thermal properties of polyether sulphone, Thermochimica Acta 256(1995) 123-135.

[22] Yucai Hu, Lu Shen, Hai Yang, Min Wang, Tianxi Liu, Tao Liang, Jiang Zhang, Nanoindentation studies on Nylon 11/clay nanocomposites, Polymer Testing 25(2006) 492–497.

[23] P. Lee-Sullivan, D. Dykeman, Guidelines for performing storage modulus measurements using the TA Instruments DMA 2980 three-point bend mode. I. Amplitude effects, Polym. Test. 19 (2000) 155-164.

[24] V. Thomas, MV Jose, S Chowdhury, JF Sullivan, DR Dean,YK Vohra, Mechano-morphological studies of aligned nanofibrous scaffolds of polycaprolactone fabricated by electrospinning, J Biomater Sci Polym Edn 17(2006) 969–984.

Chapter 6.
Modification of the mechanical properties of polyethersulfone electrospun nanofibrous membranes using zirconia nanoparticles

Chapter 6.

Modification of the mechanical properties of polyethersulfone electrospun nanofibrous membranes using zirconia nanoparticles

6.1 Introduction

As mentioned in the previous chapter, electrospun nanofibrous membranes (ENMs) despite possessing optimum filtration characteristics suffer from low mechanical properties. This problem is mainly due to their extremely high porosity which can lead to a high compaction and as a result low filtration efficiency. Hence, mechanically strengthening of electrospun nanofibrous membranes could be a very critical objective to maintain the optimum filtration efficiency. Several approaches such as heat treatment [1,2,3] and solvent induced interfiber bonding [4] have been adopted to meet this requirement.

The previous study (chapter 5) demonstrated a slightly improved mechanical properties of the PES ENMs after heat treatment due to interfiber bonding. However, the heat treated ENMs also underwent compaction and became brittle. Therefore, in the current study, as the second mechanical enhancement approach, incorporation of zirconia nanoparticles into PES nanofibers is investigated.

Incorporation of nanoparticles into polymeric materials enhances the mechanical properties of the composites. As an example, for nearly a century nanoparticular fillers (e.g. carbon black) have been used in the rubber industry to increase the mechanical strength of rubber composites. [5] This idea can be also applicable for electrospun nanofibers used as filtration membranes to strengthen them. In the review of electrospinning by Dzenis synthesis of composite nanofibers was declared to be one of the biggest breakthroughs in the field reported to date. [6]

Zirconia is a known inorganic material that through a phase transformation toughening mechanism exhibits the best mechanical properties of oxide ceramics. The mechanical stresses induce a phase transformation from metastable tetragonal grains to the monoclinic phase at the crack tip. This transformation is accompanied by volume expansion inducing compressive stresses and suppressing crack propagation. [7] Despite the promising mechanical properties, zirconia has found a few applications e.g. as a bulk material in organo-mineral (polysulfone and polyvinylidene fluoride)

ultrafiltration membranes. In such applications, zirconia has been utilized with grain sizes in the micrometer range and the properties and effects have never been examined at the nanoscale. [8] Hence, the current study is considered a novelty from such aspect.

The other goal sought after addition of zirconia nanoparticles is lowering the hydrophobicity of the membrane and optimizing anti fouling property of the ENM for some aqueous based filtration applications.

In the forthcoming research, the effect of addition of zirconia nanoparticles on mechanical performance of the PES ENM is characterized under compressive and tensile forces by nanoindentation, tensile test and dynamic mechanical analysis (DMA). Additionally, water contact angle measurement can show any alteration in hydrophobicity of the ENMs by addition of zirconia nanoparticles. Finally, water flux measurements can prove the probable improvement of filtration efficiency of the reinforced PES ENMs.

6.2 Results and Discussion

6.2.1 Zirconia particle size distribution in PES solutions and fibers

As explained in chapter 3, the composite nanofibrous membranes were prepared through physical blending of the zirconia nanoparticles with the PES solution and then electrospinning. The particle size distribution of zirconia nanoparticles before electrospinning was detertmined by Photon Correlation Spectroscopy (PCS).

In figure 6.1 particle size distribution of the zirconia particles in the PES solutions to be electrospun is observed. The agglomeration of the primary zirconia nanoparticles despite ultrasonication and stirring is inevitable. The average particle size for 1, 5 and 7 wt% zirconia are 130, 420 and 260 nm, respectively. Other than 1 wt% zirconia, the two other concentrations show a broad distribution mode (polydispersity indices (PIs) for 1, 5 and 7 wt% zirconia are 0.08, 0.16 and 0.25, respectively).

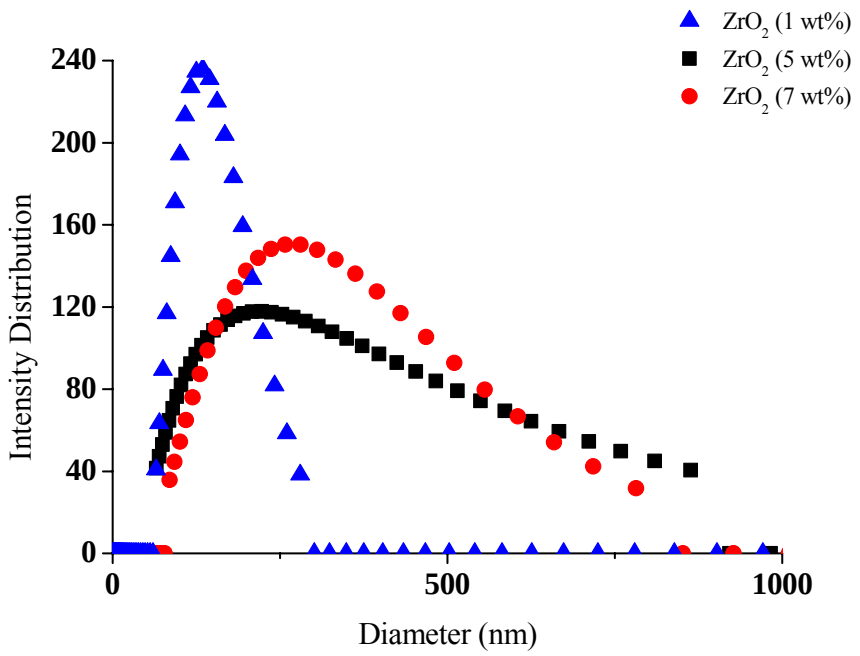

Figure 6.1: Particle size distribution of zirconia particles in the suspensions prepared for electrospinning

While particle size analysis performed on the solutions to be electrospun implied agglomeration of the nanoparticles, as seen in figures 6.2, TEM observations confirmed the presence of zirconia nanoparticles embedded into the nanofibers approximately with their original size of ~ 29–68 nm.

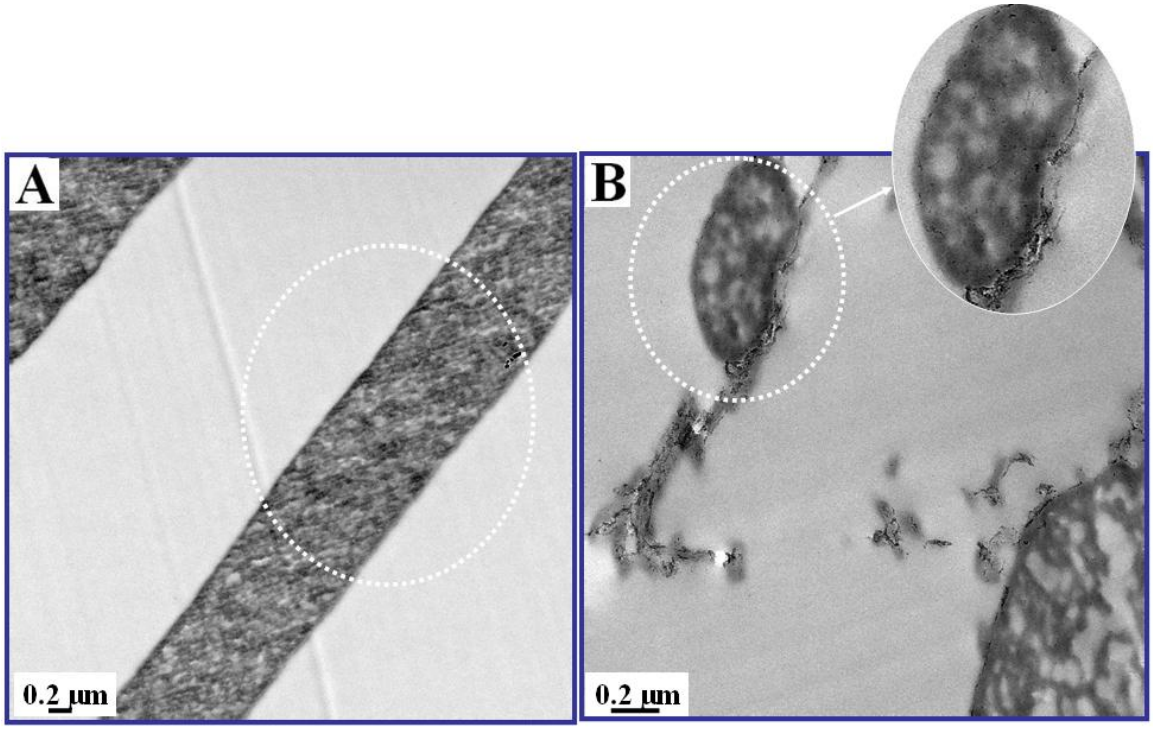

Figure 6.2: TEM pictures showing embedding of very fine nanoparticles inside the fibers containing A) 5 wt% B) 7 wt% zirconia nanoparticles

During electrospinning and especially at the beginning i.e in the transition zone between the Taylor cone and the thin jet zone, the solution jet is subjected to a high amount of longitudinal viscoelastic stress [9] which can disrupt the agglomerates of zirconia nanoparticles and make a uniform dispersion of very fine nanoparticles. However, as seen in figure 6.2, at 7 wt% zirconia, due to the "coffee stain" effect[10], most of the nanoparticles are located at the skin layer and slightly agglomerate. This difference in distribution mode of the nanoparticles compared to the previous composition (5 wt%) is due to the higher outward diffusion of the residual solvent induced by a higher applied voltage for the more viscous solution.

6.2.2 Morphological properties of the zirconia/PES nanofibrous mats

As the presence of zirconia nanoparticles might affect the morphological properties (for example by bead formation) of the electrospun nanofibers, scanning electron micrographs (SEM) were taken of the PES electrospun nanofibers with and without zirconia particles. According to the SEM images shown in figure 6.3, the nanoparticles were not visible on the surface of the nanofibers implying their encapsulation inside the nanofibers. Furthermore, no bead formation was observed for the composite nanofibers of all compositions compared to the neat ones.

Indeed, only the ENM with 5 wt% zirconia shows an exceptional behaviour. At this concentration, the nanocomposite mat constitutes of fibers with smooth surface and more uniform diameter distribution whereas all the other compositions possess a relatively rough surface.

While addition of the inorganic filler increases the viscosity and viscoelastic force, it hampers the surface tension of the PES solution to be electrospun. Consequently, formation of structural irregularities such as beads and surface roughness decreases and the fiber diameter distribution becomes more uniform. [11]

However, higher viscoelastic force leads to a higher resistance against electrostatic force stretching the jet. At higher nanofiller concentrations, i.e. 5 and 7 wt% this effect magnifies the fiber diameter.[12,13] Owing to higher nanofiller content, the highest viscoelastic force is seen at 7 wt% zirconia which inhibits a continuous jet formation. Hence, to continue electrospinning a higher voltage is needed which subsequently, as seen in figure 6.3 F, leads to nanofibers, which are thinner, and owing to higher outward diffusion of the residual solvent possess rougher and more

porous surface in comparison to the former composition i.e. 5 wt% electrospun at a lower voltage (figure 6.3 E). [14]

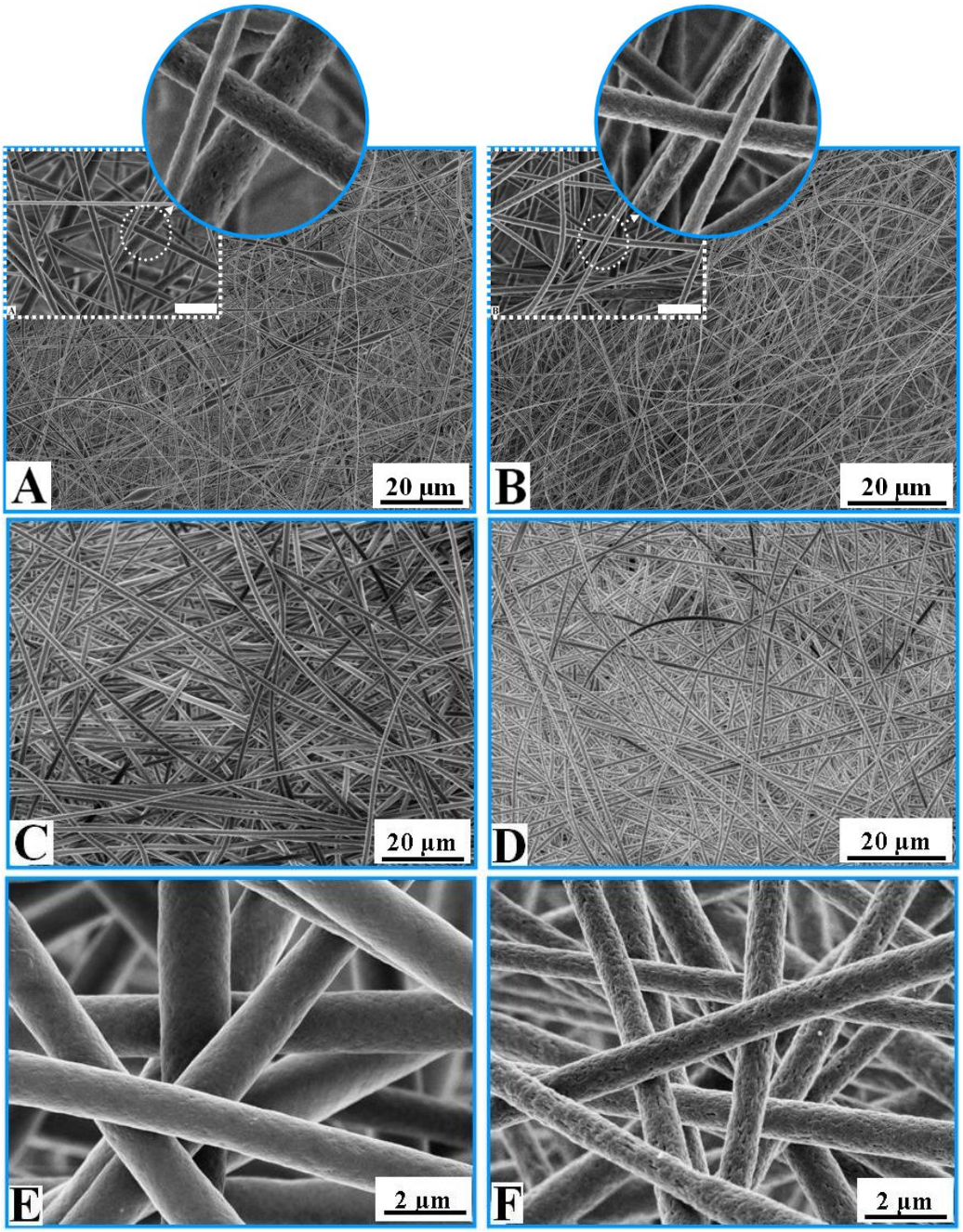

Figure 6.3: Surface morphology, bead formation and size (diameter) distribution of the nanofibers with and without the zirconia particles: the PES nanofibrous mat with A) 0 wt%, B) 1 wt%, C) 5 wt% (x 1000), D) 7 wt% (x1000), E) 5 wt% (x10,000), F) 7 wt% zirconia nanoparticles (x10,000)

The aforementioned findings about nanofiber diameter variation and diameter distribution mode, nanofiber surface roughness and embedding of the nanoparticles might influence the mechanical and wettability performance of the membranes and thus can be of significant importance.

6.2.3 Mechanical characterizations

Keeping in mind the above mentioned influential factors alterations, the mechanical properties of the electrospun membranes were investigated through several mechanical tests including nanoindentation, tensile test and DMA.

Nanoindentation tests can give us an overview about the mechanical behaviour of the ENMs especially about their compaction under a compressive force. The main desirable properties including recovery index (compaction), storage modulus (E') and the mean pressure ($\overline{P}$) are inferred from the obtained nanoindentation graphs shown in figure 6.4.

Furthermore, the calculated recovery indices according to equation 3.7, are presented in table 6.1 and figure 6.5A. It is seen that addition of zirconia up to 5 wt% results in a higher recovery index i.e. lower compaction. However, at the concentration of 7 wt% the composite nanofibers undergo a high amount of compaction comparable to the neat ones.

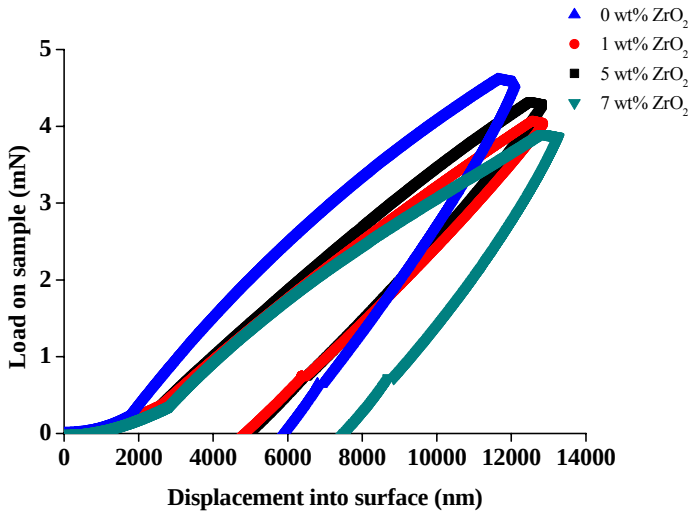

Figure 6.4: The load-displacement curve obtained by nanoindentation test for the ZrO_2 /PES nanofibrous mats

Table 6.1: Recovery index of the ZrO_2 /PES nanofibrous mats

ZrO_2 (wt%)	Recovery index (%)
0	48 ± 6
1	60 ± 1
5	59 ± 2.5
7	42.5 ± 1.4

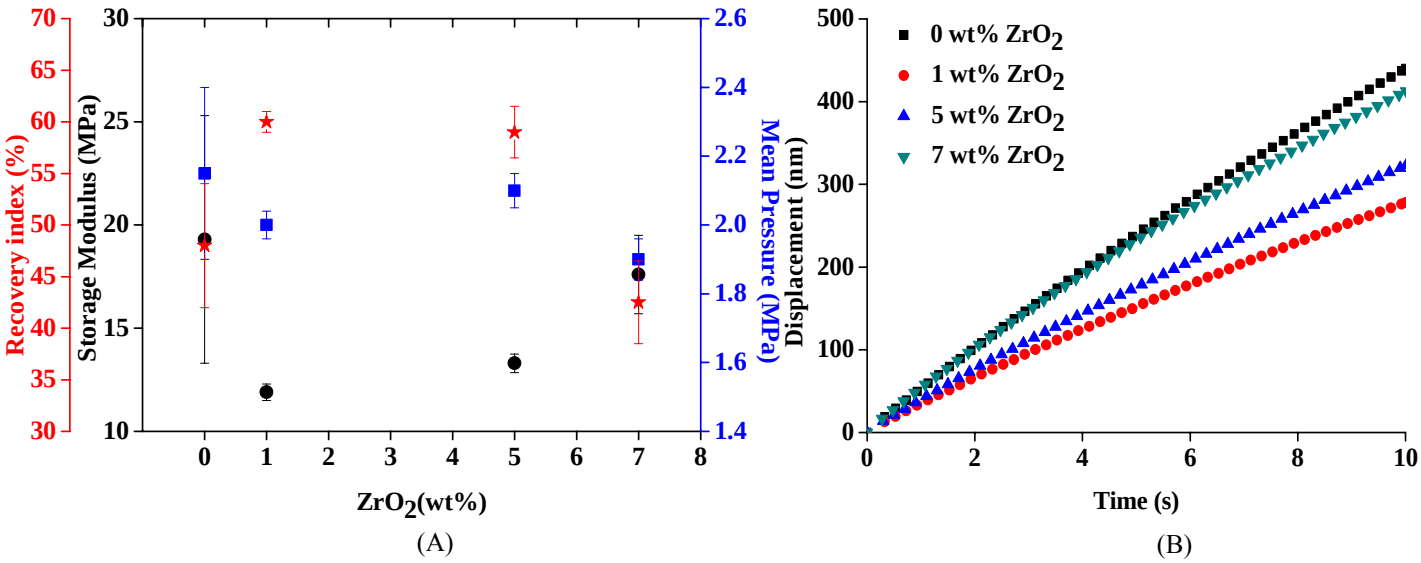

Figure 6.5: A) the storage modulus, mean pressure and recovery index of the ZrO_2 /PES nanofibrous mats obtained by nanoindentation test; B) Variation of displacement at hold segment of load representative of creep of the PES electrospun nanofibrous mats

To discuss the compaction behaviour, at first glance two main parameters appear to be more important i.e. nanofiller amount and fiber diameter. The smaller the fiber diameter and the higher the nanofiller content are, the lower compaction is expected. Indeed, smaller fiber diameter means a severer stretching of the jet while electrospinning and a higher molecular chain orientation along the fiber axis which as a result lowers ductility. [15] But when considering almost equal fiber diameters for neat fibers and those with 1 wt% zirconia and significant difference in their compaction values, it seems that the compaction should be more influenced by the nanofiller amount. However, the more similar compaction values for 1 and 5 wt% zirconia and lower value for 7 wt% contradict to the previous conclusion. Hence, it seems that some more parameters are also influential on the compaction values. For instance, according to TEM images (figure 6.2B) some agglomeration occurs at 7 wt% and due to the "coffee stain" effect [10] and outward diffusion of the residual solvent, the nanoparticles are mostly localized at the skin layer rather than in the core of the fibers. Agglomeration decreases the interaction at the particle-polymer interface thereby inhibiting an efficient load transfer. Additionally, agglomerates are weak points in the material and under stress they can break easily. A broken agglomerate then behaves as a strong stress concentrator. [16, 17, 18] Therefore a uniform dispersion of zirconia nanoparticles inside the nanofibers seems to be one of the main reasons for much lower compaction at the concentrations of 1 and 5 wt%. Along with agglomeration,

surface roughness and pores (figure 6.3F) acts as a stress concentration point and weakens the nanofibers with 7 wt% zirconia compared to those with 5 wt%. Hence, the other main reason for the higher compaction resistance of the mat containing 5 wt% nanofiller is the surface smoothness of the fibers. Such a high compaction resistance is very promising for filtration applications. A lower compaction means preservation of the porous structure (porosity and interconnectivity of the pores) of the membranes and as a result a more stable filtration efficiency during operation.

As seen in figure 6.5A, the calculated values of E' according to equation 3.6, imply higher storage moduli of the neat PES and the composite nanofibers containing 7 wt% zirconia nanoparticles than that of the composite nanofibers with 1 and 5 wt% zirconia. The most probable reason is the higher compaction and lower amount of porosity of these ENMs. [19,20] Naturally, among two composite nanofibers with lower storage moduli i.e. those with 1 and 5 wt% zirconia, 5 wt% ZrO_2/PES membranes show a higher storage modulus mainly because of more amount of dispersed nanofiller.

The mean pressure results (determined according to equation 3.5), presented in figure 6.5A, showed that the highest mean pressure belongs to the neat PES ENMs mainly due to its high compaction and smaller fiber diameter. Among the composite fibrous membranes, those with 5 and 7 wt% zirconia show the highest and lowest mean pressures attributed to high effective amount of the nanofiller uniformly embedded into the nanofibers, smooth surface and uniform diameter distribution of the fibers at 5 wt% while high surface roughness and porosity of the fibers and agglomeration at the highest filler concentration.

The hold time at the maximum load was used to show the creep effect of the electrospun nanofibrous mats. Increase of displacement (indentation depth) at the maximum load represents the creep. Figure 6.5B shows that the lowest and highest creep belong to the composite nanofibers containing 1 and 7 wt% zirconia, respectively. In contrary to the highly agglomeration suffering 7 wt% composite nanofibers, low ductility owing to uniform embedding of nanoparticles and small nanofiber diameter makes the 1 wt% composite nanofibers the most creep resistant.

The electrospun nanofibrous membranes while dead-end and cross flow filtration modes are also exposed to tension stresses. The tensile performance of the composite PES ENMs under static and dynamic forces were evaluated. As seen in figure 6.6, according to the tensile test results, tensile strength, modulus and

elongation of the PES ENMs increase with addition of zirconia amount. The maximum magnitudes of such properties are seen at 5 wt% zirconia, while at 7 wt% these properties decline compared to the previous composition indicating the important role of efficient nanoparticles embedding mode along with surface smoothness and the suppressing effect of surface roughness and porosity. A similar mechanical performance in terms of the storage and loss moduli is deduced from the DMA results shown in figure 6.7. Moreover, for all the samples, the dynamic moduli show a constant linear trend independent to the applied frequencies.

Increase of loss modulus (damping) and elongation of the reinforced membranes is a very interesting and important finding implying high ductility i.e. low brittleness of the ENMs after incorporation of the zirconia nanoparticles. This feature makes the ZrO_2/PES ENMs superior to nanofibrous membranes filled with other ceramic nanoparticles.[21]

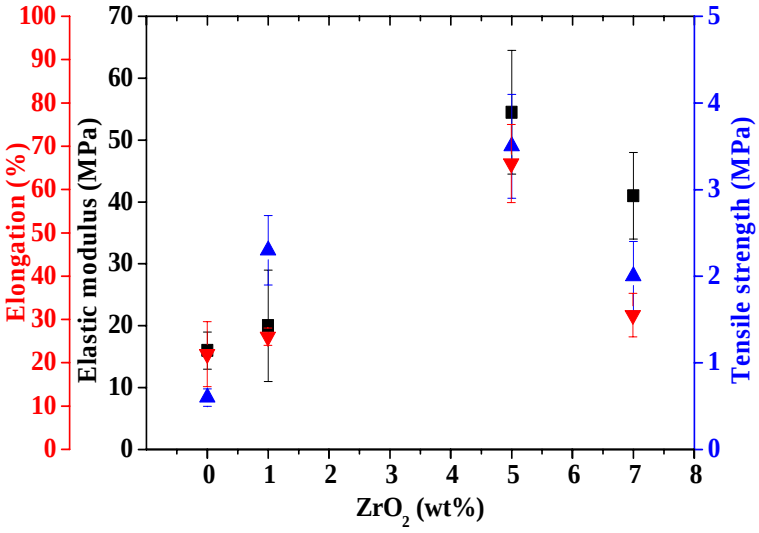

Figure 6.6: Tensile properties of the neat and reinforced PES electrospun nanofibrous mats

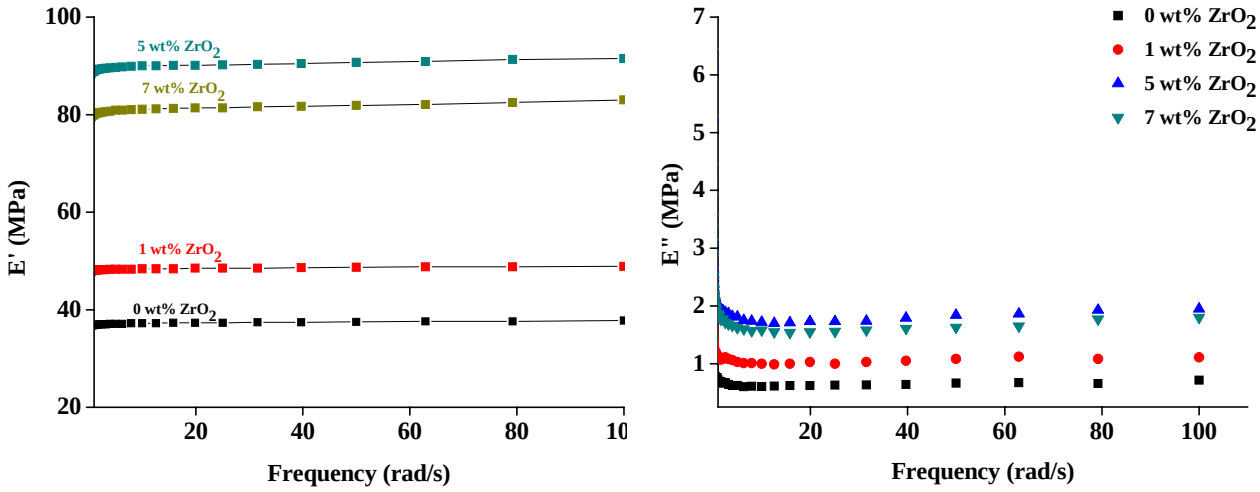

(A) (B)

Figure 6.7: Dynamic tensile properties of the neat and reinforced PES electrospun nanofibrous mats:A) storage modulus ; B) loss modulus

6.2.4 Water contact angle measurement

For the hydrophobic PES electrospun nanofibrous membrane to be proposed for water filtration, in addition to mechanical performance, wettability can also be a concern. Addition of zirconia nanoparticles could be also beneficial to increase wettability. Water contact angle (WCA) measurements, as shown in figure 6.8, imply a lower hydrophobicity of the ZrO_2/PES electrospun nanofibrous membranes as compared to the neat PES nanofibers. The water contact angle of 120° for the neat PES nanofibers decreases to 105° for those containing 5 wt% zirconia. The WCA of 7 wt% ZrO_2/PES nanofibers is slightly higher than that of the fibers containing 5 wt% zirconia due to a higher surface roughness preventing full contact of water with nanofiber surface.

In general, incorporation of polar ceramic nanoparticles such as zirconia is expected to make the hydrophobic membranes more hydrophilic. But this effect is only rather weak in our systems. Such performance can be attributed to embedding of the nanoparticles into the PES nanofibers. Such process does not let the particles be exposed on the surface. In fact the particles are mostly entrapped into the nanofibers. Therefore, the nanoparticles are more beneficial in terms of the mechanical properties rather than wettability.

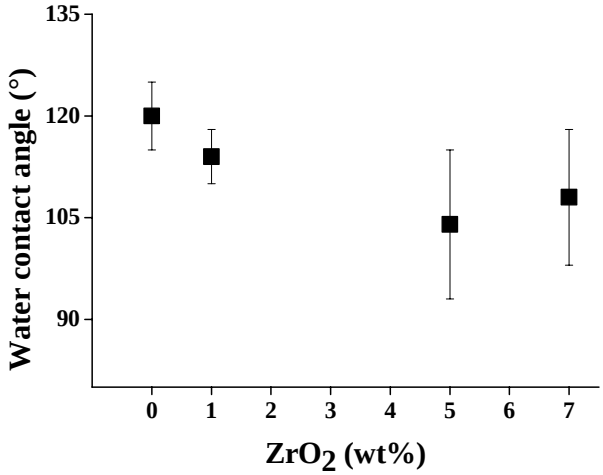

Figure 6.8: Water contact angle measured for the neat and reinforced PES electrospun nanofibrous mats

6.2.5 Water flux measurement

The zirconia nanoparticles were added to the PES electrospun nanofibers to enhance mechanical performance and wettability of the PES ENMs, consequently the filtration efficiency i.e. permeability. Water flux measurements as presented in figure 6.9, show a significantly ascending trend for the zirconia reinforced PES ENMs with a peak at 5 wt%. The results prove that addition of the inorganic filler considerably enhances permeability of the ENMs during filtration.

To discuss the permeance behavior of the composite nanofibrous membranes, three influential factors including mechanical properties, wettability, fiber diameter and subsequently pore size should be taken into account.

Considering almost comparable areal density and porosity, the fibers with bigger diameter create bigger pores. [22] According to the Hagen-Poisseule's equation (equation 6.1) increase of pore size (r) of the ENMs due to presence of bigger fibers at higher zirconia concentrations can result in a higher flux [23,24]:

$$J = \frac{\varepsilon r^2}{8\mu\tau}\frac{\Delta P}{\Delta x} \qquad \text{Eq. 6.1}$$

where J is the water flux (m^3/s), ε the porosity (-), r the pore radius (m), τ the tortuosity (-), ΔP the pressure difference across the membrane (Pa) (1 Pa=10^{-5} bar), μ the dynamic viscosity (Pa s) and Δx the membrane thickness (m).

However, at the concentration of 1 wt% zirconia despite an equal fiber diameter with the neat PES nanofibers, the composite nanofibrous membrane show an

almost two times higher water flux. This finding confirms that the main reason for such a rise in permeability is the enhanced mechanical properties obtained through embedding the inorganic filler into the electrospun nanofibers. This effect in presence of an improved wettability at higher concentrations results in a significantly higher permeability. The best mechanical performance and wettability seen at the concentration of 5 wt% zirconia leads to the highest permeance among all the ENMs investigated in this study. Compared to this composition, the highest concentration i.e. 7 wt% show a decline in permeance, mainly attributed to lower mechanical properties and wettability.

Such a promising behavior in terms of mechanical stability, wettability and permeance lead us to suggest 5 wt% ZrO_2/PES ENMs for water filtration applications. It is assumed that low compaction and high permeability of this composite membrane gives rise to a longer lifespan and lower energy consumption.

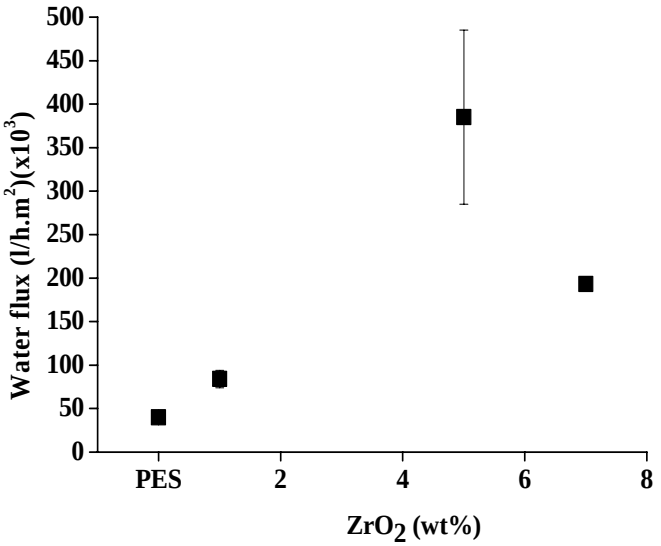

Figure 6.9: Water flux measured for the neat and zirconia nanoparticle reinforced PES electrospun nanofibrous mats

6.3 Conclusion

It was proved that mechanical stability of ENMs during different modes of filtration such as dead-end and cross flow plays the major role in preservation of their very high permeance. In fact, to prevent any kind of compaction and disintegration resulting in failure and loss of efficiency, ENMs should be somehow mechanically strengthened.

To do so, for the first time the PES ENMs were reinforced with zirconia nanoparticles. The results obtained indicate a critical amount of 5 wt% zirconia which could provide the best water permeance mainly due to a major enhancement in mechanical properties of the ENMs. This enhancement is caused by a good dispersion of the zirconia nanoparticles in the composiute fibres rather than on the surface. These nanoparticles are not only excellent inherent mechanical modifiers, but also improve structural properties of the electrospun mats such as a smooth fiber surface, no bead defects and more uniform fiber diameter distribution. This finding guarranties the more efficient filtration performance of the composite PES ENMs as compared to the neat PES ones. Mechanical reinforcement of such kind of highly porous membranes leads to preservation of their extraordinary water permeance, longer life span and lower energy consumption.

Despite a very promising enhancement of mechanical propoerties, wettability of the electrospun membrane due to embedding of the nanoparticles did not increase considerably. It is believed that another composite fabrication method able to expose more inorganic nanoparticles on the surface could be more beneficial in such a term. Higher hydrophilicity could lead to a lower filtration resistance and fouling tendency. Hence, the research is continued to meet both modification objectives including mechanical enhancement and hydrophilization.

6.4 References

[1] S.Sh.Homaeigohar, K. Buhr, K.Ebert, Polyethersulfone electrospun nanofibrous composite membrane for liquid filtration, Journal of membrane science, 365(2010)68-77.

[2] SS Choi, SG Lee, CW Joo, SS Im, SH Kim, Formation of interfiber bonding in electrospun poly(etherimide) nanofiber web**,** Journal of Materials Science 39 (2004) 1511 – 1513.

[3] Z. Ma, M. Kotaki, S. Ramakrishna, Surface modified nonwoven polysulphone (PSU) fiber mesh by electrospinning: A novel affinity membrane, Journal of Membrane Science 272 (2006) 179–187.

[4] K Yoon, BS. Hsiao, B. Chu, Formation of functional polyethersulfone electrospun membrane for water purification by mixed solvent and oxidation processes, Polymer (2009) 1–7.

[5] M. Yanagioka and CW. Frank, Effect of particle distribution on morphological and mechanical properties of filled hydrogel composites, Macromolecules 41(2008) 5441-5450.

[6] Y. Dzenis, Spinning continuous fibers for nanotechnology, Science 304(2004) 1917-1919.

[7] J. Chevalier, What future for zirconia as a biomaterial?, Biomaterials 27 (2006) 535–543.

[8] J. Kim, B. Van der Bruggen, The use of nanoparticles in polymeric and ceramic membrane structures: Review of manufacturing procedures and performance improvement for water treatment, Environmental pollution158(2010) 2335-2349.

[9] T. Han, A.L. Yarin, DH. Reneker, Viscoelastic electrospun jets: Initial stresses and elongational rheometry, Polymer 49 (2008) 1651-1658.

[10] RD. Deegan, O. Bakajin, TF. Dupont, G. Huber, SR. Nagel, TA. Witten, Capillary flow as the cause of ring stains from dried liquid drops, Nature 389(1997) 827-829.

[11] H. Fong, I. Chun and D. H. Reneker, Beaded nanofibers formed during electrospinning, Polymer 40(16) (1999) 4585-4592.

[12] C. Burger, B.S. Hsiao, B. Chu, Nanofibrous materials and their applications, Annual Review of Materials Research 36 (2006) 333-68.

[13] O.S. Yördem, M. Papila, Y.Z. Mencelog˘lu, Effects of electrospinning parameters on polyacrylonitrile nanofiber diameter: An investigation by response surface methodology, Materials and Design 29 (2008) 34–44.

[14] KM. Sawicka and P. Gouma, Electrospun composite nanofibers for functional applications, Journal of Nanoparticle Research 8(2006) 769-781.

[15] Z. Chen, B. Wei, X. Mo, C.T. Lim, S. Ramakrishna, F. Cui, Mechanical properties of electrospun collagen–chitosan complex single fibers and membrane, Materials Science and Engineering C 29 (2009) 2428–2435.

[16] R. Roger, Particulate-filled Polymer Composites, 2nd ed., Shrewsbury, Rapra Technology Limited, 2003.

[17] E.N. Lawrence, F.L. Robert, Mechanical Properties of Polymers and Composites, 2nd ed., New York, Marcel Dekker, 1994.

[18] S.Sh. Homaeigohar, A. Yari Sadi, J. Javadpour, A. Khavandi The effect of reinforcement volume fraction and particle size on the mechanical properties of β-tricalcium phosphate–high density polyethylene composites, Journal of the European Ceramic Society 26 (2006) 273–278.

[19] R. Pal, Porosity-dependence of Effective Mechanical Properties of Pore-solid Composite Materials, Journal of Composite Materials 39(2005) 1147.

[20] G. Lu, G.Q. (Max) Lu, Z.M. Xiao, Mechanical properties of porous materials, Journal of Porous materials 6 (1999) 359-368.

[21] YJ Kim, CH Ahn, MB Lee, MS Choi,Characteristics of electrospun PVDF/SiO2 composite nanofiber membranes as polymer electrolyte, Materials Chemistry and Physics 127(2011) 137-142.

[22] SJ Eichhorn, WW. Sampson, Statistical geometry of pores and statistics of porous nanofibrous assemblies, JRSoc Interface 2(4)(2005) 309-18.

[23] B. Van der Bruggen, C. Vandecasteele, T. Van Gestel, W. Doyen and R. Leysen, A Review of Pressure-Driven Membrane Processes in Wastewater Treatment and Drinking Water Production, Environmental Progress 22(1)(2003) 46-56.

[24] K. Yoon, K. Kim, X. Wang, D. Fang, BS. Hsiao, B.Chu, High flux ultrafiltration membranes based on electrospun nanofibrous PAN scaffolds and chitosan coating, Polymer 47 (2006) 2434–2441.

Chapter 7.

Enhancement of wettability, thermal and mechanical stability of PES electrospun nanofibrous membranes through incorporation of TiO_2 nanoparticles by using a sol-gel approach

Chapter 7.

Enhancement of wettability, thermal and mechanical stability of PES electrospun nanofibrous microfiltration membranes through incorporation of TiO_2 nanoparticles by using a sol-gel approach

7.1 Introduction

In recent years, electrospinning as a novel efficient manufacturing method of nanofibrous structures have been employed for a diverse range of applications including filtration.[1] High porosity (even >90%) along with interconnected pores in the size range of only a few times to a few ten times the fiber diameter are very promising structural features which make electrospun nanofibrous mats as a suitable candidate for filtration applications. The mentioned structural features result in a higher permeability and selectivity in this kind of membranes.[2,3,4,5,6,7] On the other hand, high porosity and surface area of the electrospun nanofibrous membranes make them more exposed to mechanical stresses and depending on the material hydrophobic interactions leading to clogging the pores and fouling. Therefore, to preserve high permeability and filtration efficiency of such kind of membranes, they should be mechanically reinforced and hydrophilized.

As the previous study, zirconia (ZrO_2) nanoparticles were added to poly(ether sulfone) (PES) electrospun nanofibrous membrane (ENM) to make them stronger and more hydrophilic. The ZrO_2/PES ENMs showed an optimum mechanical performance but not wettability most likely due to presence of the nanoparticles inside the nanofibers rather than on the surface. In fact, it is assumed that in the previous approach, the zirconia nanoparticles were encapsulated inside the PES nanofibers. Hence, the current study's spotlight is on mechanical and wettability modification of PES ENM to be proposed for water filtration using a more hydrophilic ceramic nanoparticle i.e. titania (TiO_2). Titania nanoparticles will be resided on the surface of the nanofibers through a sol-gel approach.[8]

Inorganic nanoparticles e.g. TiO_2 nanoparticles are inherently hydrophilic and in case of using as a filler can increase the hydrophilicity of the host polymer matrix. Recently, this group of filler materials as a modifying component has been proposed to improve the properties of polymeric membranes including antifouling, permeation,

thermal and mechanical properties. The application fields of such nanocomposite membranes have encompassed micro- and ultrafiltration, gas separation, as well as pervaporation.[9]

Titanium dioxide (TiO_2) nanoparticles are one of the mostly used inorganic nanoparticles, especially because of their high hydrophilicity, chemical stability, antibacterial property, innocuity, and low cost.[10,11,12] Such promising properties are encouraging to utilize this kind of inorganic nanoparticles to reinforce the PES ENM in two aspects of mechanical and wettability properties.

Due to different polarity status of the host polymer matrix and inorganic nanoparticles which are hydrophobic and hydrophilic, respectively, one of the major challenges in preparation of such nanocomposite membranes is the uniform dispersion of inorganic fillers in polymer matrix.[13] Physical blending of inorganic nanoparticles with polymer matrix is not a suitable approach to create a homogenous dispersion and aggregation is always problematic unless the surface of the nanoparticles are organically hydrophobized.[14] To minimize the aggregation of inorganic nanoparticles in polymer matrix two different approaches have been proposed[13]:

1) In-situ polymerization of polymer monomer in the presence of surface-modified inorganic particles.[15,16] Induction of a proper dispersibility and long term aggregation resistance to the nanoparticles, however, is an obstacle ahead.[17]
2) Inversely, the other method called sol-gel is based on in-situ generation of inorganic particles in organic phase i.e. bulk polymer, polymer solution and monomer systems.[18,19] In such an approach owing to in-situ nucleation and growth of the particles inside the host polymer matrix, they are confined and not able to contact each other and aggregate.

In order to prepare nanoparticulate composite materials with a uniform dispersion of nanofillers, the second approach seems to be more promising. The advantages include very fine particle size and low aggregation mainly due to in-situ growth of inorganic nanoparticles in a limited space of polymer matrix.

In the current study, the PES electrospun nanofibers are modified using TiO_2 nanoparticles by a sol–gel process and the properties of the modified PES ENM are characterized by different characterization tests especially water contact angle measurement and mechanical tests. To investigate the efficiency of the adopted

modification approach on filtration performance i.e. permeability a water flux test was also conducted.

7.2 Results and Discussion

7.2.1 Morphological observations

As explained in the experimental section (chapter 3), the TiO_2 nanoparticles were incorporated into the electrospun PES nanofibers through a sol-gel approach. The SEM micrographs of the PES nanofibers with varying TiO_2 contents are illustrated in figure 7.1. First, comparison of figures 7.1A and B clearly reveals that increase of the amount of TiO_2 results in less bead formation. This feature is attributed to increase of the viscosity also conductivity of the polymer solution due to presence of TBT.[1] Additionally, as shown in figures 7.1C and D, there is a low level of aggregation of TiO_2 nanoparticles in the TiO_2/PES composite nanofibers and the nanoparticles are homogenously dispersed. The TiO_2 nanoparticles formed on the surface of nanofibers possess almost a spherical morphology with an approximate size of 24 ± 8 nm.

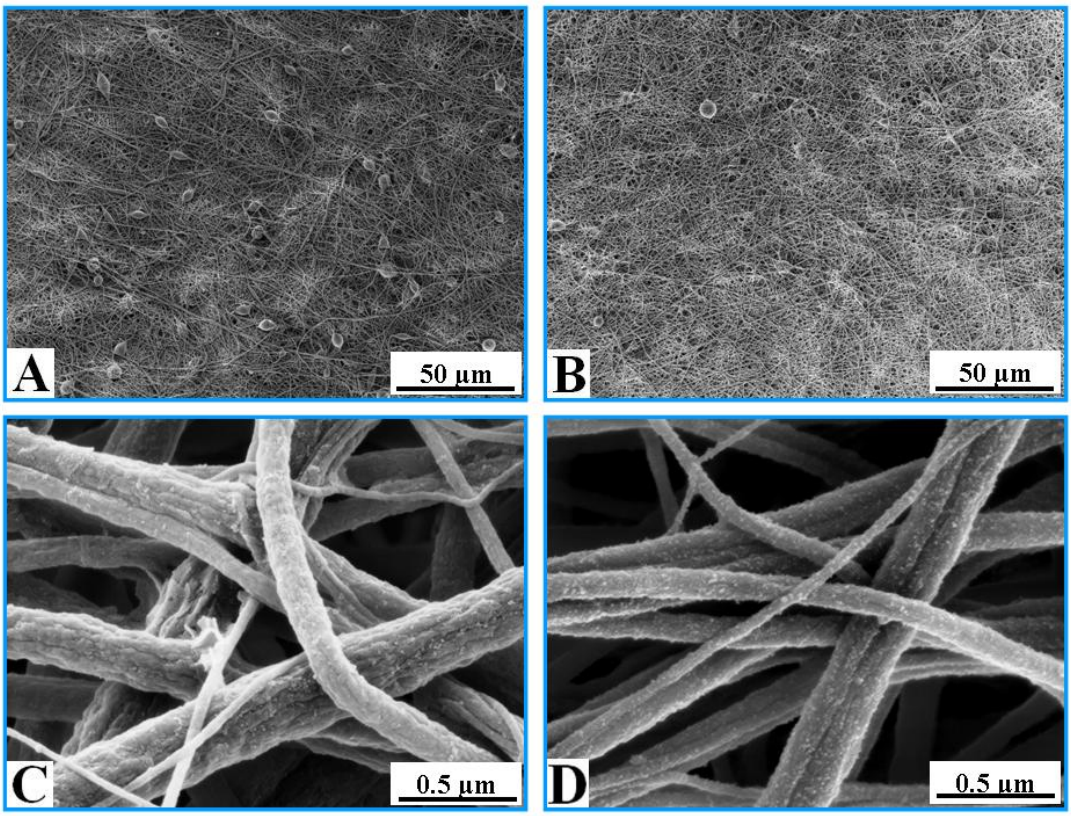

Figure 7.1: The TiO_2/PES electrospun nanofibers containing 5 (A and C) and 8 wt% (B and D) TiO_2 nanoparticles at different magnifications

TEM observations as shown in figure 7.2, also confirm the uniform dispersion of TiO_2 nanoparticles inside and mostly near/on to the surface of the nanofibers. This result is considerably promising as compared to similar researches obtaining domains of nanoparticles in nanofibers i.e. aggregation. [20] The uniform distribution of nanoparticles can be due to the last annealing stage which prevents aggregation of nanoparticles. Furthermore, the eventual chemical bond between the TiO_2 nanoparticles and the sulfone (or ether) functional group of PES can also be a reason for creation of small nanoparticles with a uniform dispersion.

Figure 7.2 demonstrates that the nanoparticles mostly settle near or on the surface of the nanofibers. The most probable reason could be ascribed to a phenomenon called "Coffee stain effect"[21]. Here, evaporation of the solvent from the surface of the jet is compensated with the interior solvent. The dissolved TBT is transferred to the surface of the jet by such an outward flow and is converted to the titania nanoparticles on or near to the surface of the nanofibers. However, this does not deny formation of titania nanoparticles in the core of the nanofibers as well. The interior nanoparticles are formed when a minor part of the TBT is converted to TiO_2 nanoparticles while preparation of the solution to be electrospun or even while the electrospinning. Such nanoparticles owing to an acidic environment caused by TFA, are highly protonated and positively charged. [22] On the other hand, the solution jet ejected from the needle connected to the positive electrode of high-voltage power supply is highly charged. The positive charges accumulating on the outer surface of the electrospinning jet are able to repel the positive charged TiO_2 nanoparticles to the middle of the nanofibers being formed.

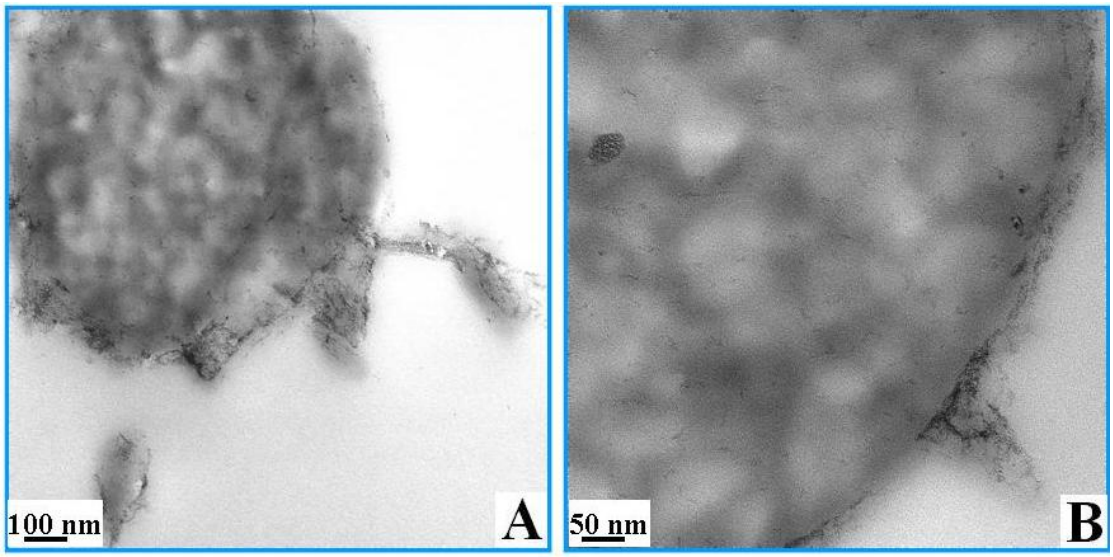

Figure 7.2: TiO_2 nanoparticles (8 wt%) spread in cross- section and on surface of the nanofibers

7.2.2 XRD analysis

Structural analyses of the neat PES and TiO_2/PES ENMs were carried out at room temperature using X-ray diffractometry (XRD). This analysis was important to verify formation of the titania nanoparticles and their probable crystallinity.

XRD pattern of the TiO_2/PES (5 wt%) ENM as compared to the neat one is shown in figure 7.3. The graphs show no significant peak other than the dispersion peak of amorphous PES. On the other hand, as seen in figure 7.3, formation of anatase in the TiO_2/PES ENMs is clearly proved by XRD graph of the pyrolized composite nanofibers. The main crystalline characteristic peaks related to anatase appears at 2θ of 25.30°, 37.8° and 48.04°.[23,24]

Generally, the titania formed through sol-gel approach is amorphous in nature.[25] Amorphous titania is less hydrophilic compared to anatase, hence it should be converted to benefit the high hydrophilic effect of anatase.

A heat treatment process at 100 °C in air can partially convert amorphous titania to anatase giving a mixture of amorphous and nanocrystalline titania.[26] Similarly, Khanna et al. [25] reported this effect for the TiO_2 nanoparticles synthesized in a polyvinyl alcohol (PVA) matrix. According to Wang et al. [27], anatase formed at this temperature is stable even up to 800 °C without conversion to rutile.

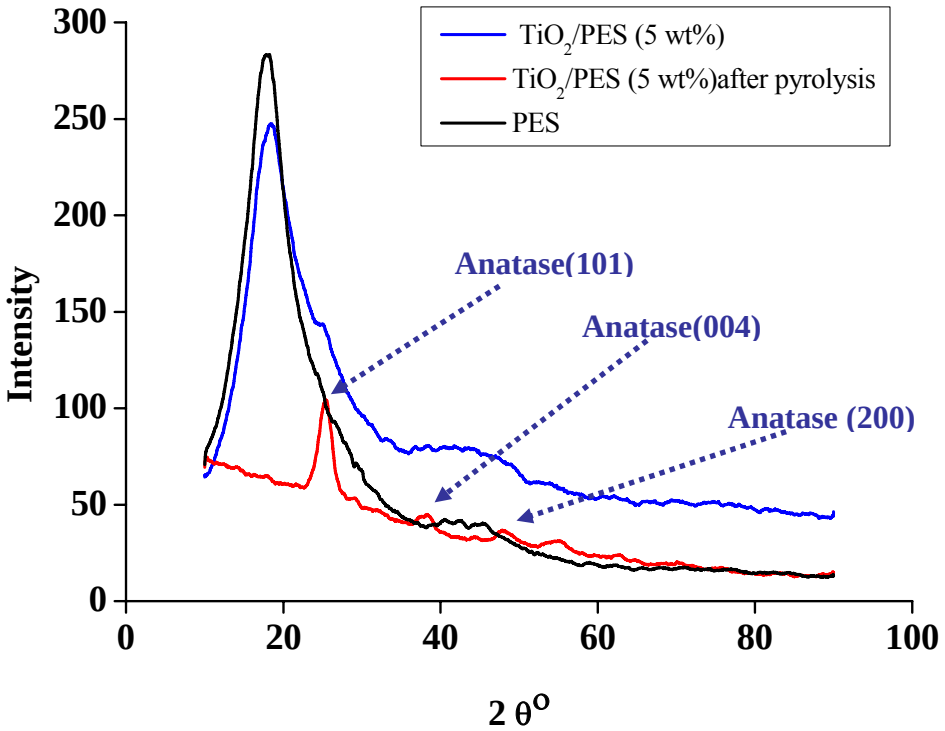

Figure 7.3: X-ray diffraction patterns of the neat PES and TiO_2 /PES ENM (5 wt%) before and after pyrolysis

Low crystallinity of the sol-gel formed titania after the heat treatment along with coincidence of the main crystalline peak of anatase (at 2θ of 25.30°) with broad dispersion peak of amorphous PES can be the reasons for similar XRD patterns of the neat PES and TiO_2/PES ENMs.

7.2.3 Water contact angle measurement

One of the main objectives of addition of titania nanoparticles to the PES ENMs was enhancement of wettability (hydrophilicity) to lower fouling tendency. The alteration of wettability of the ENMs after incorporation of titania nanoparticles can be tracked via water contact angle measurement. The results of contact angle measurements for the PES and TiO_2-incorporated PES ENMs are shown in figure 7.4.

Initially, comparison of the contact angle of PES film [28] with that of the PES electrospun nanofibrous membrane reveals a significant difference. This is due to higher roughness i.e. nanoroughness of the electrospun nanofibrous mats compared to film. Cassie-Baxter wetting model can explain this behavior as: air can remain trapped below the water drop forming "air pockets". Owing to the less contact of water with the surface, hydrophobicity increases. [29] Furthermore, high surface area of the electrospun nanofibers of hydrophobic PES also intensifies the hydrophobicity.

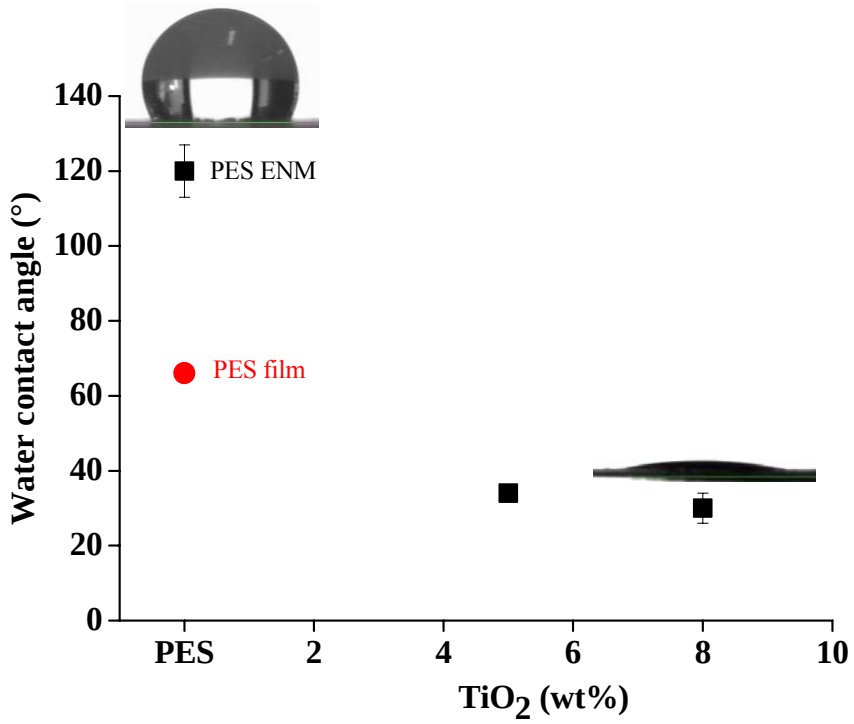

Figure 7.4: Water contact angle measured for the neat and TiO_2 reinforced PES electrospun nanofibrous mats

About the TiO_2/PES ENMs, the water contact angle decreases significantly with increase of TiO_2 amount indicating the higher affinity of the ENMs to water. As shown in figure 7.4, despite high roughness and surface area, the very low contact angle in these membranes imply a high hydrophilicity which is in contrast to the high hydrophobicity of the neat PES ENM. This property is quite promising especially for water filtration application.

7.2.4 Surface chemical properties (ATR-FTIR)

Chemical surface analysis of the neat PES and TiO_2/PES electrospun nanofibrous membranes was performed by Fourier Transform Infra Red Spectrometry (FTIR). Any probable change in surface chemical properties due to addition of the nanoparticles could be identified through this approach.

The general features of the ATR-FTIR spectra of the neat PES and the TiO_2/PES composite ENMs are shown in figure 7.5.

The absorption peaks at 1296 and 1146 cm^{-1} attribute to the asymmetrical and symmetrical vibrations of the sulfone group, respectively. The absorption peak at 1234 cm^{-1} attributes to the stretching vibration of the ether C-O-C bond in the PES polymer.[30] Comparison of the ATR-FTIR spectra of the ENMs as composite and neat reveals a shift in the position of the peak at 1234 cm^{-1} for the neat PES ENM to 1239 and 1241 cm^{-1} for the composite ENMs with 5 and 8 wt% TiO_2, respectively. This shift is due to the in situ formation of TiO_2 nanoparticles in the PES matrix. As shown in the inset figure, hydrogen bondings between the Ti-OH or Ti-$OCH_2CH_2CH_2CH_3$ and ether C-O-C bond (or sulfone SO_2 group) while the hydrolysis and condensation of TBT lead to partially cross-linking reactions thereby a shift in the peaks related to the PES functional groups.[31]

Besides peak shift, as represented in figure 7.5, intensity of the peaks also declines proportionally to titania content. The main reason for such a behavior is formation of TiO_2 nanoparticles and subsequent coverage of the surface of PES nanofibers.

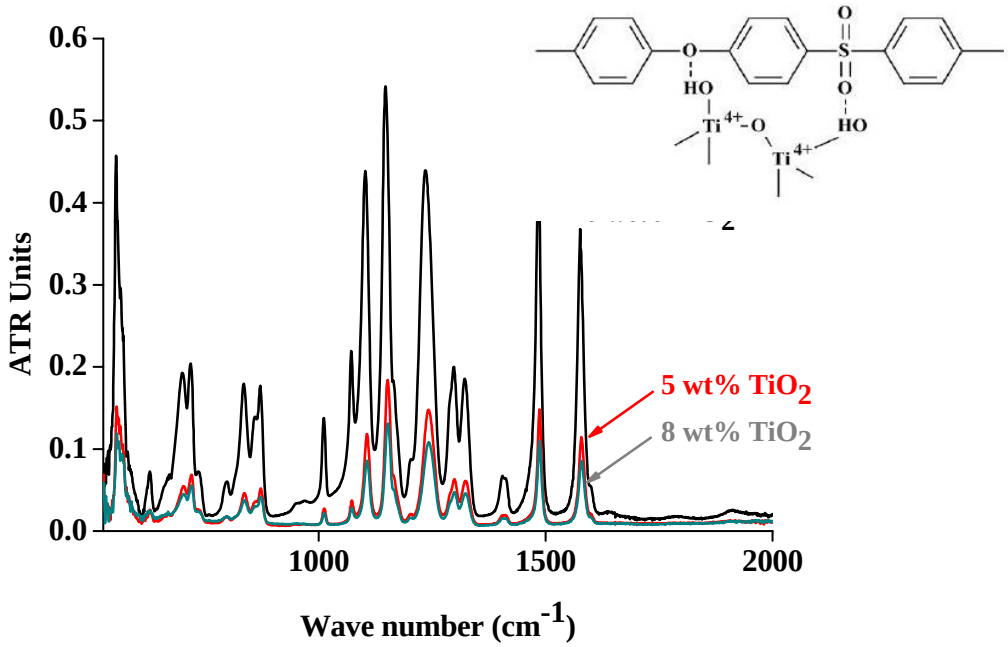

Figure 7.5: ATR-FTIR spectra of the neat PES ENM versus TiO_2/PES ENMs (the inset figure shows the chemical bond structure model of TiO_2/PES ENM [32])

7.2.5 Thermal properties (DSC and TGA)

It was assumed that incorporation of titania nanoparticles affects on thermal properties including thermal stability and the glass transition temperature (T_g) of the PES ENMs. The effect was evaluated through Differential thermal analysis (DSC) and thermal gravitational analysis (TGA).

The DSC and TGA results are shown in figures 7.6 A and B, respectively. DSC shows the glass transition temperature (T_g) of the membranes rises with increase of the amount of TiO_2. The shifting of T_g is due to the interactions between TiO_2 nanoparticles and the polymer.[13,23] The hydrogen bond between the surface hydroxyl group and the sulfone or ether group of PES (as previously shown in figure 7.5) are responsible for this increase of T_g .[23,33]

As represented in figure 7.6B, TGA results describe the thermal performance (stability) of the neat PES and TiO_2/PES ENMs. According to this results, as tabulated in table 7.1, the decomposition temperature (T_d) of the ENMs can also be determined.

As shown in figure 7.6B, thermal stability of the ENMs is improved by addition of TiO_2 amount. This behaviour is primarily due to the interaction between TiO_2 nanoparticles and PES thereby increasing the rigidity of polymer chain and the energy required for breaking down the polymer chain.[23]

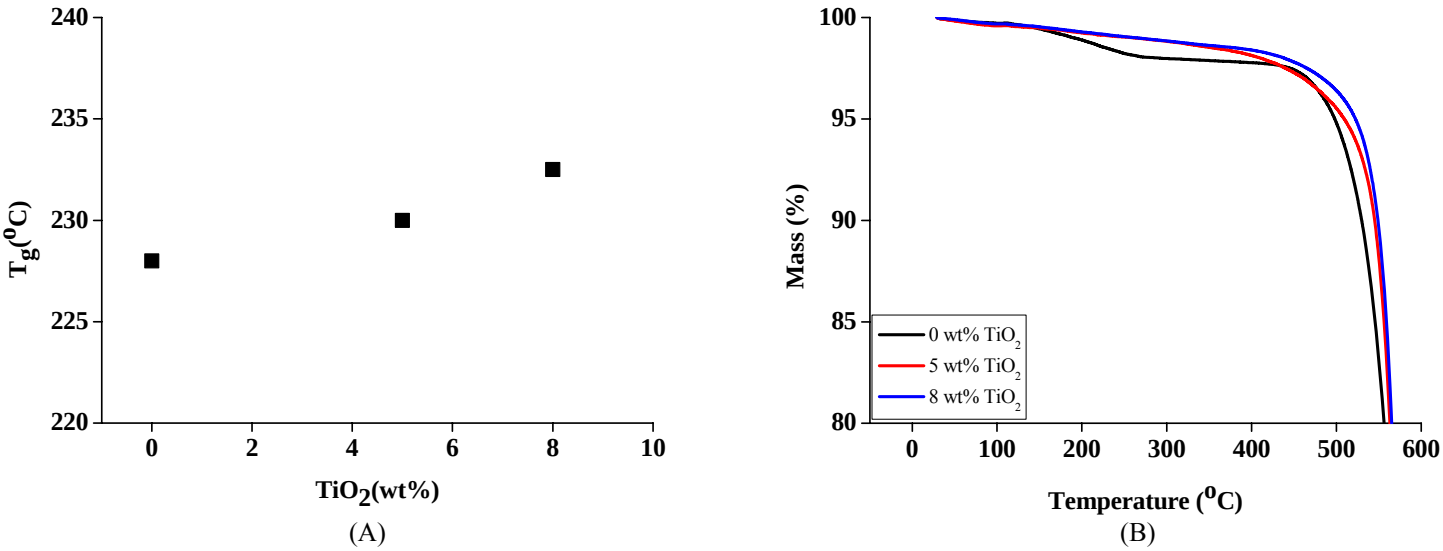

Figure 7.6: A) Variation of T_g by addition of amount of TiO_2 in the composite ENMs; B) TGA curves of the neat and TiO_2 reinforced PES electrospun nanofibrous mats

In fact, there are no significant changes of weight below 500 ◦C for the TiO_2/PES composites as compared to that for the PES ENM in same temperature range. The main weight loss for the PES ENM occurs at a temperature around 200 ◦C due to evaporation of DMAc residual solvent.

As seen in table 7.1, the decomposition temperature of the TiO_2/PES composite ENMs all rise with addition of the amount of TiO_2. For such a behavior, two possible reasons can be mentioned: 1) the physical cross-linking induced by the hydrogen bond formation between inorganic nanoparticle and polymer, constrain the PES chain and the heat oscillation of the polymer chain segment increase the decomposition temperature of the composite nanofibers [31] and 2) the higher the TiO_2 content, the more heat is absorbed by the inorganic nanofiller while heating-up, thereby decomposition of PES is postponed to higher temperatures.[12]

Table 7.1: Thermal decomposition temperature of the neat and TiO_2 reinforced PES electrospun nanofibrous mats

PES nanofiber containing	T_d (°C)
0 wt% TiO_2	498
5 wt% TiO_2	509
8 wt% TiO_2	522

7.2.6 Mechanical characterizations

In addition to wettability improvement, the other goal sought after addition of titania nanoparticles was enhancement of mechanical properties. In the previous chapters, it was sufficiently stressed on the importance of mechanical properties of an ENM for an efficient filtration performance.

The DMA results of the electrospun membranes are given in figure 7.7A, revealing a significantly higher storage modulus (E') of the TiO_2/PES composite ENMs than that of the neat PES ENM. The 5 wt% TiO_2/PES ENM show the highest storage modulus while at 8 wt% , E' declines but still two times higher than that of the neat PES ENM.

Tensile test results are demonstrated as figure 7.7B. Similar to the DMA results, elastic modulus and tensile strength increase drastically with addition of titania especially with a higher rate for the 5 wt% TiO_2/PES ENM. On the other hand, elongation to break decreases considerably as well.

On the whole, the mechanical properties are being improved by addition of titania nanoparticles especially at the concentration of 5 wt%. TiO_2 nanoparticles can cross link the polymer chains and increase their rigidity. Thus, to break down such a bond between the nanoparticles and PES chains, a higher amount of energy is required i.e. an improved mechanical property for the composite ENMs.[23] A lower increase rate of mechanical properties at the concentration of 8 wt%, can be attributed to: 1) slight agglomeration lowering the surface area of the nanoparticles and interfacial interaction between TiO_2 and PES 2) increase of the free volume of the polymer matrix around the TiO_2 nonoparticles and subsequent decrease of the mechanical properties. [31]

7.2.7 Water flux measurement

To evaluate the influence of mechanical and wettability improvement on filtration efficiency of the PES ENMs, water flux measurement was done under an applied feed pressure of 0.5 bar. An image of the set-up was represented in chapter 3.

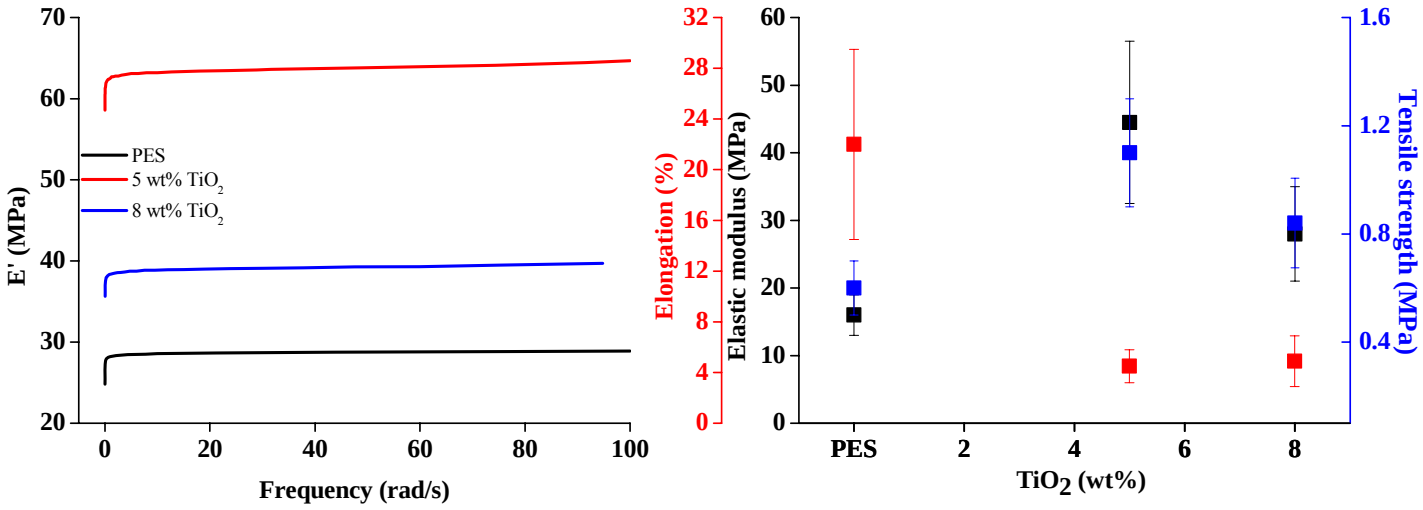

(A) (B)

Figure 7.7: A) Variation of storage modulus of the TiO_2 / PES electrospun nanofibrous membranes versus frequency; B) Tensile properties of the TiO_2 / PES electrospun nanofibrous membranes

Water flux behavior of the TiO_2/PES composite ENMs is presented as figure 7.8. Addition of titania nanoparticles increases the water permeability of the membranes significantly. This enhancement is due to the higher mechanical properties as well as hydrophilicity of the composite ENMs as compared to the neat PES ENM. This extraordinary promising finding assure us about a higher filtration efficiency of the composite ENMs leading to a lower energy consumption and need to less times of replacement of the membranes due to fouling and pore collapse. Such a performance is translated to development of a highly permeable membrane with a long life span and economically efficient.

7.3 Conclusion

Phase inverted microfiltration (MF) membranes are a well-known kind of commercial MF membranes used for various liquid filtration applications. However, as a progressive trend to create more efficient membranes researchers are attempting to develop membranes with much higher permeability and consequently lower energy consumption through structural modifications.

Electrospun nanofibers have been suggested for such an objective and substitution of conventional MF membranes. The high interconnected porosity and surface area to volume ratio leads to an extraordinary permeability and selectivity for the electrospun nanofibrous membranes.

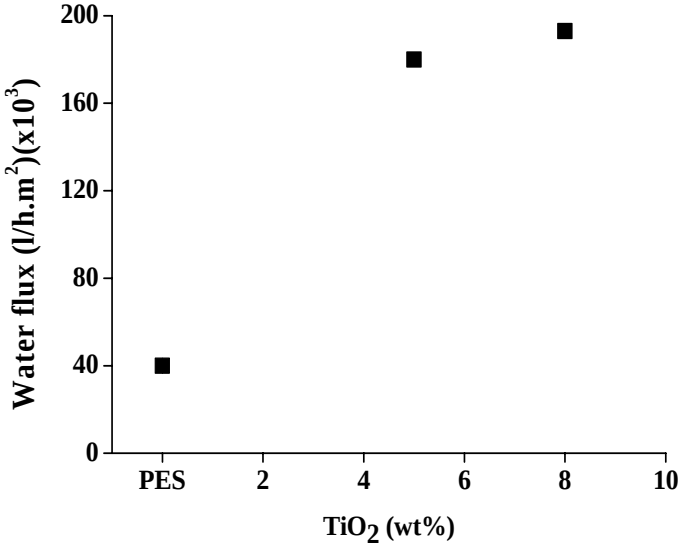

Figure 7.8: Water flux measured for the neat and titania nanoparticle reinforced PES electrospun nanofibrous mats

On the other hand, high porosity and inherent surface area of the ENMs also makes them more prone to mechanical breakdown and fouling thereby drastic loss of permeability.

In the current study, to address i.e. to prevent the aforementioned shortcomings, titania nanoparticles were employed and added to PES electrospun nanofibers through a sol-gel approach. The titania nanoparticle incorporated PES ENMs showed a very high hydrophilicity. Furthermore, the composite PES ENMs possessed a significantly higher mechanical and more optimum thermal properties than their neat counterpart. As proved through water flux measurement, such desirable combination of high hydrophilicity and mechanical stability offers the TiO_2/PES ENMs an outstanding water permeability. This membrane is highly recommended for various liquid filtration applications including water purification in rejection of non-polar foulants.

Compared with the latter composite ENMs i.e. those containing zirconia nanoparticles, the TiO_2/PES composite ENMs show some more advantages including higher hydrophilicity along with the nanofibers with smaller diameter thereby pore size which can make them a more selective membrane. However, the ZrO_2/PES ENMs show a better mechanical properties especially an optimized ductility compared to the TiO_2/PES ENMs. In general, both the composite ENMs show a

significantly enhanced water permeability compared to the neat PES ENMs attributed to their modified mechanical stability and wettability.

7.4 References

[1] ZM. Huang, Y.Z. Zhang, M. Kotaki, S. Ramakrishna, A review on polymer nanofibers by electrospinning and their applications in nanocomposites, Composites Science and Technology 63 (2003) 2223–2253.

[2] Z. Tang, C. Qiu, JR. McCutcheon, K.Yoon, H. Ma, D. Fang, E. Lee, C. Kopp, BS. Hsiao, B. Chu, Design and Fabrication of Electrospun Polyethersulfone Nanofibrous Scaffold for High-Flux Nanofiltration Membranes, J Polym Sci Part B: Polym Phys 47 (2009) 2288–2300.

[3] P. Heikkilä, A.Taipale, M. Lehtimäki, A. Harlin, Electrospinning of polyamides with different chain compositions for filtration application**.** Polym Eng Sci 48(2008)1168–1176.

[4] K. Nakata, SH. Kim, Y. Ohkoshi, Y. Gotoh, M. Nagura. Electrospinning of Poly (ether sulfone) and Evaluation of the Filtration Efficiency, Sen-I Gakkash 63(2007) 307–312.

[5] XH. Qin, SY. Wang. Filtration properties of electrospinning nanofibers. J Appl Polym Sci 102(2006) 1285–1290.

[6] WJ. Li, CT. Laurencin, EJ. Caterson, RS. Tuan, FK. Ko, Electrospun nanofibrous structure: A novel scaffold for tissue engineering, J Biomed Mater Res A 60 (2002), 613–621.

[7] C. Burger, B. S. Hsiao, and B.Chu, Nanofibrous materials and their applications, Annu. Rev. Mater. Res. 36(2006) 333–68.

[8] Y. Hong, D. Li, J. Zheng, G. Zou, Sol-gel growth of titania from electrospun polyacrylonitrile nanofibers, Nanotechnology 17 (2006) 1986–1993.

[9] JF. Li , ZL. Xu , H. Yang , LY. Yu, M. Liu, Effect of TiO2 nanoparticles on the surface morphology and performance of microporous PES membrane, Applied Surface Science 255 (2009) 4725–4732.

[10] A. Fujishima, K. Honda, Electrochemical photolysis of water at a semiconductor electrode, Nature 238 (1972) 37–38.

[11] AL. Linsebigler, G. Lu, JT. Yates, Photocatalysis on TiO_2 Surfaces: Principles, Mechanisms, and Selected Results, Chem. Rev. 95 (1995) 735.

[12] G.Wu, S. Gan, L. Cui, Y. Xu, Preparation and characterization of PES/TiO_2 composite membranes, Applied Surface Science 254 (2008) 7080–7086.

[13] X. Meng, N. Luo, S. Cao, S. Zhang, M.Yang, X. Hu, In-situ growth of titania nanoparticles in electrospun polymer nanofibers at low temperature, Materials Letters 63 (2009) 1401–1403.

[14] V. Khrenov, M. Klapper, M. Koch, K. Müllen, Surface Functionalized ZnO Particles Designed for the Use in Transparent Nanocomposites, Macromol Chem Phys 206(2005) 95–101.

[15] C. Zeng, L. James Lee. Poly(methyl methacrylate) and Polystyrene/Clay Nanocomposites Prepared by in-Situ Polymerization, Macromolecules 34(2001) 4098–103.

[16] E. Reynaud, T. Jouen, C. Gauthier, G. Vigier, J. Varlet. Nanofillers in polymeric matrix: a study on silica reinforced PA6, Polymer 42(2001) 8759–68.

[17] MM. Demir, P. Castignolles, Ü. Akbey, G. Wegner. In-Situ Bulk Polymerization of Dilute Particle/MMA Dispersions, Macromolecules 40(2007) 4190–8.

[18] T. Kyprianidou-Leodidou, P. Margraf, W. Caseri, UW. Suter, P. Walther, Polymer sheets with a thin nanocomposite layer acting as a UV filter. Polym Adv Technol 8(1997) 505–12.

[19] Mikrajuddin, I.W. Lenggoro, K. Okuyama, F.G. Shi. Luminescent Polymer Electrolytes Prepared by Growing ZnO Nanoparticles in the Matrix of Polyethylene Glycol. J Electrochem Soc 149(2002) 107–12.

[20] N. Wu, J. Wang, Q.Wei, Y. Cai, B. Lu, Morphology, thermal and mechanical properties of PVAc/ TiO_2 hybrid nanofibers,e-Polymers 2009, no.152.

[21] R.D. Deegan, O. Bakajin, T.F. Dupont, G. Huber, S.R. Nagel, T. Witten, Capillary flow as the cause of ring strains from dried liquid drops, Nature 389(1997) 827-829.

[22] Q. Hu and E. Marand, In situ formation of nanosized TiO_2 domains within poly(amide-imide) by a sol-gel process, Polymer 40(1999) 4833-4843.

[23] JF. Li, ZL. Xu, H. Yang, LY. Yu, M. Liu, Effect of TiO_2 nanoparticles on the surface morphology and performance of microporous PES membrane, Applied Surface Science 255 (2009) 4725–4732.

[24] JS. Im, MI. Kim, YS. Lee, Preparation of PAN-based electrospun nanofiber webs containing TiO_2 for photocatalytic degradation, Materials Letters 62 (2008) 3652–3655.

[25] P.K. Khanna, N. Singh, S. Charan, Synthesis of nano-particles of anatase-TiO_2 and preparation of its optically transparent film in PVA, Materials Letters 61 (2007) 4725–4730.

[26] CC. Wang, JY. Ying, Sol-Gel Synthesis and Hydrothermal Processing of Anatase and Rutile Titania Nanocrystals, Chem. Mater. 11(1999) 3113-3120.

[27] D. Wang, C. Song, Y. Lin, Z. Hu, Preparation and characterization of TiO_2 hollow spheres , Mater. Lett. 60 (2006) 77-80.

[28] A. Rahimpour, S.S. Madaeni, A.H. Taheri, Y. Mansourpanah, Coupling TiO_2 nanoparticles with UV irradiation for modification of polyethersulfone ultrafiltration membranes, Journal of Membrane Science 313 (2008) 158–169.

[29] E. Bormashenko, Y. Bormashenko, T. Stein, G. Whyman, E. Bormashenko,Why do pigeon feathers repel water? Hydrophobicity of pennae, Cassie–Baxter wetting hypothesis and Cassie–Wenzel capillarity-induced wetting transition, Journal of Colloid and Interface Science 311(2007) 212–216.

[30] S. Belfer, R. Fainchtain, Y. Purinson, O. Kedem, Surface characterization by FTIR-ATR spectroscopy of polyethersulfone membranes-unmodified, modified and protein fouled, J. Membrane Sci. 172 (2000) 113–124.

[31] M. Luo, W. Tang, J. Zhao, C. Pu, Hydrophilic modification of poly(ether sulfone) used TiO_2 nanoparticles by a sol–gel process, Journal of Materials Processing Technology 172 (2006) 431–436.

[32] A.F. Ismail, A.R. Hassan, Effect of additive contents on the performances and structural properties of asymmetric polyethersulfone (PES) nanofiltration membranes, Sep. Purif. Technol. 55 (2007) 98–109.

[33] TH. Bae, IC. Kim, TM. Tak, Preparation and characterization of fouling-resistant TiO_2 self-assembled nanocomposite membranes. J. Membr. Sci. 275 (2006) 1-5.

Chapter 8. Outlook

Biofunctionalized Electrospun Nanofibrous Membranes for nanofluid filtration

Chapter 8. Outlook

Biofunctionalized Electrospun Nanofibrous Membranes for nanofluid filtration

Among the new membrane technologies, electrospun nanofibrous membranes (ENMs) are emerging as a distinct novel class possessing promising potentials for liquid filtrations. Primarily their high interconnected porosity is of interest which can lead to a very high permeability thereby low energy consumption. However, the other main part of function i.e. selectivity is limited to size based rejection of only coarse (micro) suspended solids due to their relatively bigger pore size.[1,2,3,4] In other words, ENMs are unable to filter out a nanofluid i.e. a fluid containing the nanoparticles with a size below 100 nm. To broaden the range of applicability to removal of nanosubstances, ENMs should be equipped to the other separation mechanism i.e. adsorption as well.

In a novel biomimic idea (patented by the number of EP111698189) called "Carnivorous plant" approach, nanofibers are surface functionalized via protein immobilization. Upon increase of pH to above isoelectric point of the protein, e.g. by wetting, the protein undergoes conformational change. This transformation leads to emergence of some more functional groups able to bind to water molecules (thereby protein swelling) and nanosolids to be filtered. Moreover, the swollen functional protein makes a higher steric hindrance facilitating the capturing of the nanosolids and maximizing the rejection efficiency. In this carnivorous plant-like membrane, the swollen protein immobilized nanofibers act as the spread leaves of the plant and the emerged functional groups able to catch the nanoparticles as sticky mucilage. Figure 8.1 shows a carnivorous plant called venus flytrap.

As the preliminary study, a protein /nanofiber hybrid membrane was developed for rejection of metal nanoparticles from water streams. For the first time, Bovine Serum Albumin (BSA) protein was immobilized onto the surface of Poly(AcryloNitrile-co-Glycidyl MethAcrylate) (PANGMA) electrospun nanofibers to make a novel functionalized membrane with superior retention capacity.

As the capturer component, BSA is a very conventional and cheap serum albumin protein, which has been widely used in numerous biochemical applications.

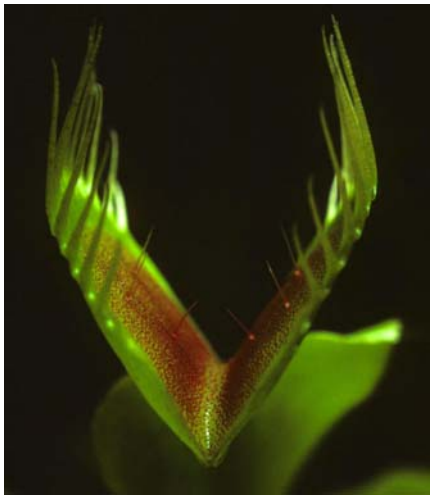

Figure 8.1: A carnivorous plant[5]

On the other hand, PANGMA as a new polymeric material is a copolymer of acrylonitrile (AN) and glycidyl methacrylate (GMA). This polymer has not only the advantage of the chemical stability induced by the strong backbone of polyacrylonitrile but also a high functionality offered by the free and active epoxy group on GMA allowing a variety of activation/coupling chemistries for the covalent binding of capturers. In the current study, the nanofibers are functionalized based on the extremely simple and conventional epoxy-amino reaction between the amine groups on BSA and epoxy groups on PANGMA. [6]

First, the PANGMA nanofibers were made via electrospinning under the following conditions: PANGMA concentration (20 wt%), DMF as solvent, voltage of 15-20 kV, collecting plate of Aluminum foil, spinning distance of 25 cm, and feed rate of 1.1 ml/h. Subsequently, the PANGMA ENMs were immersed into the BSA/PBS buffer solution with the concentration of 5 mg/mL and the pH values of 6.8 and the mixture was moderately shaken at 55 °C up to 24 h. After the reaction, the membranes were taken out and washed several times by PBS buffer (pH 6.8) under shaking condition until the complete removal of unbound BSA.

Functionalization mechanism of PANGMA is based on ring opening of the epoxide groups of its GMA part when attacked by amine containing BSA. The result of such a reaction is formation of the secondary amine and hydroxyl groups. Such an assumption is proved by surface chemical analysis (ATR-FTIR) results shown in figure 8.2. Successful reaction between primary amine groups of BSA and epoxides of PANGMA is emphasized by vanishing the characteristic peak of epoxy group appearing at 908 cm^{-1} for the neat nanofibers. In addition, the peaks emerging at 1650

cm^{-1} and 1530 cm^{-1} are the vibration peaks of amide I and amide II groups in BSA molecules. The peaks appreaed at 3300 and 3600 cm^{-1} are related to the secondary amine and hydroxyl groups, respectively, generated during the opening of the epoxy group by the primary amine groups of BSA.[7]

Primarily, BSA protein was immobilized onto the PANGMA nanofibers for an adsorption based water separation. However, this approach could be beneficial in terms of mechanical and chemical features of the membrane as well. Possessing lots of primary amine groups, BSA can also react with two adjacent PANGMA nanofibers leading to a cross linked structure. While, the overview pictures shown in figures 8.3 A,B reveal no significant difference in term of porosity between the neat and functionalized nanofibrous mats, the cross sectional image indicated as figure 8.3C clearly indicate that the submicrometer fibers are interconnected by nanometer protein wires. The latter behaviour was not observed for the neat ENM. Such an increase of the netting points of the web and interfiber bondings are expected to strengthen the membrane.[8,9] This effect is intensified by crosslinking of the PANGMA molecules inside the nanofibers while functionalization. Indeed, the biofunctionalization giving rise to inter/intrafiber bondings leads to a significantly higher mechanical stability in terms of elastic modulus and tensile strength as demonstrated in figure 8.4. A mechanically strong nanofibrous membrane can resist against pore collapse while filtration subsequently possesses a longer life span and lower energy consumption. Water filtration under a 1 bar pressure readily showed that the mechanically stronger BSA/PANGMA ENM is much more permeable (~ 45 $kl/h.m^2$) than its neat counterpart. Yet, some part of this higher permeability is attributed to the superhydrophilicity effect as shown in figure 8.5 caused by emergence of the secondary functional groups such as hydroxyl and amine while functionalization.

Retention ability of the BSA/PANGMA ENMs for gold (Au) nanoparticles is demonstrated in figure 8.6A. As the control experiment to compare the filtration performance of the functionalized PANGMA ENM with its neat counterpart, the suspension containing 40 nm Au nanoparticles was randomly selected. While the neat PANGMA ENM is able to reject a negligible part (1.5 %) of the 40 nm Au nanoparticles, the biofunctionalized ENM rejects 72.5% of the nanoparticles of the same size.

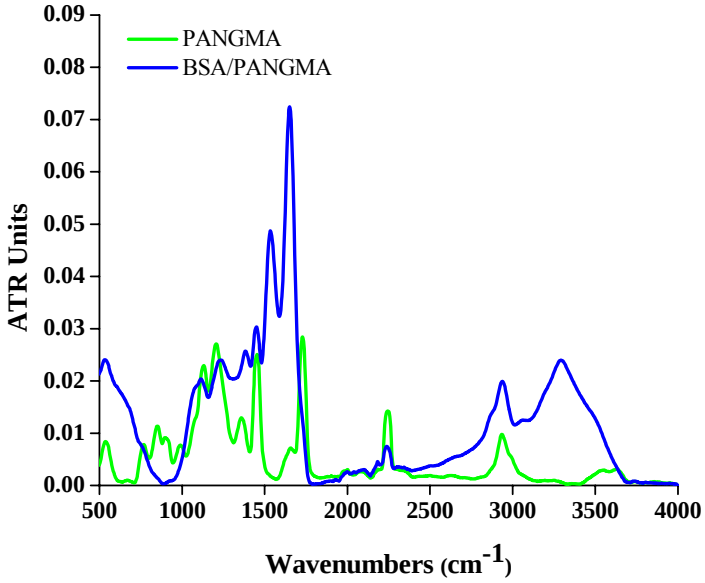

Figure 8.2: ATR-FTIR spectra of the PANGMA ENMs before and after BSA immobilization

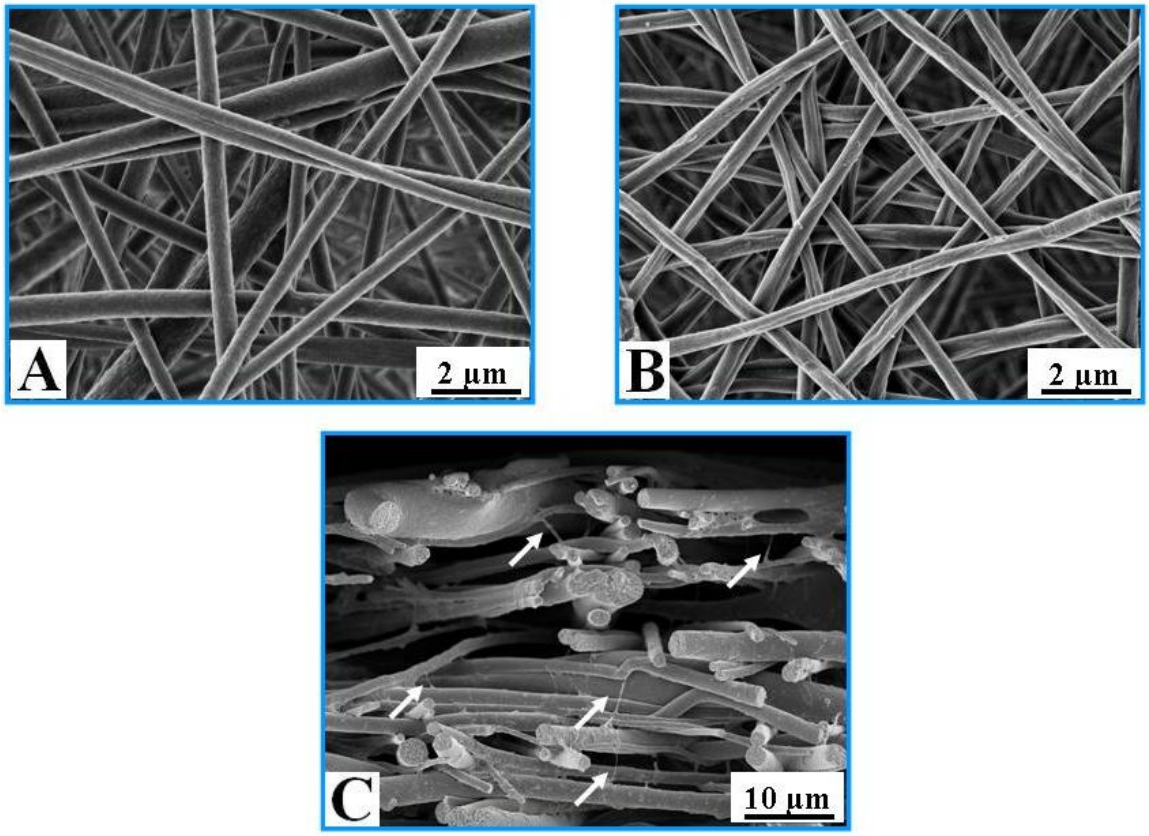

Figure 8.3: SEM micrographs of the PANGMA nanofibers: (A) neat nanofibers; (B) BSA immobilized nanofibers; (C) the cross sectional image indicating the BSA induced cross linking of the nanofibers

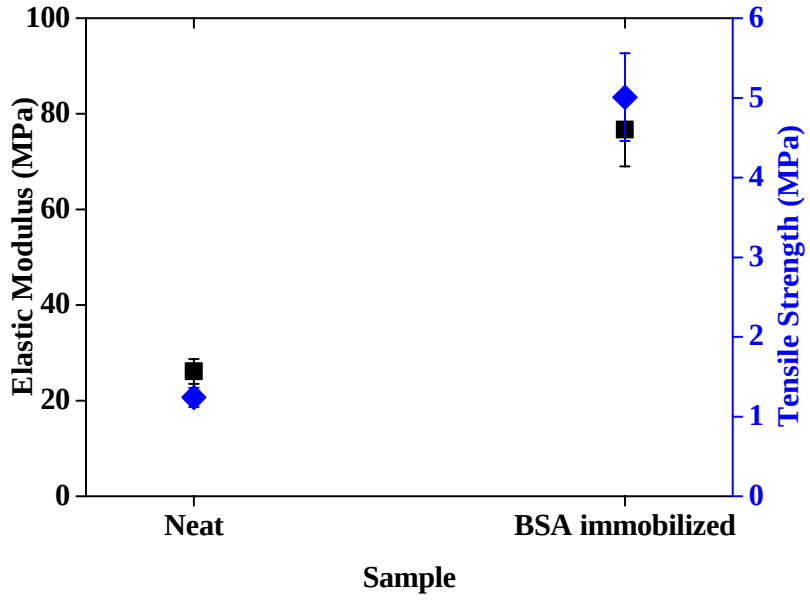

Figure 8.4: Mechanical properties of the PANGMA electrospun nanofibrous membranes

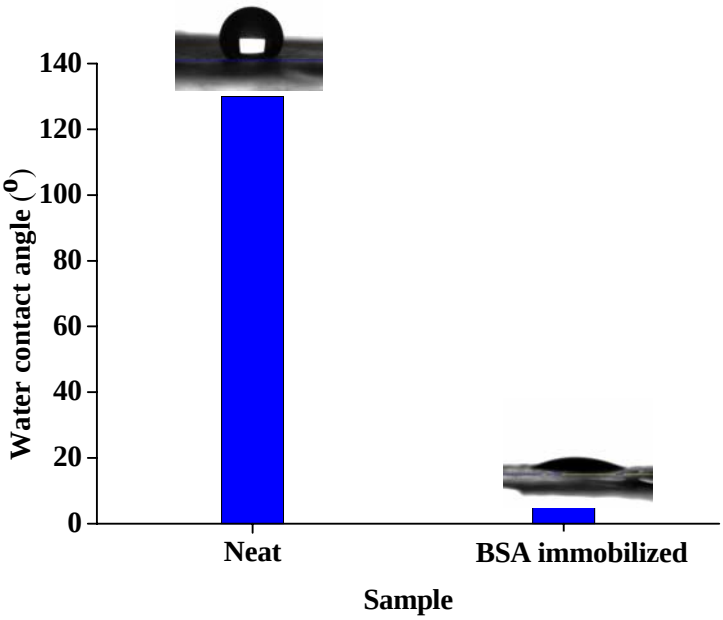

Figure 8.5: Wettability of the PANGMA electrospun nanofibrous membranes

Visual inspection of the feed and permeate samples clearly reveals the high retention ability of the BSA/PANGMA ENM compared to its neat counterpart. As seen in figure 8.6B, color intensity of the feed sample drastically decreases after permeation through the biofunctionalized ENM. The retention efficiency for 80 nm Au nanoparticles is even more as high as 97 %, whereas this value for the 20 nm nanoparticles reduces to 70%, still high and promising. In addition to such an extraordinary retention efficiency, the permeate flux recorded when filtration of 80

nm Au nanosuspension, was also considerable as high as 9000 l/h.m^2 much higher than that reported for conventional micro/ultrafiltration membranes.[10] Noteworthy, there was no major feed pressure while filtration and experiment was performed under the atmospheric pressure implying a very low energy consumption.

The reason for such a high retention efficiency by the BSA/PANGMA ENMs should be sought in pH- dependent conformational change of BSA. Upon wetting, when pH increases to above isoelectric point of BSA i.e. 4.7, conformational changes occur.[11] Such a transformation leads to binding considerably more water[11] giving rise to a swollen structure. From one hand, the swollen functional protein on the surface of the nanofibers makes a smaller pore size and more steric hindrance by growing nanofibers. On the other hand through emergence of the new functional groups upon conformational change and strong protein- metal nanoparticle interactions such as ionic interaction, hydrogen bonding, Van der Waals and hydrophilic interactions[12,13,14] Au nanoparticles stick to BSA protein. Combination of these effects reminds us the hunting behaviour of a carnivorous plant and results in a significantly high retention efficiency for the membrane being studied.

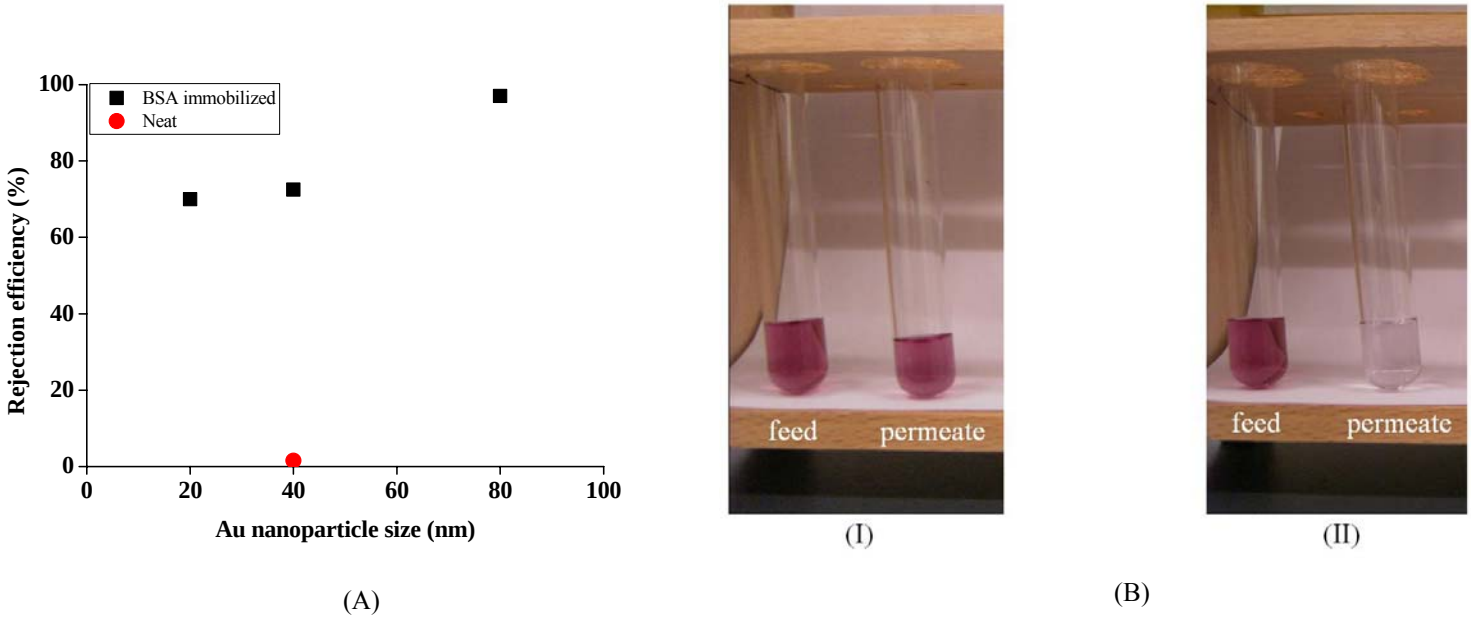

Figure 8.6: A) Extraordinary retention efficiency of the biofunctionalized PANGMA ENMs for gold (Au) nanoparticles; B) visual comparisons between the feed and permeated samples through the neat (I) and BSA/PANGMA ENMs (II)

As seen in figure 8.7, morphological observation of the membranes after the filtration process reveal a highly uniform dispersion of gold nanoparticles onto the biofunctionalized nanofibers i.e. formation of a bionanohybrid structure. Indeed, the adopted approach to functionalize the nanofibers and their decoration via filtration of a suspension containing functional nanoparticles can be claimed as a novel bioactivity based route to create a metal-polymer nanohybrid structure. Such a bionanohybrid can be utilized as a multifunctional hybrid material for a diverse range of applications including filtration, catalysis, photonic, electronic etc.

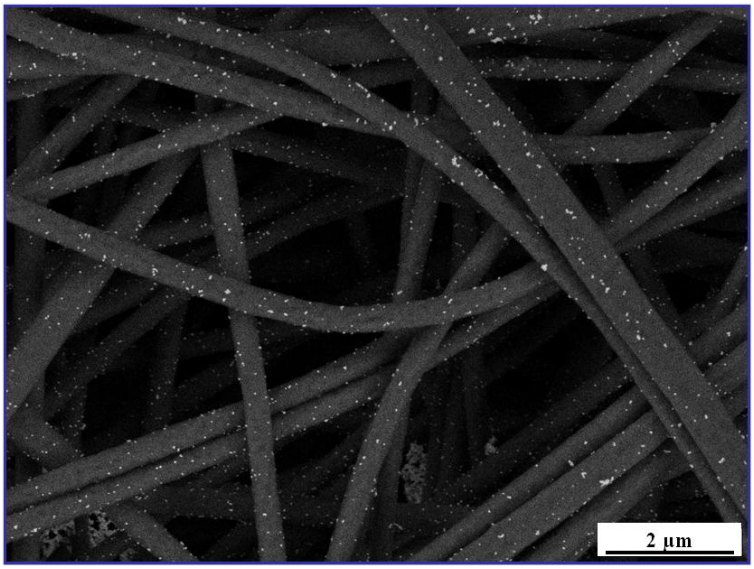

Figure 8.7: The gold nanoparticles adsorbed onto the BSA/PANGMA nanofibers

On the whole, through this preliminary study to be continued for other filtration systems, a novel bio functionalized electrospun nanofibrous membrane was developed for nanofluid filtration. Depending on the nanoparticle size, this membrane was successful in rejection of 70-100% of the nanoparticles. Moreover, protein induced cross linking of the nanofibers and ring opening of the epoxide groups of GMA part of the polymer led to a higher mechanical stability and wettability, respectively. Such promising features could induce a higher permeability and less fouling tendency. The final remaining structure after filtration is a bionanohybrid which acts as a multifunctional membrane for different advanced applications.

Considering the high potential of the novel class of functionalized electrospun nanofibrous membranes, study in this area to benefit them for advanced filtration

applications is severely demanded and will be emphasized by the "Nanochemistry and Nanoengineering group".

References

[1] S.Sh.Homaeigohar, K. Buhr, K.Ebert, Polyethersulfone electrospun nanofibrous composite membrane for liquid filtration, J. Mem. Sci. 365 (2010) 68-77.

[2] R. Gopal, S. Kaur, C.Y. Feng, C. Chan, S. Ramakrishna, S. Tabe, T.Matsuura, Electrospun nanofibrous polysulfone membranes as pre-filers:particulate removal, J. Mem. Sci. 289(2007) 210–219.

[3] D. Aussawasathien, C. Teerawattananon, A. Vongachariya, Separation of micron to sub-micron particles from water: Electrospun nylon-6 nanofibrous membranes as pre-filters, J.Mem. Sci. 315 (2008) 11–19.

[4] R. Gopal, S. Kaur, Z. Ma, C. Chan, S. Ramakrishna, T. Matsuura, Electrospun nanofibrous filtration membrane, J. Mem. Sci. 281 (2006) 581–586.

[5] www.Honda-e.com

[6] T.Godjevargova, V. Konsulov, A. Dimov, Preparation of an ultrafiltration membrane from the copolymer of Acrylonitrile-glycidylmethacrylate utilized for immobilization of glucose oxidase, J. Mem. Sci. 152 (1999) 235-240.

[7] J. González-Benito, The nature of the structural gradient in epoxy curing at a glass fiber/epoxy matrix interface using FTIR imaging, J. Coll. and Interf. Sci. 267(2003) 326–332.

[8] A. Romo-Uribe, L. Arizmendi, ME Romero-Guzman, S. Sepulveda-Guzman, R. Cruz-Silva, Electrospun Nylon Nanofibers as Effective Reinforcement to Polyaniline Membranes, Appl. Mater. and interfac. 1(2009) 2502–2508.

[9] S. Ba, Experimental study of mechanical and electrical properties of carbon nanofiber/epoxy composites, Materials and Design 31(2010) 2406–2413.

[10] S. Ramakrishna, R. Jose, PS. Archana, AS. Nair, R. Balamurugan, J. Venugupal, WE Teo, Science and engineering of electrospun nanofibers for advances in clean energy, water filtration, and regenerative medicine, J. Mater. Sci. 45(2010) 6283–6312.

[11]DH. Chou and CV. Morr, Protein-Water Interactions and functional properties, J. Am. Oil. Chemists' Soc. 56(1979) 53A-62A.

[12] I. Lynch and KA.Dawson, Protein-nanoparticle interactions, Nanotoday 3(2008) 40-47.

[13] T Cedervall et al., Understanding the nanoparticle–protein corona using methods to quantify exchange rates and affinities of proteins for nanoparticles, PNAS 104(2007) 2050-2055.

[14]XL Kong et al., High-Affinity Capture of Proteins by Diamond Nanoparticles for Mass Spectrometric Analysis, Anal. Chem. 77(2005) 259-265.

Chapter 9.

Summary

Chapter 9. Summary

Water crisis is undoubtedly a global developing challenge. This problem derives from water pollution, shrinking the available water supplies, climate change, escalating world population and industries highly demanding water. One solution for such a challenge is filtration of available even polluted water sources to remove the contaminants and to make the water drinkable. Hence, tremendous efforts in terms of research investment, manpower training and membrane developments have been put forth by governments and industries to expand existing membrane technologies as well as to identify novel membrane technologies with enhanced filtration efficiency.

Water purification can be effectively achieved using novel nanofibrous membranes due to their high interconnected porosity and tunable pore size giving rise to very promising filtration abilities in terms of permeability, selectivity and low fouling.

Pursuing the trend to evaluate the potentials and to meet the industrial (practical) requirements, as the PhD research work, electrospun nanofibers were implemented for water filtration. As the membrane material, polyethersulfone (PES) was selected due to its high mechanical property, thermal and chemical resistance. A promising combination of suitable membrane material and structural characteristics was the initial assumption to develop an efficient water membrane with extraordinary filtration performance.

The PES electrospun nanofibrous membrane (ENM) was prepared through an electrospinning method and mounted on a poly(ethylene terephtalate) (PET) non-woven to alleviate difficult handling of the nanofibrous web. Heat treatment was adopted as an effective approach to enhance the integration of the composite membrane in order to prevent delamination of the nanofibrous layer. Pure water flux measurements demonstrated the high permeability of this nanofibrous composite membrane. However, the compaction of the PES nanofibrous layer at high feed pressures (the simulated conditions by a multi layer i.e. cartridge filter structure) could lower the water permeation. In a novel particle challenge test based on particulate aqueous suspensions, this nanofibrous composite membrane showed a high permeability while rejecting microparticles efficiently. However, in the case of nanoparticles much smaller than the average pore size, in spite of an optimum rejection efficiency, the permeation declined

drastically due to a cake layer formation. Considering the characteristics of real particulate suspensions in water treatment, containing a mixture of micro and nanoparticles, this electrospun nanofibrous membrane has the potential to be used in pre-treatment of water, one step before ultra and nanofiltration membranes.

To scale up and overcome the encountered limitations, the ENM needs to be mechanically stable also wettable. Primarily, the mechanical performance should be understood at different operating modes under compressive and tensile stresses. Accordingly, the membrane should be augmented. Despite slightly enhanced mechanical properties of the heat treated ENM, it was still susceptible to compaction. In addition, wettability is not expected to rise through such an approach. Hence, the nanocomposite strategy was considered to fulfill the requirements. Two groups of nanofillers including zirconia and titania were selected primarily owing to their high mechanical and wettability induction, respectively. Noteworthy, zirconia nanoparticles are envisaged a novel nanofiller in the membrane technology. Intentionally, physical blending was adopted to incorporate zirconia nanoparticles into the PES nanofibers. Embedding of the nanofiller could significantly optimize the mechanical properties of the ENM especially its compaction resistance. Reflected in the water permeability, pore collapse was prevented and the porosity was preserved. Yet, wettability was slightly enhanced. To compensate the lack of wettability of the membranes, titania nanoparticles were chosen as the nanofiller well known for their high hydrophilicity. Moreover, sol-gel was taken as the fabrication method to induce surface residence of the nanoparticles with least agglomeration. The nanocomposite electrospun nanofibrous membranes showed amazing properties in terms of mechanical stability also wettability. The resultant performance is bloomed as incredibly high water permeability thereby low energy consumption and long life span. This implies their highly desirable potential to be utilized for industrial filtration applications.

Acknowledgements

Acknowledgements

I would like to thank my advisor, Prof. Mady Elbahri, for his great guidance over the course of my graduate career, and his unwavering support for me to ”bridge the gap” between science and engineering. I appreciate his patience, friendly attitude and flexibility in allowing me to pursue novel research areas such as advanced nanostructured membranes, nanocomposites, and bioinspired nanomaterials. In addition, I should appreciate deeply Prof. Volker Abetz, head of the Polymer institute, who gave me the opportunity to accomplish this dissertation. The suitable and friendly atmosphere of the institute along with modern equipments facilitate accomplishment of advanced researches. Without any question, he has the key role in this regard. I would also like to thank Dr. Katrin Ebert who from my first week in the Polymer institute, Helmholtz-Zentrum Geesthacht (HZG), supported me to get familiar with the disciplines of the institute and even the German culture. She was also an excellent advisor for me throughout my first year of the PhD research.

Helmholtz association, German Academic Exchange Service (Deutscher Academischer Austausch Dienst ;DAAD) and Nanochemistry and nanoengineering group are greatly acknowledged for the financial support as a PhD fellowship. Joachim, Regina, Kristian, Carsten and Berthold deserve another big thanks for all their immense helps. I would also like to thank Dr. Erica Lilleodden, Clarissa, Karen, Heinrich, Silvio and Sabrina for all their assistances throughout characterizations of my very complicated samples.

A big thanks to all my good friends with whom I spent memorable times throughout my staying in Geesthacht especially Shahrokh, his wife Farzaneh and his son Arman, Suran and Massoud, Maab, Gagik, Neda, Maryam, Hossein, Alireza and his wife Sepideh, Dai, Usman, Rakib, my other friends from Kiel including Mehdi, Mostafa, Ali, Jason, Ramzy and all the DAAD friends.

Finally, my biggest thanks goes to my family including my father, mother and younger brothers Farzin and Farzan for all their love and encouragement throughout my life. Undoubtedly, without their unconditional support, I would not be where I am today. I wish them a long happy life.

Patents and Publications:

Patents

1) M. Elbahri, **S.SH. Homaeigohar,** Nanoceramic reinforced electrospun nanofibrous membranes with superior permeability for water filtration, European patent, EP11153217, 2011.

2) M. Elbahri, **S.SH. Homaeigohar,** T. Dai, R. Abdelaziz, A novel biofunctionalized electrospun nanofibrous membranes for nanofluid filtration, European patent, EP111698189, 2011.

Publications

1) **S.SH. Homaeigohar**, E. T. Lilleodden, V. Abetz, M. Elbahri, Evaluation of the mechanical properties of Polyethersulfone electrospun nanofibrous membranes used for liquid filtration, Submitted.

2) **S.SH. Homaeigohar**, M. Elbahri, Zirconia nanoparticle doped Polyethersulfone nanofibers; An electrospun nanocomposite mat for water filtration, ***Materials Chemistry and Physics, under revision.***

3) **S.SH. Homaeigohar**, H. Mahdavi, M. Elbahri, Extraordinarily water permeable sol-gel formed nanocomposite nanofibrous membranes, ***Journal of Colloid and Interface Science, In press***.

4) M. Elbahri, **S.SH. Homaeigohar,** T. Dai**,** R. Abdelaziz, R. Khalil, A Zillohu, Carnivorous plant-like nanofibrous membranes for an energy saving nanofluid filtration and nanohybrid fabrication, Submitted.

5) **S. SH. Homaeigohar**, K. Buhr, K. Ebert, Polyethersulfone electrospun nanofibrous composite membrane for liquid filtration, ***Journal of Membrane Science,*** Volume 365, Pages:68-77, 2010.

Conferences

1) **S.SH. Homaeigohar**, M. Elbahri, Ceramic nanoparticles doped Polymeric nanofibrous membranes;An electrospun nanocomposite mat for water filtration, **ICOM 2011**, Amsterdam, The Netherlands, July 23-29, 2011.

2) M. Elbahri, **S.SH. Homaeigohar**, T.Dai, Nanofluid filtration using electrospun nanofibers, **ICOM 2011**, Amsterdam, The Netherlands, July 23-29, 2011.

3) **S.SH. Homaeigohar**, M. Elbahri, K.Ebert, V. Abetz, Filtration potential and mechanical performance of an electrospun nanofibrous composite membrane used for liquid filtration, **Electrospin 2010**, Australia, Melbourne, Jan.26-29, 2010.